POLITECNICO DI MILANO

Dipartimento di Ingegneria Civile e Ambientale

Corso di laurea in Ingegneria Civile Idraulica

Soil water dynamics with phase changes: mathematical modeling, numerical simulations and laboratory experiments

Relatore: Prof. Ing. Carlo De Michele

Correlatore: Ing. Marco Caruso

Ing. Francesco Avanzi

Tesi di Laurea di:

Cristina Deidda

Matr. 837698

Anno Accademico 2017-2018

Abstract

The aim of the thesis is to study the dynamics of water in soils under freezing conditions. The seasonal creation of ice in underlying soils can cause the upward movement of the ground surface. This process is called "Frost Heave" and generates lot of engineering problems creating damage to roads, pipelines and infrastructures for billion dollars.

The study of literature highlight the complexity of the process which is a hydro-thermal-mechanical problem. The system of main governing equations is very complex both for the number of equations and for the non-linearity of the equations.

Many authors propose different approaches in describing from a mathematical point of view the frost heave process. The exhaustive study of the State of Art suggested to classify the different models in two main group. The first one, introduces models that studies saturated condition. These models are very specific studying the dynamics of frost heave process, the creation of the lenses and the cryostatic suction. The soil is subdivided in various layers (below, and upper the ice lens) with different equations and hypothesis governing each layer. Various mechanical models are presented but the governing equations are written in a not rigorous way. Moreover,the pressure exerted on the soil skeleton, at pore-size dimension, is often calculated with empirical formulation based on strong approximations. Indeed, it is not taken into consideration the pressure exerted due the thermal expansion of freezing water.

The second group of models, studies unsaturated soils in freezing conditions and

considers the frost heave process completely negligible. Indeed, there is a lack of a mechanical model: the pressure and stress field in freezing conditions are not analyzed and not considered. Another common approximation regards the ice gauge pressure which is considered equal to zero. In other word, the pressure exerted by the ice in freezing conditions is considered negligible. However, these models are based on rigorous formulation: the mass conservation equations and energy equations are written in a rigorous and complete mathematical form.

On the basis of the State of Art analysis, the first stage of this work concerns a mathematical study of a system of equations which can be applied both for saturated and unsaturated soils and which take into consideration the change of phase phenomena. The aim of this system of equations is to include the frost heave process and the ice pressure exerted on the solid skeleton in the equations; utilizing a rigorous mathematical formulation. The main governing equations are studied and written such as to consider the ice pressure contribute and the cryostatic suction.

The complexity of the system implies the necessity of more elaborate studies and advanced numerical and computational instrument to solve entirely it. So, the experimental and numerical part of the study is focused on the resolution of an easier case. In particular, considering saturated conditions, the energy equation is solved both for soils and water.

Moreover, considering the pore-size dimension a coupled thermo-mechanical model is presented to study the pressure exerted on the soil skeleton by the freezing water. Focusing on a water volume, the temperature trend and pressure exerted in freezing conditions are studied experimentally and with coupled numerical simulations. As a proof a concept, it has been founded a correlation between the pressure exerted at pore-size dimension and the pressure exerted by the soil registered with the experimental test.

A innovative laboratory experiment has been designed and built in all its component to register temperature and pressure data in freezing sample of soil and water. Considering a

water sample of 5 cm of diameter and 2,5 cm of height, a pressure of 10151.91 kPa (20000 N) has been registered. This is not the maximum force that can be exerted by the water because the test was stopped since the chosen load sensor can support a maximum force of 20000 N. From the soils sample test the maximum pressure registered is of 130.43 kPa (corresponding to a force of 255 N). The experimental results follow the theory: in soils the freezing temperature is below 0 C, reaching a value of -4 C in some experiments.

The temperature trend in a soil probe has been simulated solving the energy equations for soils, using the software COMSOL. The model manage to simulate with a certain precision the experimental results. The comparison has been done looking at the temperature trend registered and simulated in a point.

A coupled thermo-mechanical model has been utilized to simulate the pressure exerted by water in freezing condition. The comparison with the experimental results shows that , under specific boundary conditions, the model is able to reproduce the pressure trend. The last comparison with the experimental results has been done considering the pressure exerted by freezing soils. It has been considered the force exerted by a volume of water of the same dimension of the water volume presents on the soil sample (so considering the sample porosity). Comparing this estimated values of soil force with the experimental values, it can be seen that they are comparable and of the same order of magnitude. So, with further studies, this can be a way of proceeding to evaluated the pressure exerted on solid skeleton, taking into account of ice pressure.

Looking at the future applications of the entire project, the laboratory experiment set-up can be easily modified to do a huge range of studies such as considering different type of soils in different conditions. For instance, it can be added a liquid water reserve to take into account of the cryostatic suction.

The numerical modeling it is at a first stage for soils, but can be implemented to solve also the hydrological part of the phenomena. The energy equations gives as an output

the temperature and change of mass parameter for each time. These two unknowns of the general system can be inserted into the mass conservation equation and Clapeyron equation. Moreover, further researches on the proposed mechanical model can lead to the evaluation of another unknown of the system: the pressure exerted on the solid skeleton.

The study in every aspects (mathematical, experimental and numerical) has a huge potentiality to reach a better understand of freezing soils phenomena and it set the basis for an exhaustive and complete model which can represents a possible way of resolution of this complex problem.

Sintesi del lavoro

Lo scopo della tesi é lo studio della dinamica dell'acqua nei suoli in condizioni di congelamento. La formazione di ghiaccio nel sottosuolo puó causare il movimento verso l'alto della superficie del suolo. Questo processo é chiamato "Frost Heave", o criosollevamento, ed é causa di notevoli problematiche ingegneristiche, ad esempio danni alle strade, alle condotte e alle infrastrutture.

L' analisi della letteratura evidenzia la complessitá di questo processo che consiste in un problema termo-idro-meccanico. Il sistema di equazioni che governano questo fenomeno é molto complesso sia per il numero di equazioni che per la non linearitá delle equazioni stesse.

Molti autori, durante gli anni, hanno proposto diversi approcci per descrivere matematicamente il problema. Lo studio approfondito della letteratura suggerisce una classificazione dei diversi modelli in due gruppi.

Da una parte, abbiamo i modelli che studiano il suolo in condizioni sature. Questi modelli risultano molto specifici, analizzando nel dettaglio il fenomeno del criosollevamento, creazione delle lenti e "cryostatic suction". In questi modelli il terreno é suddiviso in diversi strati (al di sotto, e sopra la lente di ghiaccio) e ognuno di questi livelli presenta diverse equazioni e ipotesi che lo governano. I modelli comprendono uno studio meccanico ma le equazioni non sono spesso scritte seguendo una trattazione matematica rigorosa. Un'altra criticitá é collegata alla pressione esercitata sullo scheletro solido, a livello di dimensione

del pori, che é spesso calcolata con una formulazione empirica. Inoltre,non tiene conto della forza risultante dall'espansione termica durante il cambio di fase.

D'altra parte, i modelli che studiano terreni insaturi, considerano totalmente trascurabile il processo del criosollevamento. Infatti, vi é la mancanza di un modello meccanico, e le forze generate in condizioni di congelamento non sono analizzate. Un'altra approssimazione comune riguarda la pressione relativa del ghiaccio, che é considerata uguale a zero. In altre parole, la pressione esercitata dal ghiaccio in condizioni di congelamento viene considerata trascurabile.

Sulla base dello studio dello Stato dell'Arte, la prima fase di questo lavoro di tesi riguarda uno studio matematico di un sistema di equazioni che puó essere applicato sia per i suoli saturi che insaturi e che tiene in considerazione il fenomeno del cambiamento di fase. Sono state studiate e scritte le principali equazioni che governano il processo, in modo tale da considerare la pressione esercitata dal ghiaccio e la "criostatic sunction" .

La complessitá del sistema matematico implica la necessitá di studi piú elaborati e avanzati strumenti numerico e computazionali per la sua completa risoluzione. Per questa ragione, la parte sperimentale e la parte numerica di questo lavoro si concentrano sulla risoluzione di un caso semplificato. In particolare,considerando condizioni sature, l'equazione di energia é risolta sia per i suoli che per l'acqua.

Inoltre, considerando lo studio a livello della dimensione dei pori, viene presentato un modello termo-meccanico per studiare la pressione esercitata sullo scheletro del suolo dall'acqua in fase di congelamento. Considerando un volume d'acqua, sono state studiate sperimentalmente e con un modello termo-meccanico, sia l'andamento della temperatura che la pressione esercitata in condizioni di congelamento. L'obiettivo di questo modello é la simulazione della pressione esercitata dal ghiaccio in fase di congelamento a dimensione di poro. Inoltre, come primo passo per uno studio piú approfondito, é stata trovata una correlazione tra i valori di pressione a scala di poro e i valori di pressione esercitati dal

terreno ottenuti sperimentalmente.

Per effettuare le prove sperimentali, e'stato progettato e costruito un esperimento di laboratorio innovativo, per registrare i dati di temperatura e pressione in campione di acqua e suolo in condizioni di congelamento. Considerando un campione d'acqua di 5 cm di diametro e 2.5 cm di altezza, é stata registrata una pressione di 10151,91 kPa (20000 N). Questa non é la forza massima che puó essere esercitata dal provino poiché il test é stato interrotto, in quanto la cella di carico scelta poteva supportare una forza massima di 20000 N. Dall'esame del campione di suolo la massima pressione registrata é di 130,43 kPa (corrispondente a una forza di 255 N). I risultati sperimentali seguono la teoria: nel suolo la temperatura di congelamento é inferiore a 0C, in particolare, in alcuni esperimenti, raggiunge un valore di -4 C.

Un modello termo-meccanico é stato utilizzato per simulare le pressioni esercitate dall'acqua in condizioni di congelamento. Dal confronto con i risultati sperimentali si evince che il modello é in grado di simulare l'andamento delle pressioni dell'acqua, considerando oppurtune condizioni al contorno. Inoltre, é stata valutata la forza esercitata da un volume d'acqua di grandezza pari al volume d'acqua presente nei pori del terreno (quindi considerando la porositá). Confrontando questi valori di forza con le forze esercitate dal terreno misurate sperimentalmente, si puó vedere che esiste una correlazione. I valori trovati sono confrontabili e dello stesso ordine di grandezza. Alla luce di questi risultati, piú approfonditi studi su questa relazione, possono portare alla valutazione delle pressioni esercitate sul terreno.

L'equazione di conservazione dell'energia é stata risolta anche per il suolo, per fare un confronto tra l'andamento della temperatura simulato con i risultati sperimentali. Confrontando le due curve, si puó vedere che la simulazione ha la stessa tendenza dei dati sperimentali.

Analizzando le applicazioni future dell 'intero progetto, il set up dell'esperimento

di laboratorio puó essere adottato per fare una vasta gamma di studi, ad esempio: la considerazione di diversi tipi di terreno in condizioni diverse. Inoltre il sistema puó essere facilmente modificato per tener conto della "criostatic sunction", aggiungendo una riserva idrica liquida. La modellazione numerica é ad uno stadio iniziale per quanto riguarda i suoli, ma puó essere implementata per risolvere anche la parte idrologica del fenomeno.I risultati della simulazione bidimensionale dell'equazione dell'energia nel terreno, danno come risultato il valore di temperatura in ogni punto del suolo e in ogni momento. Inoltre fornisce come risultati la variazione del contenuto di acqua dovuta al congelamento, in tal modo si conosce la massa d'acqua e la massa di ghiaccio presenti in ogni istante.

L'equazione di energia fornisce come uscita la temperatura e il cambio del parametro di massa per ogni istante. Queste due incognite del sistema generale possono essere inserite nell' equazione di conservazione della massa e nell'equazione di Clapeyron. Inoltre, con successivi studi sul modello meccanico proposto, si puó arrivare alla valutazione di un'altra incognita del problema: la pressione esercitata sullo scheletro solido. Lo studio svolto in questa tesi, in tutti gli aspetti (matematico, sperimentale e numerico), presenta una grande potenzialitá per raggiungere una migliore comprensione del fenomeno di congelamento del suolo e fonda la base per un modello esaustivo e completo che puó essere una chiave di risoluzione di questo complesso problema.

List of Figures

Contents

Chapter 1

Problem Statement and thesis organization

The physics of multiphase flow in porous media in variably saturated conditions is an argument largely discussed into the years. The cycle of freezing-thawing of the water in porous media is a complex process which combines hydrological, geotecnical and thermodynamical aspects. The seasonal formation of ice in the underlying soils can cause the upward movement of the ground surface (frost heave) which is the responsible of damage to road, pipelines and infrastructure. To this reason during the years much attention has been focused on this problem.

The aim of this work is to analyze and investigate the dynamics of water in soils under freezing conditions by the mathematical, laboratory and computational point of view.

In the first chapter the physics of heaving due to frozen soils is described, underlining the importance of the researches focused on this process. The global warming and the increasing average temperature is getting larger the thickness of the soil which is seasonally subjected to cycles of thawing and freezing. This causes not only ecological but also engineering grave consequences, creating unstable ground susceptible to soil creep and

severe frost heaving. The researches done in this field, make clear the complexity under this process. The frost heave is not only caused by the water volume expansion induced by the phase change, but it is also caused by the creation of i ice lenses parallel to the land surface. The difference between ice and water pressure, namely cryostatic suction, has a fundamental role on the increasing of the lenses thickness and so on the final greatness of soil heaving.

In the second chapter, the State of Art is analyzed. In literature there are lot of models which describe the freezing soils in saturated and unsaturated conditions. The general problem is governed by a system of various equations: the mass conservation equation and the energy conservation are the main governing equation. The complexity of the resolution of this problem lies on the highly non-linearity of the equations, most of all of the energy conservation equation. There are different parameters which depends on both pressure and saturation of the two phases (water and ice) and moreover the phase change has to be considered. Although the models are based on the same main governing equations, every author write the final system in different ways and following different assumptions.
Moreover, the models which treat the saturated conditions and the ones which treat unsaturated conditions are very different. In the first case, the models are very specific analyzing the creation of lenses and frost heave process. The model which study the unsaturated conditions, however, do not consider the frost heave process and also all the mechanical aspects are not examined.

The study of State of Art puts in light the various and different way of writing of the main governing equations and the different assumptions under them. For this reason, the second part of this work, described in the fourth chapter, is focused on the study of a system of equations which can combines the various phenomena presented both in saturated and unsaturated models. The model is written with the aim to maintain the scientific accuracy on the mathematical equations form and also to include the physical

process which are relevant to describe the frost heave process.
At this stage, the system of equations has to be considered as a study of the governing equations based on the State of Art analysis. This step has been useful to have a deeper comprehension of the complexity of the phenomena and of the various processes involved. The aim of this system of equation is to put the the basis for the formulation of a unique system of equations which takes into account the frost heave process also in unsaturated conditions and considering also a deformable volume.

The analysis of State of Art system and the writing of a system of equations has been a deep analysis of the physical law which governs the phenomena and the mathematical equations utilized to model it. By the literature models, some points still unknown and insidious can be under light. First of all, there is not a mechanical model which takes into consideration the volume expansion of water in the pore. In most of the saturated soil model the cryostatic suction $(p_w - p_i)$ is calculated using the Van Genuchten equation under the freezing= drying assumption. This assumption states that the freezing process can be considered equal to the drying process, and so the pressure of ice can be considered as the pressure of air, using the Van Genuchten equation. This assumption is surely a good way to find a solution of a very complex system, but it is a strong approximation of the real value of ice pressure. The unsaturated soils model, however, did not consider at all the cryostatic suction and frost heave process and there is always a lack of a mechanical model. Moreover, the pressure on solid skeleton, indicates as p_s, which describes the ice stress state is calculated with empirical parameter.

Facing a very complex problem and in base of the critical issue and approximations of the resolving systems; this study focused on the pressure exerted by water freezing at the pore dimension. The aim is to model the pressure exerted on the pore skeleton by the freezing water, with a coupled model which consider the temperature and mechanical aspects. Starting from the physics of water expansion studied with laboratory experiment

the objective is to describe the mechanical action of ice on the soils. Water and soil sample have been utilized to measure experimentally pressure and temperature trend. Then, at a first stage, only the water volume is modeled with a software of numerical simulation (COMSOL) to modeling the temperature and pressure data at pore-dimension. The results of the numerical simulations has been compared with the experimental results. As second step, the temperature equation has been solved also for soils.

In the third chapter the laboratory experiments are presented. A whole experiment set-up has been built to measure the force exerted by freezing samples. The laboratory plant is composed by a rigid structure specifically built for the experiment,a load sensor, an mould and temperature's sensors. Two electrical circuits have been built to collect the data of both sensors. Various test has been done using water and soil sample. The general procedure consists on consolidate the sample (in case of soil sample) inside the mould, then this is placed in contact with the load sensor (which is rigidly connected to the steel structure) and everything is putted inside the fridge. The data registered are the force exerted by the sample during freezing and the temperature trend in a point of the domain.

In the fifth chapter the computational simulations are presented. The COMSOL software is utilized to simulate the temperature and pressure trend focusing at the pore size, and so considering an only-water sample. The energy conservation equation is modeled, taking into account of the phase change. The trend of temperature in a point of the domain, follows what has been founded in the experimental part. Moreover, a simulation of the force behavior has been presented using the mechanical study, a section between the COMSOL physics. In the simulation, the sample is considered as a solid and the expansion is governed by the thermal expansion coefficient. The results has the same order of magnitude of the pressure registered in the experimental part.

In this study, it is presented a laboratory experiment which put in light the relation between pressure and temperature in freezing soils. Moreover, a computer simulation

of the energetic and mechanical aspects focused on the pore size dimension is presented. The analysis of the literature, the laboratory experiments and the thermo-mechanical simulation at pore size dimensions are the basis for a future more complex model which can simulate the frost heave process in the soil taking also into account of the mechanical features.

Chapter 2

Freezing soils

2.1 Permafrost

Permafrost, or perennially cryotic ground, refers to ground (i.e., soil and rock) that remains at or below 0°C for at least two years [1]. It can be found in about a fifth of the land surface of the Earth, covering 23 million km^2. Over half of Canada and Russia, most of Alaska, and north-east China are covered by continental permafrost. In Europe, alpine permafrost is found at high elevations in middle and low latitudes and some permafrost is found in Scandinavia [2] [1] (fig.2.1).

The spatial extent and thickness of permafrost generally changes with climate and depends on many factor that regulate heat fluxes and consequently soil temperature. Some of these factors are geographic position and exposure, precipitation,vegetation and properties of the earth materials under the ground surface [4]. The variability of perennially frozen ground's characteristics permits to define different type of permafrost.

Continuous permafrost includes the areas at high latitude where 90% of the ground is underlain by permafrost that reach few hundred meters deep. *Discontinuous permafrost*, of few ten meters depth, can be found in warmer regions where the temperature over 0°C

more frequently.[2] Where the mean annual surface temperature reach 0°C, the thickness of the permafrost can reach few meter and in areas of enhanced solar radiation, it can even disappear. In this case it is called "sporadic permafrost".

Figure 2.1: Permafrost extent in the Northern Hemisphere- Souce: UNEP

Analyzing the soil structure, permafrost terrains are characterized by different layers, the upper is controlled by seasonal heat exchange with atmosphere and the lower by geothermal flux.

Permafrost is separated from the atmosphere by a boundary layer consisting of the active layer (fig.2.2). The active layer is subjected to cycles of thawing and freezing following the seasonal change of climate. This layer is the support for plant and animal communities. It transmits heat to and from permafrost, is the medium through which

moisture and gases are exchanged between the permafrost and the atmosphere, and provides water and nutrients for biological processes [2].

Below the active layer, the upper portion of permafrost is governed by convective and conductive heat flux and is known as the permafrost table. The bottom depth of permafrost (permafrost base) is limited by the geothermal gradient and mean annual surface temperature [3].

Inside the ice-rich permafrost stratum, unfrozen ground can be found (talik). They are often positioned beneath rivers and lakes.

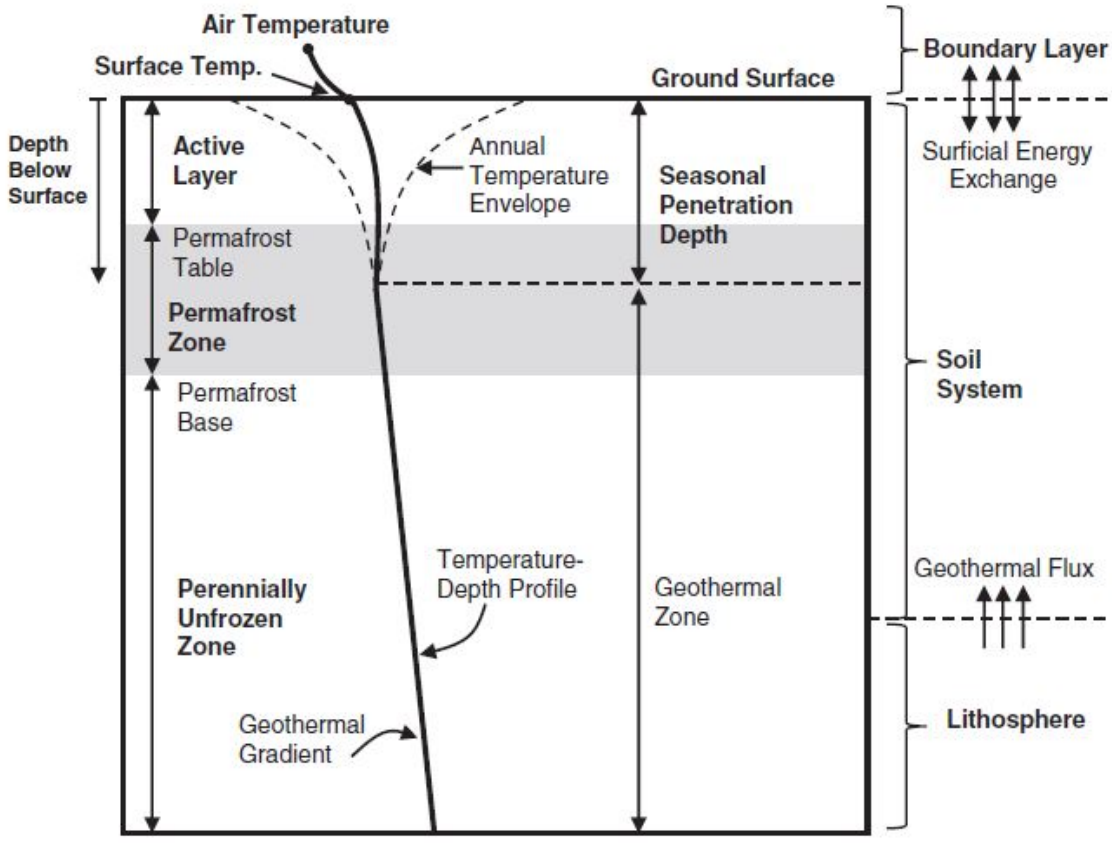

Figure 2.2: Soil structure based on atmosphere temperature and thermal flux [1].

2.1.1 Impacts of Global Warming

The climate change that is occurring in the last decades is producing hydrologic and ecologic changes most of all at high latitudes. According to NASA "the 10 warmest years in the 136-year record all have occurred since 2000, with the exception of 1998. The year 2016 ranks as the warmest on record" [16].

The consequences of global warming are the decreasing sea ice, permafrost warming or degradation, increased carbon dioxide release from soils, decreased glacier ice mass and shifting biological indicators. [3]

Figure 2.3: Sinking house. Effects of non-thaw stable permafrost on heated foundations in the in hills surrounding Fairbanks

Focusing on the permafrost zone the increasing of surface temperature has both ecological and engineering consequences. Long-term measurements of active layer thicknesses in different regions show an increasing trend connected to surface temperature anomalies.

Monitoring of the active layer was developed at a global scale in the 1990s and currently incorporates more than 125 sites in the Arctic, the Antarctic and several mid-latitude mountain ranges. The worldwide warming surface temperature induces the base permafrost to thaw causing an increase of the active layer's thickness and a reduction of permafrost

aerial extent.

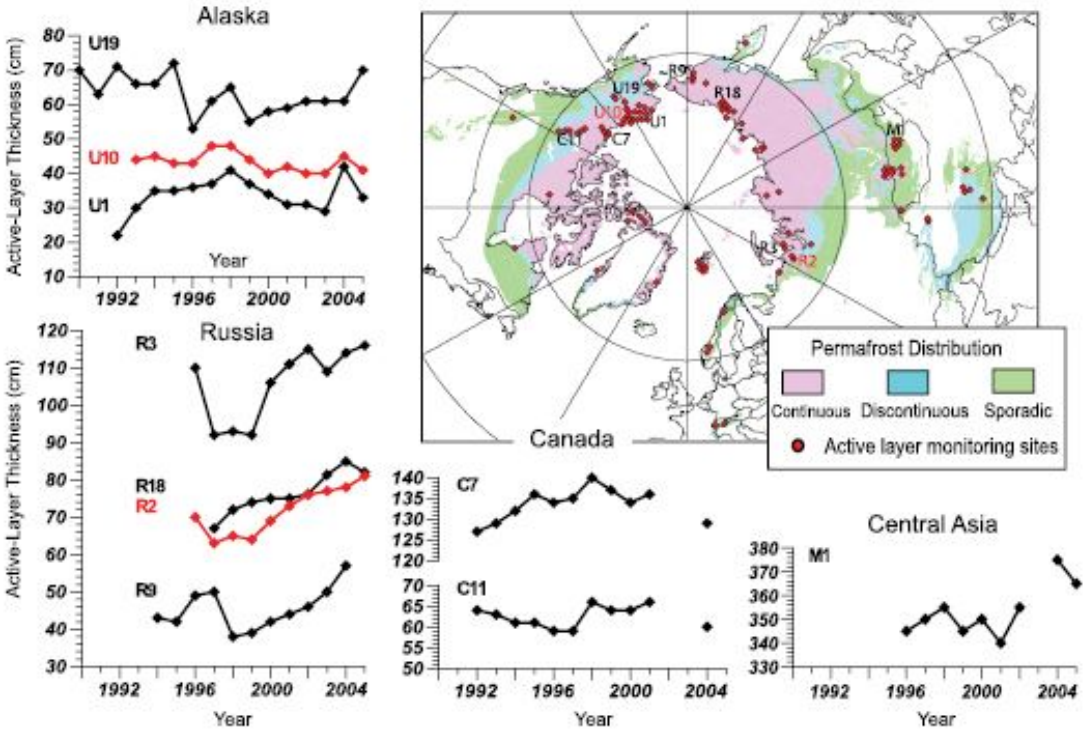

Figure 2.4: Locations of sites and changes in active layer thickness from selected sites (after Nelson, 2004a,b)

Thawing of the permafrost layer generate landslides, coastal erosion and many engineering damage to construction and infrastructures built on frozen ground. The consequences are unstable ground susceptible to soil creep and landform, slumping and severe frost heaving.

2.2 Frost Heave

Frost heave is a physical process involving the cyclic freezing and thawing of water in soil or rock. Heave in this context refers to the upward movement of the ground surface that occurs in response to the seasonal formation of ice in the underlying soil. During the years much attention has been focused on this problem because of its importance in the construction and maintenance of roads, railroads and oil industry pipelines. Every year frost action destroys public and private property for billions of dollars generating various problem to construction as pavements, railways and building foundations (see fig.2.5) [10].

Region	Cost of damage/year	Reference
USA	$13 billion	Puppala and Cerato (2009)
UK	£400 million	Driscoll and Crilly (2000)
France	€3-3 billion	Johnson (1973)
Saudi Arabia	$300 million	Ruwaih (1987)
China	¥100 million	Ng *et al.* (2003)
Victoria, Australia	$150 million	Osman *et al.* (2005)

Figure 2.5: Annual cost of damage to structures constructed on heaving expansive soils for several regions.

Experimental researches reveal the complicate mechanism which is beyond the phenomena of Frost Heave. The uplift of the ground can not be explained only by the increasing of volume of water during freezing but by more complex mechanisms which govern the phenomena. This results in an open issue that is still object of intense research.

Figure 2.6: Frost heave on this Bismarck street has lifted parts of the road surface about 46cm.

Figure 2.7: Heavy damage to a road in Duluth, Minnesota June 2014

2.2.1 Physical process of Frost Heave

Experimental observations suggest that frost heave is caused by the formation of ice lenses into the ground.

Ice lenses are made of pure ice and grow with their long axis parallel to ground surface creating a series of lens separated vertically by a layer of frozen soils (fig.2.8). The thickness of the lenses vary from microscopic dimension to several decimeter.

In the soils the heat flux is direct by the internal part of the planet to the surface. The process of freezing occurs from the surface down, parallel to the the surface and perpendicular to the direction of heat, creating a geothermal gradient.

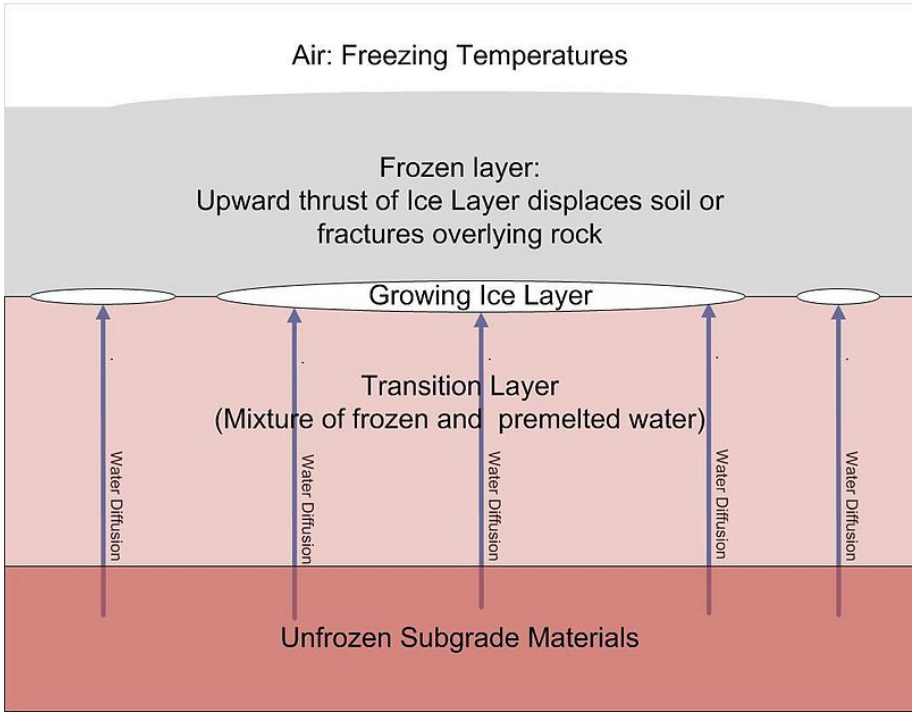

Figure 2.8: Ice lens formation resulting in frost heave.

The formation of the lenses and the mechanisms of heave are governed by two important features regarding pore pressure.

Disjoining Pressure and Regelation The growth of a lense is governed by a thermodynamic process: the creation of a nanometer-thick premelted film that separate the surface of ice and soil grain.

As water into the soil pores solidify into ice, a film of water remains unfrozen at temperature below the freezing temperature (fig.2.9). This thin film of liquid separates the soil particles and the solid ice, creates a liquid pressure gradient causing the migration of water toward the film and the accumulation of ice in the upper part.[8]

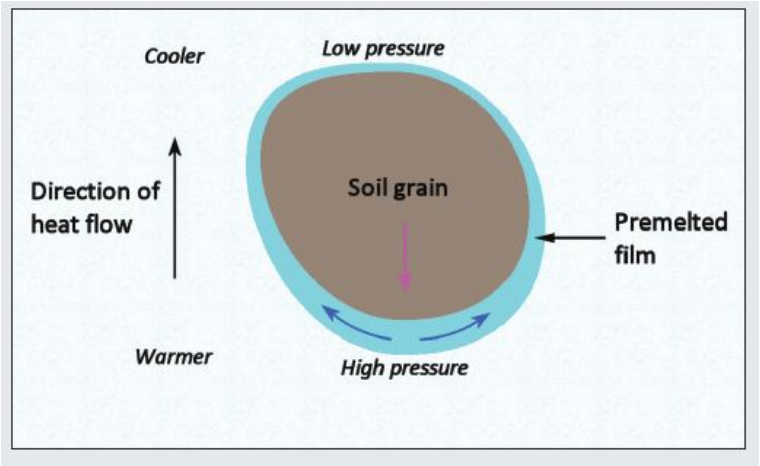

Figure 2.9: Segregation of soil and ice by regelation.

The liquid film is thicker on the warmer side (the lower) and this difference of thickness between the two side generate a change of pressure, called disjoining pressure. This pressure gradient is in the opposite direction to thermal gradient and causes the migration of water from the downside to the upper side. The water accumulate and refreeze forcing the soil particle to move downward with a certain velocity.

The existence of a disjoining pressure is essential in order that soil particles are forced apart allowing ice lenses to form. The magnitude of the disjoining pressure does not affect the amount of heave but it is important to the film thickness.[6]

Cryostatic suction Mizoguchi in 1990 performed freezing experiments on sandy loam samples. The experiment consists on freezing from the top of the samples and measuring after 12,24,50 hours the total water content at the various depth. The results of this experiment shows that the total water content (liquid plus ice) increase in the upper part of the cylinder as the sample freezing (fig.2.10).

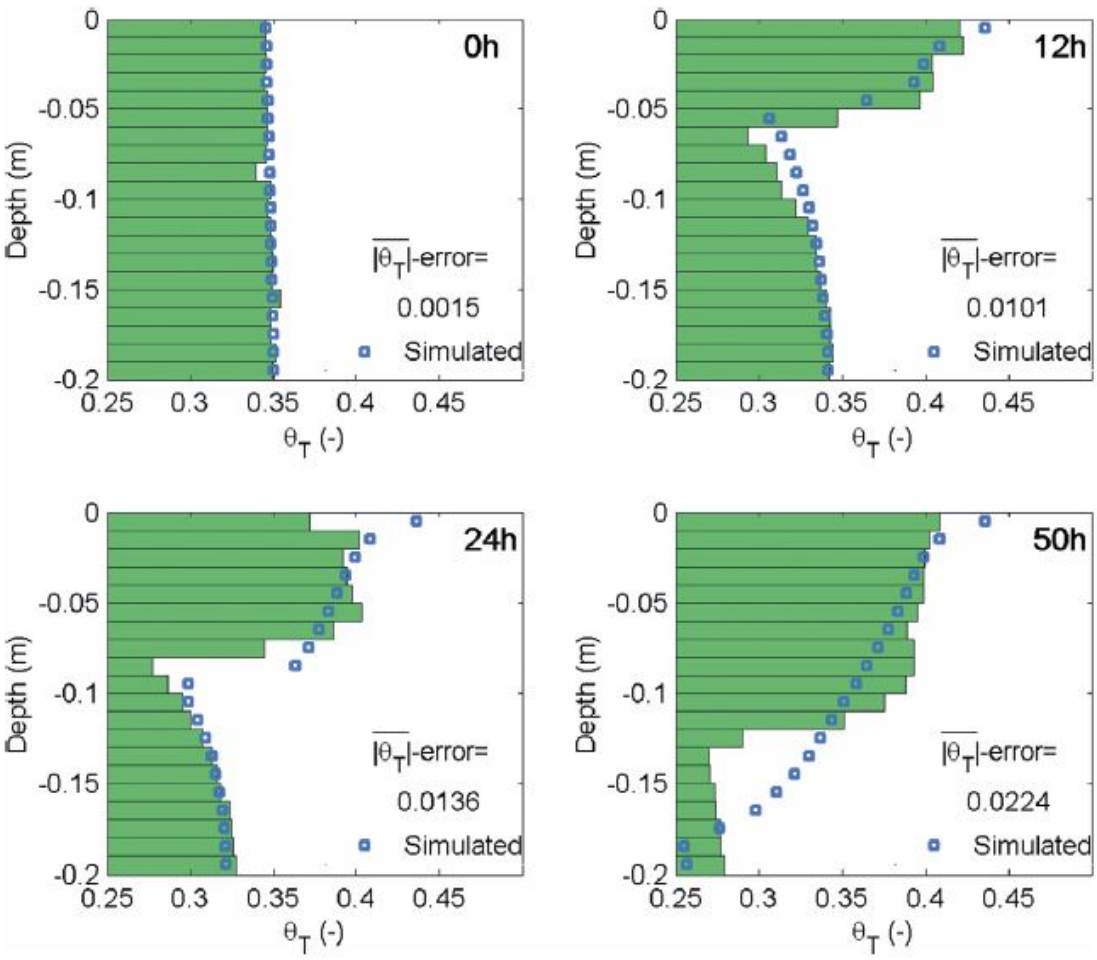

Figure 2.10: Simulated and measured values of Hansson's model of the total volumetric water content 0, 12, 24, and 50 h after freezing started.[10]

This physical behavior can be explained as a flux of water toward the freezing front in which it refreeze. It is caused by a pressure gradient in the pore water, called cryostatic suction. This excess of water flux is the fundamental responsible of heaving.

2.2.2 Creation and growth of Ice lenses

A good comprehension of the physic governing the creation of pure-ice lenses is necessary to understand the models and the equations used to describe the frost heave process. The development of ice lenses depends on two different direction of freezing and of unfrozen water.

1. The soil freeze from the ground surface to the inner part of the soil, namely, *frost front* is directed downward (white arrows in 2.11).

2. The flow of unfrozen water, due to the mechanisms previously described, is directed upwards (blue arrow in fig.2.11).

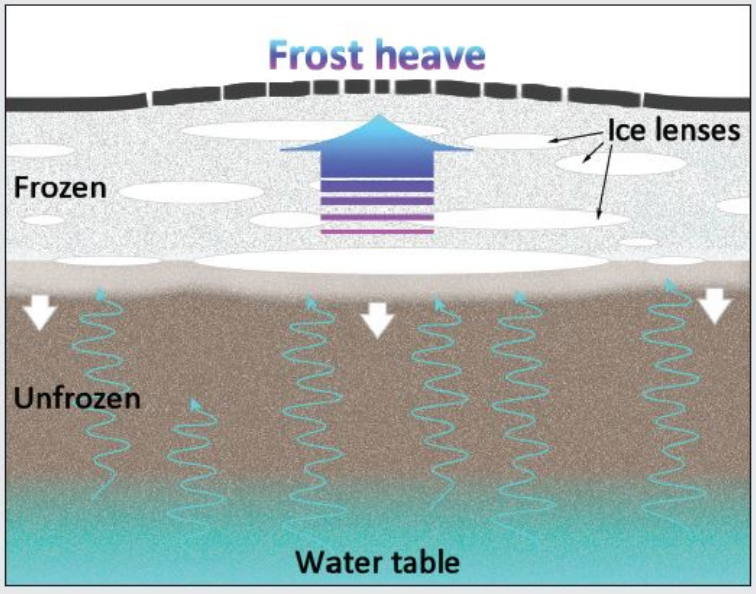

Figure 2.11: Formation of ice lenses in frozen ground below pavement [5].

The slightly layer between frozen and frozen zone (fig. 2.11) represents the *frozen fringe*. It is a zone in which water and ice coexist, is a partially frozen zone between the warmers side of the lens and the freezing front below [7].

"Within this region, unfrozen water is being drawn up by cryostatic suction" [11] so in the frozen fringe cryostatic suction forces are produced [5].

The cryostatic suction is the responsable of the generation of a continuous water flux from the water table (in the lower zone of soil).

This additional water flows through the unfrozen film surrounding grain particles, refreezes and causes the accretion of the lens, this phenomena is called as "regelation" [7]. The entire process is sustained by the continuous supply of liquid water from below the frozen fringe.

Even though the temperature is a few degrees below freezing conditions in the frozen fringe there is still liquid water in equilibrium with ice. This is caused by the Gibbs-Thomson effect and analytically means that another equation is needed to calculate the temperature of freezing, the *Clapeyron Equation*.

The freezing of water and thawing of ice in soils occurs over a range of "freezing points" that can be calculated with the Clapeyron equation and change as the unfrozen water content increase or decrease [12].

Chapter 3

State of Art

The dynamics of water in saturated and variably saturated soils subjected to freezing-thawing cyles are becoming increasingly important in civil engineering, soil science and environmental engineering. An in-depth review of the literature reveals indeed that different models have been formulated since the 70s.

This process is generally described by a system of mass conservation equations for each phase and an energy equation. In the case of unsaturated soil the mass conservation equation is the well-known Richard's equation [15]. Due to the Thomson-Gibb's effect the water in porous media do not freeze at 0°C, so the Clapeyron equation is needed to calculate the depression of freezing temperature.

Although these are the main governing equations of this process, in the literature different way to write them can be found. Moreover, every author made different assumptions: most of the models do not consider a deformable volume or do not take into consideration the changes to water volume and density due to freezing (see the next sections for details).

In conclusion, there are several models based on different hypotheses and assumptions and different way to express the same main governing equations. Accordingly, we have noticed a lack of a general and unique system of equations. This chapter will present

the differences between the existing models and will introduce the main motivations and objectives of the thesis in light of the literature on this topic.

3.1 Saturated, rigid volume models

Miller and O'Brian 1985

Miller and O'Brian put the basis for a frost heave model considering saturated, solute-free, air-free soils. They propose the differentiation between different way of heaving. The *Primary heave* is intended as a layer of ice growing on the top of some unfrozen soil, through which water is drawn to join the ice. In this case no ice penetrates the remaining frozen soil. Alternatively, speaking of *Secondary heave*, the ice penetrate the soil and the liquid flow towards the ice feeds an accumulation of ice in the frozen soil causing a discontinuous forces movements. This secondary mode of heave is the one in which the greatest load are lifted and causes the greatest engineering problems.

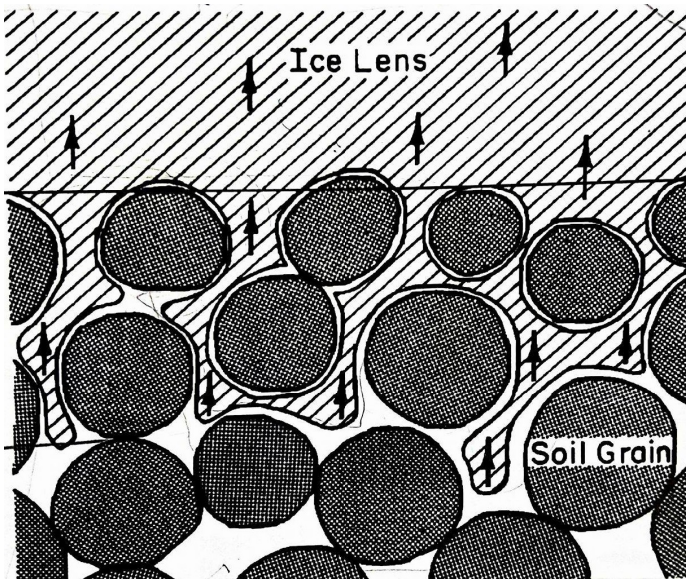

Figure 3.1: Schematic diagram of the frozen fringe, with the lense above [7].

The physical process of segregated ice lenses growth within the soil is analyzed and

different assumptions based on that are proposed. These hypotheses have made Miller's works a milestone in saturated freezing soil model literature. Indeed, several recent models still base on Miller's assumptions.

- **"Rigid ice approximation"**. During freezing all new ice continuously formed on preexisting ice creating a continuous and unique mass. Ice migrates through the grain due to regelation and moves as a solid body with a spatially uniform velocity (fig.3.1). They assumes that "soil ice tends to form on preexisting ice and thus grow through the pore system to form one solid body" [7].

- **"Freezing and drying equivalence"**. This correlation means that the mechanism of freezing can be studied as the mechanism of drying. When only water and air are present around a soil particle (that is, no ice is present), water experiences a stronger attraction to soil than air. This implies that a grain immersed in water will be surrounded by a microscopic "hydrostatic" pressure field. This adsorbed film of mobile water which sorrounds the particles depends upon the difference between water and air pressure outside a certain range of the adsorption force [7]. It the temperatures are not too far below 0°C the mechanical concepts of adsorption space and capillary space enters in the displacement of ice and water. So ice behaves like air and ice pressure can be considered equal to air pressure. In the practice it enables to exploit the theory of unsaturated soil and to calculate the unfrozen water content (W) as a function of the difference between ice pressure and water pressure (ϕ_{iw}).

$$W = W(p_i - p_w) = W(\phi_{iw}) \tag{3.1}$$

Note that, in reality, ice pressure varies the reality vary in space and in time depending on transient conditions.

The dynamics of frozen soils have been modeled considering a rigid system, so negleting compressibility, in the unknowns: temperature and water pressure.

Fowler and Krantz 1994

Fowler and Krantz studied formation of ice lenses and developed a model on the base of Miller's previous studies. The aim of this model is to overcome some of the draw-back of Miller's model as the numerical difficulties and the general complexity.

This model defines three domain in the freezing soil: frozen fringe,within this region unfrozen water is drawn up by cryostatic suction, the region above the frozen fringe (ice lenses region) and region below the frozen fringe in which there is soil satured of unfrozen water (fig.3.2).

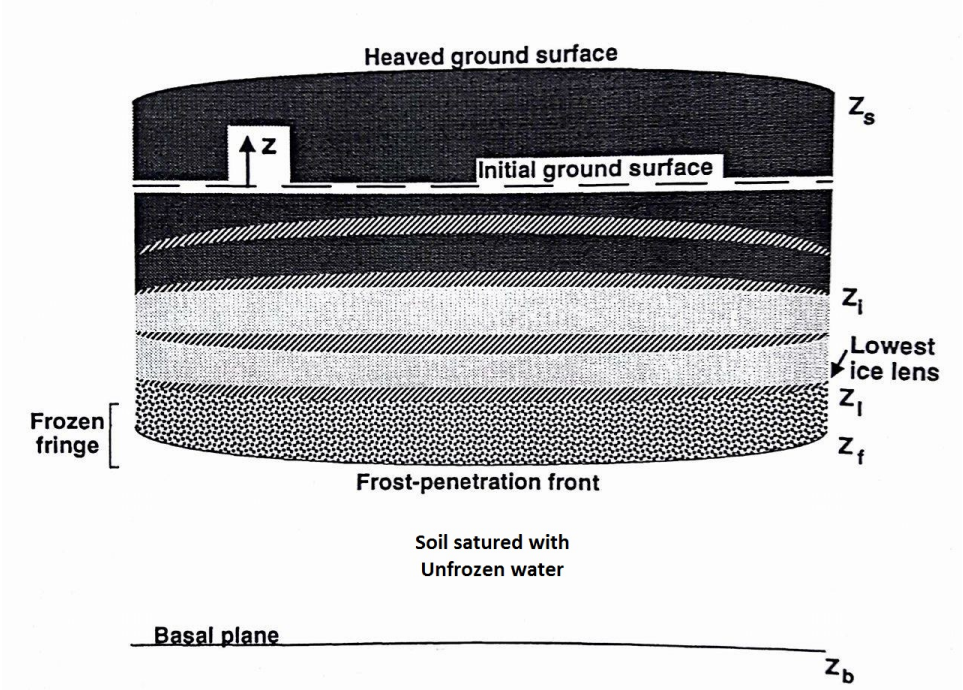

Figure 3.2: Cross section of soil: the heaved ground surface is defined by z_s. The frost penetration depth (z_f) divide the zone beside that which is assumed saturated with unfrozen water and the zone above it which is the frozen fringe [6].

In the frozen fringe unfrozen water and ice coexist so the ice and water mass conservation

and the energy conservation equations are given for that zone. Moreover, the Clapeyron equation is utilized taking into account" the effect both of pore pressure and capillary suction on the freezing temperature"[6].

$$T = T_0\{1 + \frac{p_w}{\rho_w L} - \frac{p_i}{\rho^i L}\} \tag{3.2}$$

The Clapeyron equation in this form considers different density for water and ice. Also, ice pressure is different from that of air.

This model considers "differential frost heave" which means a nonuniform and random heaving [6]. In this model the Miller "rigid ice approximation" is relaxed and the ice velocity depends on space.

In the region above the frozen fringe water permeation is not possible due to the impermeable ice lenses. Besides, in the region under the frozen fringe no freezing occurs; however both energy transport and water permeation occurs.

A criterion for the formation of a new lens is given: in order for ice lens to form discretely rather than continuously the effective (absolute) pressure exerted by the soil particles must be greater or equal to zero [6].

Moreover, their model follows the Miller's assumption based on the analogy with drying-wetting processes of unsaturated soil. In practice, one can write the capillary suction as a function of the local volumetric water fraction (W) within the frozen fringe. The capillary suction is defined as the difference between ice and water pressure.

$$p_i - p_w = f(W) \tag{3.3}$$

These curves depend on pressure at liquid-ice interface and are found experimentally for each type of soils.

Daichao Sheng and Knutsson 1995

Sheng and Knutsson developed a model to have a better computational behaviour and a better agreement between model and experiment. Modifications are provided in the expression of heat and mass equation and of neutral stress. A mathematical model for ice lenses formation and frost heave is presented, in saturated and salt-free soil. Also in this model a separation of depth zones is indicated: differentiating the processes which occur in the frozen fringe from that in the unfrozen zone below (fig.3.3).

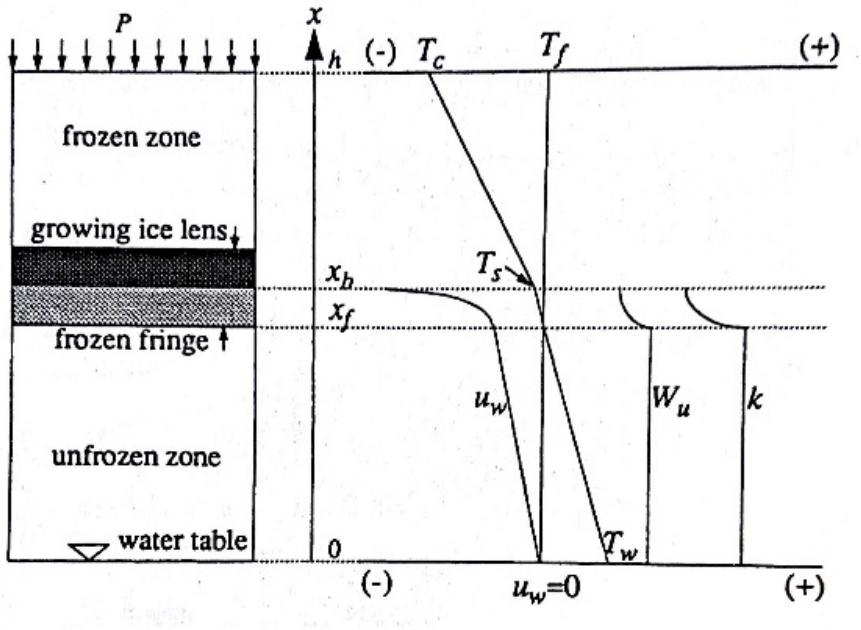

Figure 3.3: Temperature, pore water pressure, permeability and unfrozen water content [9].

Indeed, the model is focused on the *frozen fringe* calculating pore water pressure, ice pressure and water flow in that zone. The permeability of that area is studied and assumed to decrease exponentially.

The flow rate in the frozen fringe is considered constant and the pore water pressure can be integrated from the Darcy law, whereas the ice pressure is calculated using Clapeyron Equation, where T_s is the segregational temperature through the frozen fringe.

$$\frac{u_w}{\rho_w} - \frac{u_i}{\rho_i} \equiv L\frac{T_s}{T} \tag{3.4}$$

A criterion for the formation of a new lens is given related to effective stress value.

This model follows Miller "Rigid ice" hypothesis and includes the ice velocity in the heat balance. The porosity (n) less ice volumetric content (I) is calculated with a formula given by Kujala based on laboratory measurements and not as function of pressure difference of water and ice.

$$n - I = W_0(T) = W_0 e^{\alpha(T)^\beta} \tag{3.5}$$

Where W_0 is the initial volumetric water content and α and β are parameters dependent on soil specific surface area and pore geometry.

They do not use the relation between the volumetric water content and capillary suction proposed by Miller under the hypothesis "freezing=drying".

$$W_u = f(\phi_{iw}) = f(u_i - u_w) \tag{3.6}$$

That choice is justified by the fact that the parameter in the formula are not easy to determine and limited experimental data are available. [9].

This model "takes into account the basic feature of the phenomenon, but which exclude strange parameter" and is thought "to solve pratical problem" [9].

3.2 Variably saturated, rigid system models

Hansson 2004

Hansson studied the variably saturated soil case. This model considers a modified Richards'equation taking into consideration both ice and water phase written in terms of volumetric content and the energy conservation. Following the unsaturated soil theory they calculate the effective saturation with Van Genuchten equations.

Their model is based on the hypothesis that ice gauge pressure, with the reference pressure being atmospheric, is zero and osmotic pressure is zero.

The applicability of this assumption has been often debated. This approximation is justified by the fact that in unsaturated soils the potential of heaving is reduced and so the zero ice pressure is more likely to hold.

This hypothesis implies that the process of frost heaving is not considered because "the ice lenses rapresent situations where the ice gauge pressure is not equal to zero" [10]. Consequently, all the aspects of physic processes at the base of frost heave are not taken into consideration. The mechanical analysis are not considered so there is a lack of pressure relations and the only pressure considered is the pressure head.

The temperature drop is not cited and the Clapeyron equation is utilized in a simplified form:

$$\frac{dP}{dT} = \frac{L_f}{V_w T} \tag{3.7}$$

This equation is then inserted in the apparent volumetric heat capacity to relate capillary pressure and temperature.

The unknowns of the model are the variation of total water content and pressure head in the Richards'equation and ice content and temperature in the heat transport.

This model has been evaluated comparing the predictions with results of laboratory

column freezing experiments. This approach enabled a numerically stable method to solve problem involving simultaneous heat transport and water flow.

Dall' Amico and Rigon 2011

Dall'Amico and Rigon wrote a model which considers saturated and unsaturated case, valid in both condition of freezing and thawing.

The study considers two cases: temperature higher or lower of the melting temperature. In the first case the soil is unfrozen, whereas in the second case is under freezing conditions.

The final system is composed by a mass conservation equation written in terms of total water content (liquid and ice) and a energy conservation equation, written in terms of matric potential. The formulation of liquid pressure head ($\psi(T)$) under freezing condition take into consideration both saturated and unsaturated cases:

$$\begin{cases} \psi(T) = \psi_{w0}(T) + \frac{L_f}{gT^*}(T - T^*) & if\ T < T^* \\ \psi(T) = \psi_{w0}(T) & if\ T \geq T^* \end{cases} \tag{3.8}$$

When $T \geq T^*$, T^* is the melting temperature, the freezing process is not activated and liquid pressure head is equal to ψ_{w0}. In the other case,a simplify Clapeyron equation is inserted to take into account the phase change. The Clapeyron equation utilized,following the "freezing=drying" Miller's assumption, considers ice gauge pressure equal to zero:

$$\rho_w L_f \frac{dT}{T} = p_w \tag{3.9}$$

The model is based on the hypothesis of a rigid soil scheme: the volume is constant and no volume expansion during freezing is allowed. Accordingly, water and ice densities are assumed equal, because otherwise the change of water density during freezing would lead to an expansion of soil which is not considered due to the lack of a mechanical model.

Benes and Krupicka 2015

Benes and Krupicka wrote a model similar to the previous described. It is based on the hypothesis of rigid solid skeleton, the capillary theory is considered valid both for the frozen and unfrozen zone and the gas contribution is considered negligible for heat and mass transport. They consider the two cases of temperature under and over freezing/melting temperature to differentiate the unfrozen and frozen conditions. Water retention curves are utilized to calculate the amount of water present at a certain matric potential of porous media. The Clapeyron equation is utilized, considering ice gauge pressure equal to zero, to calculate the depression of temperature of freezing due to freezing of water in pore.

3.3 Deformable volume

Gray 2008

In the book "Essentials of multiphase Flow and Transport in Porous Media" [14] a system of mass conservation equations is presented which considers a slightly deformable medium. Only compression is considered. The mass conservation equations take into consideration some new terms: fluid compressibility, solid compressibility and matrix compressibility. Considering the solid to respond elastically and isotropically to the pressure, the variation of density of solid due to pressure change is called *solid compressibility*.

$$\beta^s = \frac{1}{\rho^s}\frac{\partial \rho^s}{\partial p^s} \tag{3.10}$$

The compressibility, is positive since the density will increase as the pressure increases [14]. *Rock matrix compressibility* is the fractional change in volume of the solid rock materials (grains) with a unit change in pressure.

$$\alpha^{\beta} = \frac{1}{(1-\varepsilon)\rho^s} \frac{\partial[(1-\varepsilon)\rho^s]}{p^s} \tag{3.11}$$

With the terms of compressibility, the equations take into account of exchange of pressure mechanisms between the solid phase and the other two phases.

The mass conservation equation are derived under the hypothesis that the effects of temperature and chemical composition on the density are negligible and density depends only on pressure. This model can be applied for two immiscible fluids in a solid porous matrix. In this book the change of phase is not considered and the energy conservation equation is not presented.

Schrefler 1987

In the book "The Finite Element Method in the static and dynamic deformation and consolidation of porous media" a similar system of mass conservation equation can be found.

Comparing with the Gray system of equations, also in this system the deformation is taking into account with the compressibility terms. However, this model is based on the hypothesis that solid density depends on pressure exerted by the phase occupying pores, on the temperature and on first invariant of the effective stress.
Consequently, the mass conservation equations are quite similar to Gray's equations but for the terms which take into consideration the variation of density due to temperature and the stress applied.

In addition, in this book the energy conservation equation is inserted and linked to mass conservation equation through the change of mass term.
Koniorczyk, Marcin and Schrefler define also a model in which they utilize this system to study the frost damage for cement based material [19].

The Schrefler system of equations is complete and comprehensive of all the possibly variation in density and pressure, but their complexity make it difficult to manage in a numerical simulation.

3.4 Overview

Two main directions of research emerge from our literature review: on the one hand we have a number of very specific models that analyzed in details the frost heave process and the creation of lenses in saturated conditions; on the other hand we have models that consider unsaturated conditions, but neglect this process.

The most common hypotheses and approximations are:

1. Water density is considered equal to ice density, so the increase in volume during freezing is not considered.

2. It is usually not included a mechanical model which accounts for the exchange of phase pressure and stress field.

3. The volume is considered undeformable, matrix and solid compressibility is neglected and porosity is considered constant in time.

4. Ice pressure is considered equal to zero so that frost heave is not examined.

5. The Clapeyron equation is utilized in different and generally simplified forms.

Many of that assumptions lead to large approximations and cannot consider the real physics of freezing-thawing soil. Moreover,cryosuction and the interaction between soil particle and water are generally ignored.

Another important issue is that models by different authors generally adopt different formulations for the same general equation. Even though this issue is analytical in essence, the lack of a unique, common way to write the main system of equations also makes it difficult to understand the differences between models and ultimately may hamper the definition of a general theory of multiphase flow in porous media.

Chapter 4

Governing equations

The first stage of this work concerns a mathematical study of a system of equations which can be applied both for saturated and unsaturated soils and which take into consideration the change of phase phenomena. It has been considered a slightly deformable porous volume composed by soil particles and water in two phase: liquid and solid. The main governing equations are studied and written such as to consider the ice pressure contribute and the cryostatic suction.

The mass conservation equation for both phase are derived under the hypothesis that the density depends by pressure. In this way the equations take also in consideration the deformability of the pore. The other equations presented in the system derived from the study of literature models taking into consideration the physical and thermodynamic phenomena in freezing porous media.

4.1 Hypothesis

The system of equations is based on the following hypothesis:

1. Soil is modeled as a multi-phase mixture consisting on different α phases: soil particles ($\alpha = s$), liquid water ($\alpha = w$) and ice ($\alpha = i$);
2. The soil is solute-free, chemical salt reaction are not considered.
3. The ice velocity is considered negligible.
4. The mass contribution of air is negligible respect to the other phases;
5. All processes are single valued i.e. hysteresis is not present in the characteristic curves so it is considered only freezing;
6. Only the phases liquid water and ice are considered in local thermodynamic equilibrium;
7. The generalized Clayperon equation is used to calculate the freezing temperature due to pressure change;
8. Effects of temperature and chemical composition on the density are negligible. Density depends only on pressure.;

4.2 Mass Conservation equation

The mass conservation equation is written following the approach utilized by Pinder and Gray in the book "Essentials of multiphase Flow and Transport in Porous Media". Assuming that no solid and water phase is pumped into or from the system and that no chemical reaction occurs we obtain a general form of equations written considering the α phases:

$$\varepsilon\rho^{\alpha}\frac{\partial s^{\alpha}}{\partial t}+s^{\alpha}\rho^{\alpha}\{[\alpha^{\beta}+(1-\varepsilon)\beta^{s}]\frac{\partial p^{s}}{\partial t}+\varepsilon\beta^{\alpha}\frac{\partial p^{\alpha}}{\partial t}\}-\nabla\cdot[\rho^{\alpha}\frac{\mathbf{k}^{s\alpha}}{\mu^{\alpha}}\cdot(\nabla p^{\alpha}-\rho^{\alpha}g)]=e^{\alpha}_{\alpha s}+e^{\alpha}_{wn}. \quad (4.1)$$

$\alpha = w, i, a$

Symbols	Parameters	Units
ρ^{α}	Density of α phase	Kg/m^3
ε	Porosity	-
s^{α}	Saturation of α phase	-
α^{β}	Matrix compressibility	m^2/N
β^{s}	Solid compressibility	m^2/N
β^{α}	Compressibility of alpha phase	m^2/N
p^{s}	Pressure exerted on the solid skeleton	Pa
p^{α}	Pressure exerted by α phase	Pa
$\mathbf{k}^{sw}$	Relative permeability	m^2
μ^{α}	Dynamic viscosity of α phase	Pas
g	Gravitational acceleration constant	m/s^2
e^{α}_{wn}	Mass exchange between phases	$kg/(m^3s)$
$e^{\alpha}_{\alpha s}$	Mass exchange between solid phase and α phase	$kg/(m^3s)$

Taking into consideration that the density of fluids is considered constant and does not vary with temperature and pressure (α^β and β^α can be neglected) and considering that there is not mass exchange between solid phase and fluids ($e^\alpha_{\alpha s} = 0$, adsorbtion is not considered) we obtain the final form:

$$\varepsilon\rho^\alpha\frac{\partial s^\alpha}{\partial t} + s^\alpha\rho^\alpha\alpha^\beta\frac{\partial p^s}{\partial t} - \nabla\cdot[\rho^\alpha\frac{\mathbf{k}^{s\alpha}}{\mu^\alpha}\cdot(\nabla p^\alpha - \rho^\alpha g)] = e^\alpha_{wn}. \tag{4.2}$$

$\alpha = w, i$

4.2.1 Liquid water mass conservation equation ($\alpha = w$)

$$\varepsilon\rho^w\frac{\partial s^w}{\partial t} + s^w\rho^w\alpha^\beta\frac{\partial p^s}{\partial t} - \nabla\cdot[\rho^w\frac{\mathbf{k}^{sw}}{\mu^w}\cdot(\nabla p^w - \rho^w\mathbf{g})] = e^w_{wi}. \tag{4.3}$$

4.2.2 Ice mass conservation equation ($\alpha = i$)

$$\varepsilon\rho^i\frac{\partial s^i}{\partial t} + s^i\rho^i\alpha^\beta\frac{\partial p^s}{\partial t} = e^i_{wi}. \tag{4.4}$$

Permeability

The presence of two phase in pore space decreases the space available for flow for each phase. This fact is taken into account in the permeability term $\mathbf{k}^{sw}$. The apparent intrinsic permeability depends not only on solid property but also on the presence of the other phase.

$\mathbf{k}^{s\alpha} = k^\alpha_{rel}\mathbf{k^s}$

In which $\mathbf{k}^s$ is the intrinsic permeability and k^α_{rel} is called the relative permeability and is a function of s^α that ranges from 0 to 1.

Pressure on solid skeleton

The symbol p^s is used to represent the force per area exerted on the solid by the two fluid. It can be calculated:

$$p^s = \chi p^w + (1 - \chi)p^i \tag{4.5}$$

where χ is called Bishop parameter and is a function of saturation, $0 \leq \chi \leq 1$ [14]. Physically, the Bishop parameter is a measure of the fraction of the solid phase surface in contact with the water phase and $1 - \chi$ the fraction of solid surface in contact with the ice phase. There are different relation to calculate the relation between χ and s^α (see Miller 1970 [7]) it can be simplify using: $s^w = \chi$.

Matrix compressibility

When the matrix is subjected at stress there is a change in volume of pores. If we consider an elastic matrix and the stress exerted on the bulk solid due to the pressure of α phase, the fractional volume occupied by the solid will decrease as the pressure of the fluid increases. So it can be defined the matrix compressibility:

$$\alpha^\beta = \frac{1}{(1-\varepsilon)\rho^s} \frac{\partial[(1-\varepsilon)\rho^s]}{p^s} \tag{4.6}$$

Mass exchange between phases

The term e^α_{wn} indicates the mass exchange between liquid and ice phase due to the change of phase. It will be calculated through the energy equation. Obviously $e^w_{wi} = -e^i_{wi}$, so this term will be indicated from now on as e.

4.3 Energy conservation equation

The energy conservation equation describe the temperature variation due to the conduction and advection phenomena plus the change of phase. The energy content in a volume can be quantified considering the internal energy U [18]. It is defined as

$$U = U_s + U_i + U_w \tag{4.7}$$

where U_s, U_i and U_w are the internal energies of solid, ice and liquid water.

Each of these internal energies can be written with respect to a reference temperature (T_{ref}), in K, see again [18]:

- $U_s = \rho^s c^s (1-\varepsilon)(T - T_{ref})$
- $U_i = \rho^i c^i \varepsilon s^i (T - T_{ref})$
- $U_w = \rho^w \varepsilon s^w \left[L_f + c_w (T - T_{ref})\right]$

where c_s, c_w and c_i are specific thermal capacities for minerals, liquid water and ice (in J/kg/K) and L_f is the latent heat of fusion (in J/kg). It follows that

$$U = C_{eff}\,(T - T_{ref}) + \rho^w L_f \varepsilon s^w \tag{4.8}$$

, with

$(C_p)_{eff} = \rho^s (1-\varepsilon) C_p^s + \rho^w \varepsilon s^w C_p^w + \rho^i \varepsilon s^i C_p^i$

is usually called total (or volumetric) thermal capacity of the soil volume [10, 18]. Henceforth, $T - T_{ref} = T^\star$.

The one-dimensional conservation equation for U reads:

$$\frac{\partial U}{\partial t} + \nabla \cdot (\mathbf{G} + \mathbf{J}) = -L_f e \tag{4.9}$$

And following some mathematics passages (reported in Appendix), the final form of the equation is

$$(\rho C_p)_{eff}\frac{\partial T^*}{\partial t} + (\rho_w C_p^w v^w)\nabla T^* - \nabla \cdot (\lambda_{eff}\nabla T^*) = -L_f e \tag{4.10}$$

Where:

$(\rho C_p)_{eff} = \rho^s(1-\varepsilon)C_p^s + \rho^w \varepsilon s^w C_p^w + \rho^i \varepsilon s^i C_p^i$

$\lambda_{eff} = \lambda^s + \lambda^w + \lambda^i$

$T^* = T - T_{f/m}$

Note that this definition neglects the energy of air and the work involved in the volume expansion from liquid water to ice [18].

Symbols	Parameters	Units
T	Temperature	K
C_p	Effective heat capacity	$J/(kgK)$
λ	Effective thermal conductivity	$W/(mK)$
L_f	Latent heat	J/kg
e	Mass exchange due to phase change	$kg/(m^3 s)$

4.4 Clapeyron equation

The relationship between water and ice in porous medium has been a subject of interest for many years. It is clear that the well-known Clapeyron relation has a evident importance in the knowledge of this argument. An important evidence derived by the study of freezing water in porous media is that the coexistence of water and ice in porous media creates a depression of the freezing temperature. "Evidently the freezing of water, or thawing of ice, in soils actually occurs over a range of freezing poins: that is, the equilibrium freezing point must be changing as the unfrozen water content is decreasing or increasing" [12].

There are different way to express the Clapeyron Equation, which permit to calculate under equilibrium conditions the change in freezing point due to change of pressure and volume. This equation can be written in different way considering pressure of water and ice applied equally to both phase or considering different pressure scenarios.

$$T_{f/m} = T_{ref} exp[\frac{1}{\rho^w L_f}(p^w - \frac{\rho^w}{\rho^i} p^i)] \tag{4.11}$$

4.5 Capillary suction

Considering the equations 4.3, 4.4,4.5 ,4.10,4.11 there are five equations and six unknowns: $s^w, s^i, p^w, p^i, p^s, e$. The system is underdetermined and one more condition is needed to make the problem determined. A relation is needed to put in correlation the pressure difference $p_i - p_w$ with the saturation. This gradient of pressure, namely criostatic suction, has a important rule on the heaving process.

Direct observation showed that the pressure difference between the two phase is related to the curved ice-water interface. Curvature decrease with decreasing temperature. In terms of the Laplace surface tension equation, a decrease in the mean radius of curvature indicates an increase in the pressure difference:

$$u_i - u_w = \frac{2\gamma_{iw}}{r_{pore}} \tag{4.12}$$

In which γ_{iw} is the ice-water surface tension and r_{pore} the radius of curvature. The liquid water saturation during freezing of a porous material, can be found with a constitutive relation:

$$s^w = s^w(p^w) = s_w(p^{atm} - \frac{2\gamma_{iw}}{r_{pore}}) = s^w(r_{pore}) \tag{4.13}$$

$$\begin{cases} p^i - p^w = \frac{2\gamma_{il}}{r_{pore}} \\ \\ s^w = \sum_{k=1}^{4} a_i log(r)^k \end{cases} \tag{4.14}$$

4.6 Final System

The final system is:

$$
\begin{cases}
\varepsilon\rho^w \frac{\partial s^w}{\partial t} + s^w\rho^w\alpha^\beta \frac{\partial p^s}{\partial t} - \nabla\cdot[\rho^w \frac{k^{sw}}{\mu^w}\cdot(\nabla p^w - \rho^w g)] = e^w_{wi}. \\
\varepsilon\rho^i \frac{\partial s^i}{\partial t} + s^i\rho^i\alpha^\beta \frac{\partial p^s}{\partial t} = e^i_{wi}. \\
(\rho C_p)_{eff}\frac{\partial T^*}{\partial t} + (\rho_w C_p^w v^w)\nabla T^* - \nabla\cdot(\lambda_{eff}\nabla T^*) = -L_f e^w_{wi} \\
T_{f/m} = T_{ref} exp[\frac{1}{\rho^w L_f}(p^w - \frac{\rho^w}{\rho^i}p^i)] \\
p^i - p^w = \frac{2\gamma_{il}}{r_{pore}} \\
s^w = \sum_{k=1}^4 a_i log(r)^k \\
p^s = (1-\chi)(p^i - p^w) + p^w \\
e^i_{wi} = -e^w_{wi}
\end{cases}
\tag{4.15}
$$

The unknowns are:

$s^w, s^i, p^w, p^i, p^s, e^\alpha_{wn}, T$

Where:

$(\rho C_p)_{eff} = \rho^s(1-\varepsilon)C_p^s + \rho^w\varepsilon s^w C_p^w + \rho^i\varepsilon s^i C_p^i$

$\lambda_{eff} = \lambda^s + \lambda^w + \lambda^i$

$T^* = T - T_{f/m}$

Analyzing the whole system and studying the way of resolution of other models presented in the literature it is clear the complexity of the problem. The complexity regards not only the number of equations and but also the non-linearity of the equations.

The energy conservation equation is highly non linear because the coefficients depends on the saturation of the two phases and in addiction there is complexity of the phase-change. The saturation of both phases is a function of temperature and pressure. The freezing point depression, explained by the Clapeyron equations, varies depending on the value of cryostatic pressure at each time.

Moreover, analyzing the numerical simulation presented in the literature, to over-come the highly non-linearity of the equations some strong approximations are done. For instance, most of the time the variation of water content with the temperature is given as an input relation and not results as an output of the energy equation.

Facing a preliminary attempt of the resolution of the entire system of equations it was clear that there was the necessity of more elaborate studies focused on the physics of the problem. For this reason, it has been decided to focus the analysis on a simpler problem and to perform some laboratory experiment to understand better the physics process described by the system.

The laboratory and numerical analysis are focused on the three unknowns: temperature T, mass change of phase e and the pressure exerted on the solid skeleton at pore-size p^s.

The energy conservation equation is solved both considering soils and only water sample. The results of numerical simulation for the soil case has been compared with the experimental results. In this way, the temperature trend is modeled and the terms of exchange of mass, e, results as an output of the simulation.

Moreover, considering the pore-size dimension a coupled thermo-mechanical model is presented to study and model the pressure exerted on the soil skeleton by the freezing water. A simplified mechanical model is presented to simulate the pressure exerted by

a volume of water in freezing conditions. The results of the model in terms of pressure exerted, considering only water, has been compared with the experimental results.

In the following chapter, the temperature trend and pressure exerted in freezing conditions are studied experimentally and numerically.

4.7 Application: Saturated case

Considering to apply the system presented in the chapter 2 to a saturated case, it is obtained that:

$s^w + s^i = 1$

Considering an undeformable matrix (constant porosity) the term $\frac{\partial p^s}{\partial t}$ can be neglected by the equation. The mass conservation equation of water and ice phase becomes:

$$\begin{cases} \varepsilon \rho^w \frac{\partial s^w}{\partial t} - \nabla \cdot [\rho^w \frac{k^{sw}}{\mu^w} \cdot (\nabla p^w - \rho^w g)] = e^w_{wi}. \\ \varepsilon \rho^i \frac{\partial s^i}{\partial t} = e^i_{wi}. \\ e^i_{wi} = -e^w_{wi} \end{cases} \tag{4.16}$$

So the energy conservation equation becomes:

$$(\rho C_p)_{eff} \frac{\partial T^*}{\partial t} + (\rho_w C^w_p v^w) \nabla T^* - \nabla \cdot (\lambda_{eff} \nabla T^*) = +L_f (\varepsilon \rho^i \frac{\partial s^i}{\partial t}) \tag{4.17}$$

But the saturation of both phases are a function of temperature, so the last derivative can be written as: $\frac{\partial s^i}{\partial t} = \frac{\partial s^i}{\partial T} \frac{\partial T}{\partial t}$. Moving the last term before the equal and collecting the $\frac{\partial T}{\partial t}$ term, it is:

$$\left((\rho C_p)_{eff} - L_f \varepsilon \rho^i \frac{\partial s^i}{\partial t}\right) \frac{\partial T^*}{\partial t} + (\rho_w C_p^w v^w) \nabla T^* - \nabla \cdot (\lambda_{eff} \nabla T^*) = 0 \tag{4.18}$$

In this way, the Apparent Heat Capacity formulation has been obtained. Indeed calling Ca, the apparent capacity coefficient and considering that $s^i = 1 - s^w$ and the derivation propriety : $\frac{\partial s^w}{\partial t} = -\frac{\partial (1-s^w)}{\partial t}$ it can be obtained the final form of the energy equation is:

$$C_a \frac{\partial T^*}{\partial t} + (\rho_w C_p^w v^w) \nabla T^* - \nabla \cdot (\lambda_{eff} \nabla T^*) = 0 \tag{4.19}$$

Where:

$C_a = (\rho C_p)_{eff} + L_f \varepsilon \rho^i \frac{\partial s^w}{\partial t} = \rho^s (1-\varepsilon) C_p^s + \rho^w \varepsilon s^w C_p^w + \rho^i \varepsilon s^i C_p^i + L_f \varepsilon \rho^i \frac{\partial s^w}{\partial t}$

Chapter 5

Laboratory experiments

The Frost heave process is a complex process characterized by hydrological, geotecnical and thermodynamical aspects. While the hydrological features are clear and there is a good comprehension of the main governing equations; the thermal and mechanical aspects are still an open research argument.

Due to the complexity of the process, it is necessary an experimental study to understand the physics of the phenomena and to find the constitutive laws. As already said in the previous chapter, the pressure and the correlation between pressure and temperature have a relevant importance on the process. To this reason the second part of this work is focused on the experimental measure of pressure and temperature on freezing samples. The aim is to study the physical processes to have a deeper comprehension of the phenomena.

The laboratory experiments has been done with an experimental equipment totally designed, built and realized appositely for this test.

5.1 Testing equipment

An experiment has been designed to perform one-dimensional swelling force test with saturated soil sample. The experiment set-up allow also to measure the force generated by

the freezing water volume.

The testing equipment has been designed and built to satisfy some specific requirements of the test. First of all, the maximum value of force exerted by freezing soils registered in other literature experiments has been take into consideration as the basis for the design.

A confining structure was needed to support the force exerted by the freezing sample. There was the need to have a mould that can prevent the sample from radially deformation and at the same time some elements which not allow hydraulics exchange with the external ambient. A fridge which can reach -40C , already present in the laboratory, has been utilized. To the pressure and temperature measurement there was the necessity to find sensors which were impermeable and also which can work at very high negative temperature, till -40C.

Moreover, a data acquisition system (DAQ) has to be design and created to transform the output of the two sensors into values, numbers in a computer. The data acquisition system has been connected to an Analog to Digital Converter (ADC), in this way the temperature and pressure data can be visualized in real time into a screen.

The innovation of this experiment lead to the necessity of the creation of various elements and to act a process of selection to satisfy different requirements and necessities. The final testing equipment is composed by a rigid structure, a load sensor to measure the force, a data acquisition system connected to a computer, a mould, temperature sensors and a fridge.

5.1.1 Soil cell and confining system

The design of the confining system has been done to satisfy some specific requirement. First of all, the structure has to support the high stress due to the freezing process so it was necessary it has a good resistance. Secondly, the entire structure was to be manageable and with the right dimensions to be insert into the fridge. To contain the force generated by the deformation of freezing soils a steel structure was built welding four HEA 100 beams. The steel structure performs as a continuous rigid body. The design of the structure has been thought to enter in the fridge and to minimize the weight (fig.5.1).

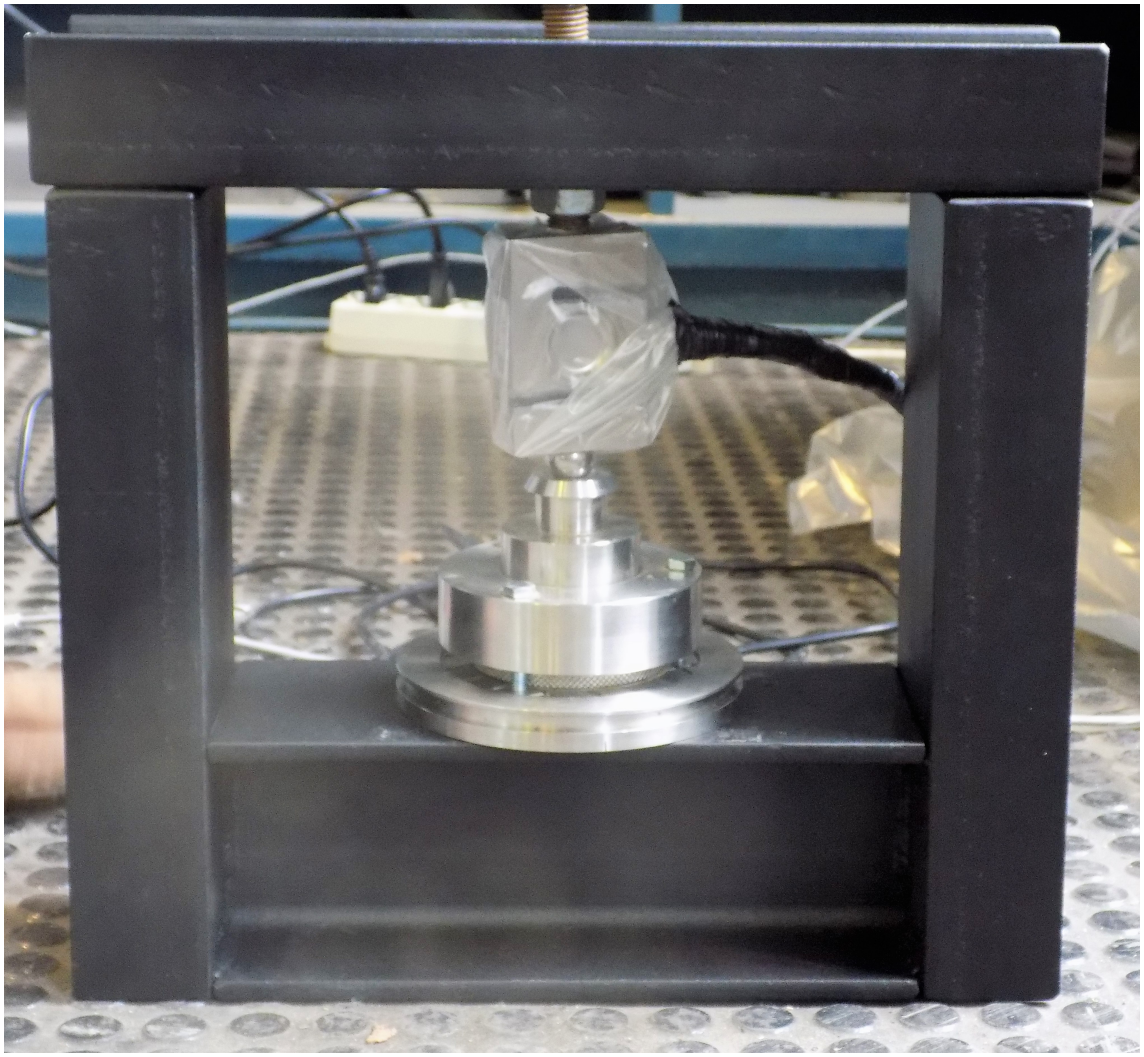

Figure 5.1: Testing equipment: rigid structure with load sensor and mould.

To create a soil cell, the mould which was a part of an oedometer has been utilized, (see fig.5.3). The oedometer is a instrument composed by an impermeable rigid ring and two porous bases. That instrument prevent the sample from deforming radially; only axial deformation is allowed. The maximal dimensions of the sample are: 5 cm of diameter and 3 cm of height.

A piston and a sphere is available to make the contact. Two little discs have been designed to confine the sample above and in the inferior part and to avoid whatever hydraulics exchange with the external environment, see fig.5.2.

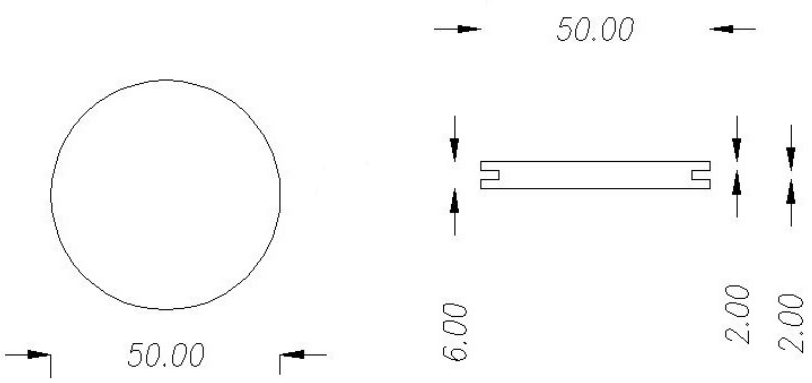

Figure 5.2: Design of the two plastic discs in mm.

The plastic discs has a diameter of 5 cm and is 6 mm thicker. Every little discs had a cavity in the external part, in which an O-Ring has been placed. The O-Ring is a plastic ring used in static and dynamics application, it guarantee the impermeability of the contact and prevent the water leaks.

Figure 5.3: Photo of the soil cell elements: on the right two O-Ring and the two plastic discs with the O-ring. On the left the mould utilized.

5.1.2 The fridge

The fridge utilized in the experiment was the only component of the testing equipment already presented in the laboratory. The fridge utilized is a POLAR 110 H, the volume utilizable is of 113 l and it can works in a temperature range of $-40°C$ to $-85°C$, and the adsorbed power is 0.66 kW. The internal dimensions are: 45x56x45 cm (LxPxH).

Some preliminary test were done to study the mode of operation of the fridge with the structure inside it. The set-up of the experiment consist on insert the entire rigid structure inside the fridge. The aim of these test was to check that the fridge was able to freeze at temperature of $-40°C$ while the structure was inside and with the waves exiting from the fridge. The result of the test point out that the fridge managed to go at temperature also with the instrumental waves passing through the closure part of it.

Inserting the structure into the fridge the temperature rise from $-40°C$ to $-23°C$, then it takes 57 minute to reach again the temperature of $-40°C$. Then it follows the cycle of the fridge, fig. 5.4.

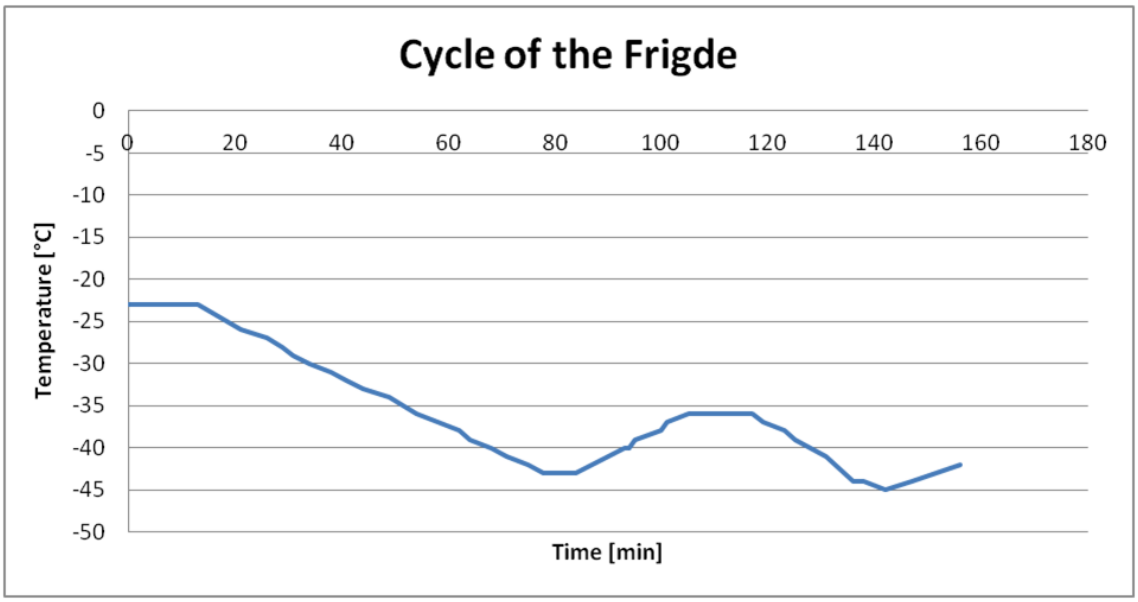

Figure 5.4: Cycle of the fridge, with the confining structure inside it.

Measuring sensors

The load sensor is an electronic device, transducer, used to measure the traction or compression force. The value of the force is measured in terms of electrical signal which varies due to the deformation of the strain gauge. The load cell capacity is 2000 kg and it is certified by the manufacture to work at high negative temperature (up to $-50°C$), fig.5.5. The load sensor model is YZC-516. The output sensibility is 2-0.004 mv/v, temperature effect on sensibility is 0.02 % °C ,input resistence 405-30 ohm, recommanded excitation voltage 12V, hysteresis 0.02.

The signal of that instrument is in mV so requires amplification.

Figure 5.5: load sensor to measure the force.

The load sensor is connected at the rigid structure trough a threaded bar ,fig.5.6. The threaded bar is clamped to the rigid structure by two bolts, preventing any vertical displacements of the load cell. The bolts allow also to regulate the load sensor position to reach the perfectly contact with the top piston of the mould. These two bolts are very important for the contact. Screwing them an initial force is imposed to the sample, that

force can vary from few to hundred Newton. In the inferior part, the connection with the mould is done with a steel piston and a sphere or with a plastic disc.

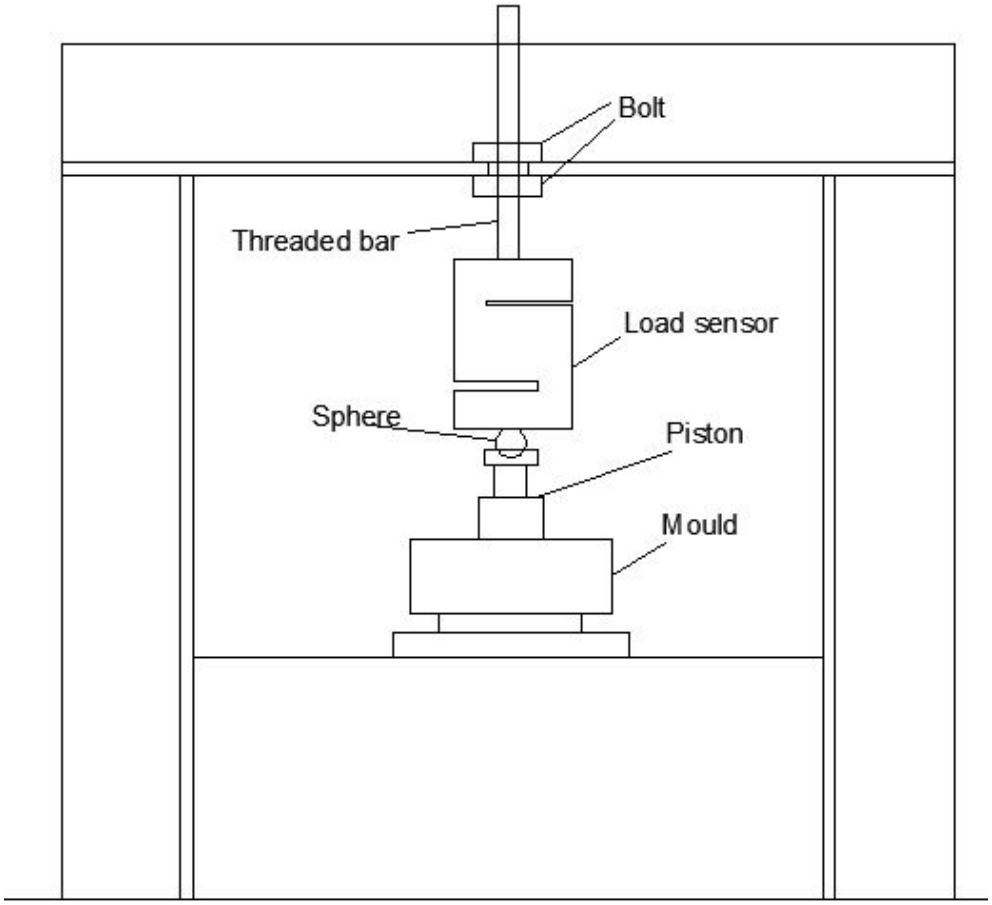

Figure 5.6: Scheme of the contact between load sensor, the rigid structure and the mould.

Since the various element are rigidly connected the monitoring of temperature data needs the utilize of a particular type of temperature sensor. The set-up of the soil cell, with the mould do not permit a easily insertion of a temperature sensor. The only way to insert the sensor at the center of the sample is to make the thin waves passing through the little cavities of the inferior plate of the mould, see fig. 5.8. So, it was necessary to find a very thin and flexible sensor, impermeable and with thin waves. After having compared different sensors with different characteristics; it has been chosen a flexible NTC

thermistor ultra-thin, see fig.5.7. A thermistor is an element with an electrical resistance that changes in response to temperature.

Figure 5.7: Ultra-thin thermistor.

The sensor utilized in the experiment is thin only 0,5 mm and 20 mm long and it has a superior insulating film. The accuracy is 1%, operating temperature range: -50 to +90 °C. This type of sensor can be bent into the smallest of spaces and have a fast-response making them ideal for surface-sensing applications.

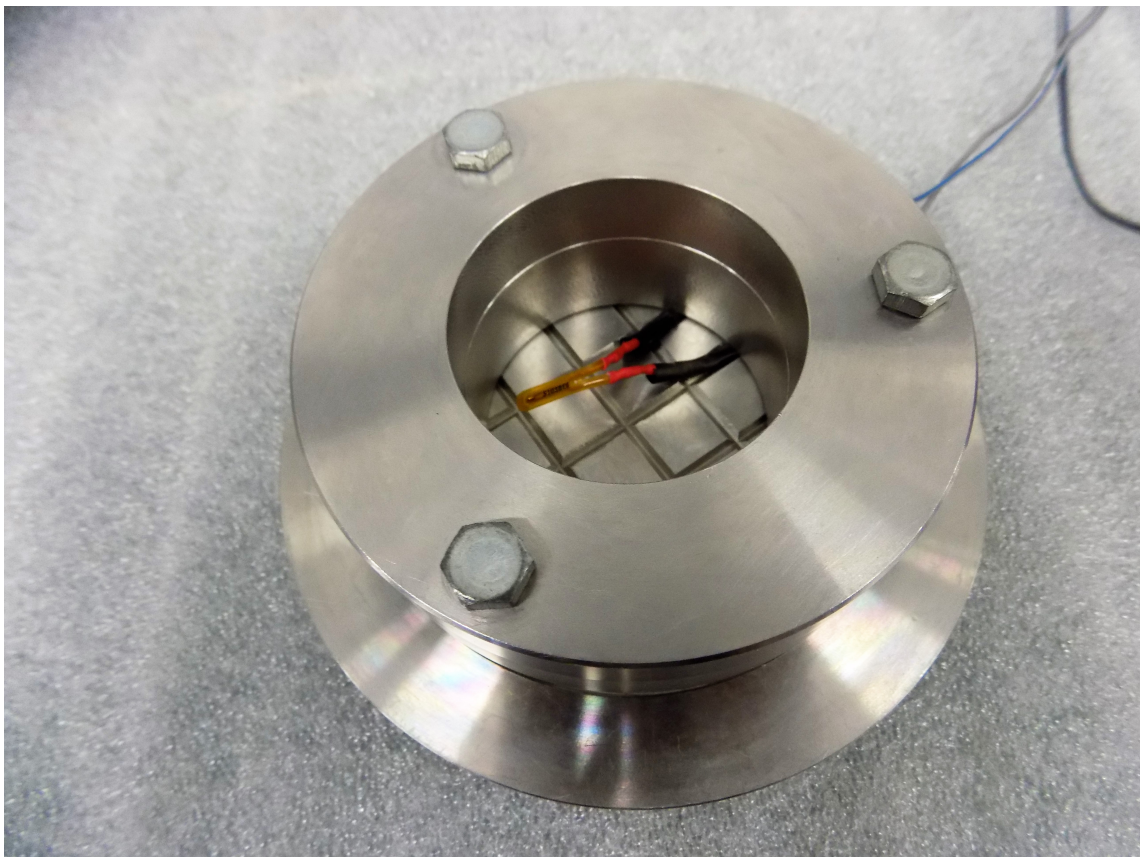

Figure 5.8: The sensor positioned in the little cavities in the inferior plate of the mould

The curve resistance-temperature of he thermistor can be seen in fig.5.9.

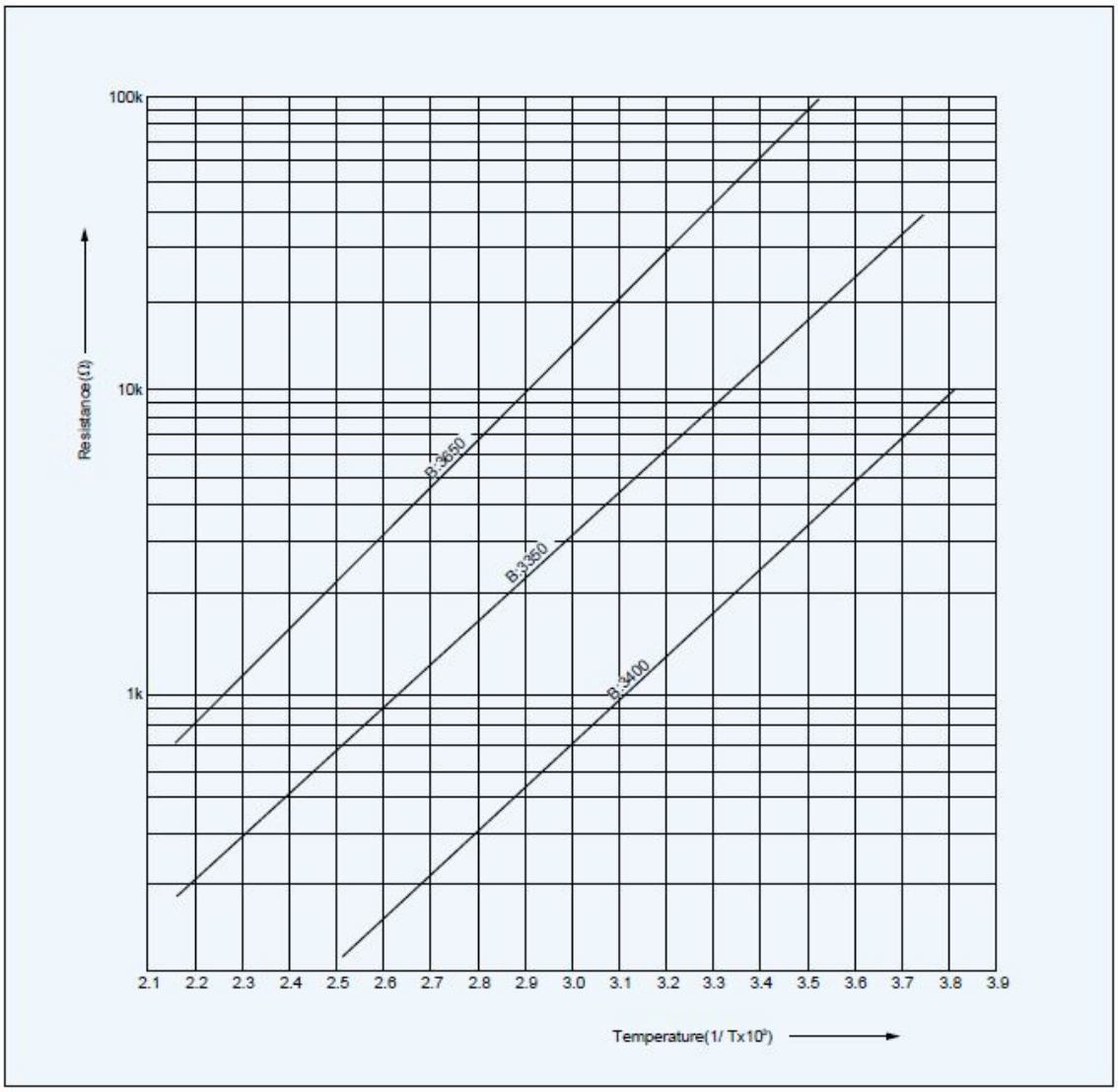

Figure 5.9: Resistance -Temperature characteristics curve of the thermistor ($\beta = 3435K$).

Data acquisition system (DAQ)

The data acquisition system is composed by three main components: a power generator of 24 V, and amplifier and power supply for the load sensor and a screw terminal, fig.5.10. The grey one in the photo is the amplifier and power supply for the load sensor. It receives the signal from the load cell and amplifies the signal in the interval from 0 to 10 Volt. It is also connected to the power generator. The screw terminal, the green element in the photo, is needed to make the connection with the Analog to Digital Converter (ADC) of the computer. The ADC is an electronic circuit which converts an analogical signal (the output voltage of the two sensors) into a series of discrete values.

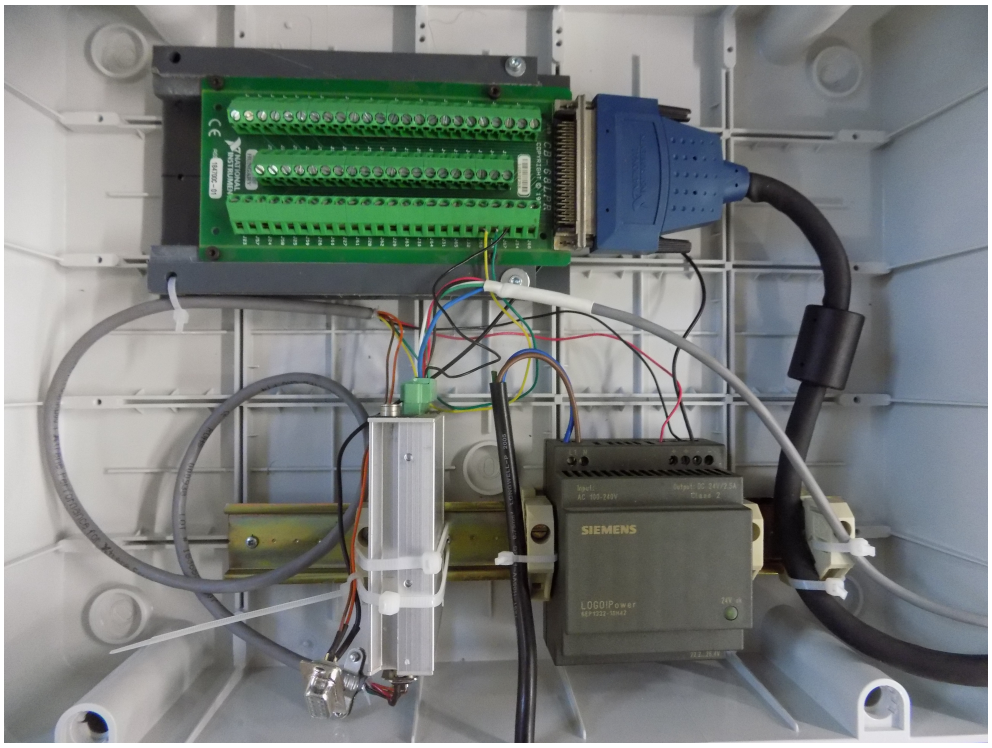

Figure 5.10: Data acquisition system

The ADC can read only voltage signal in the interval of $0 - 10V$, so as the thermistor gives as output a resistance value it has been necessary to convert the resistance signal into a voltage signal. This has been done realizing an electrical circuit with a non inverting

amplifier. Has been chosen a MCP 6001 supplied by a tension of 5 V. The scheme of the non inverting amplifier is reported in fig.5.11.

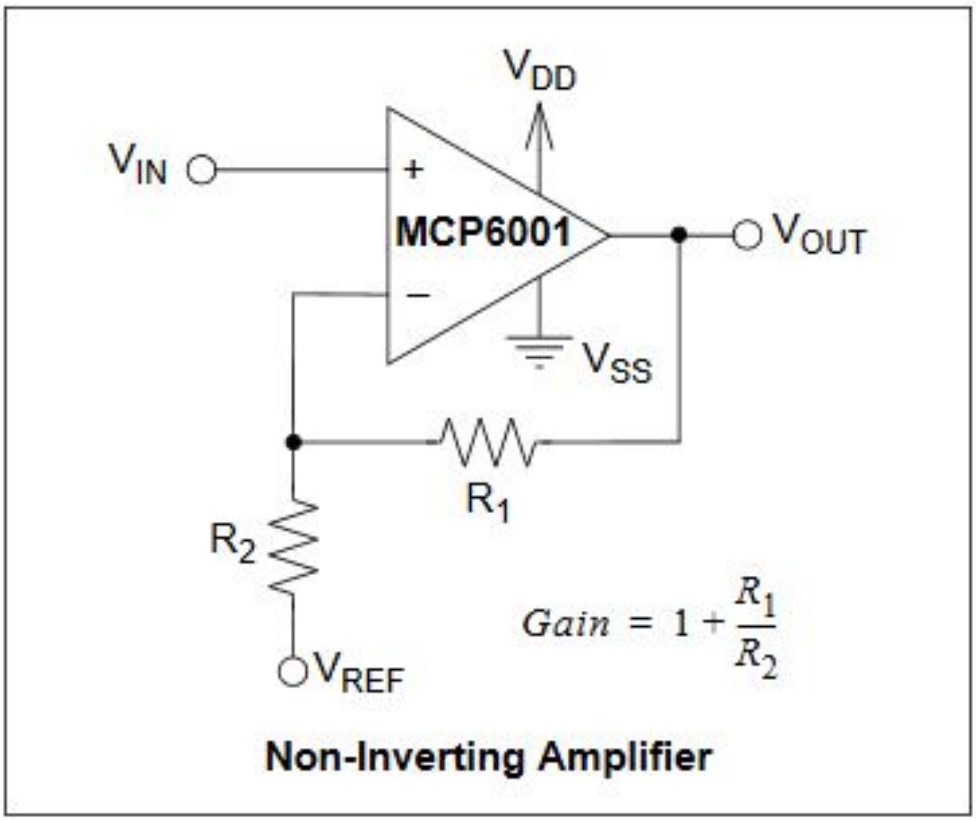

Figure 5.11: Scheme of non inverting amplifier for the temperature sensor

$V_{IN} - V_{REF} = 0.75V$, $R_1 = 400\Omega$ and R_2 is the resistance value obtained by the thermistor. The power supply voltage is obtained with a series of CC-CC converter which drop the voltage to the required value. In this way, it is obtained as an output a difference of voltage. The final circuit can be seen in fig.5.12, it has been connected than to the screw terminal.

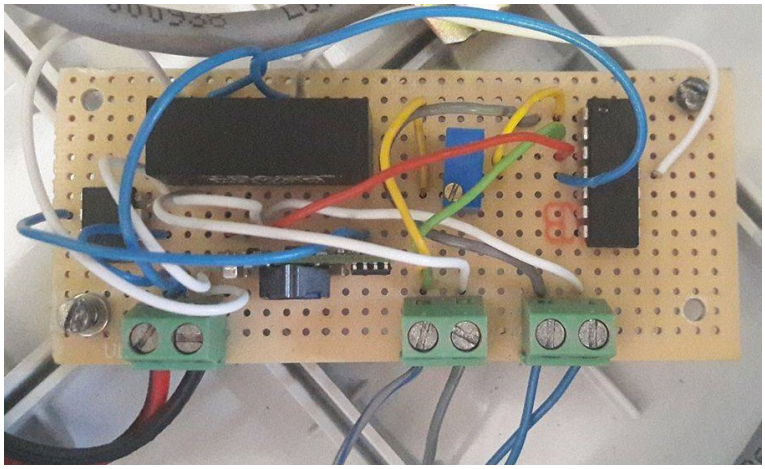

Figure 5.12: Electrical circuit connected with the thermistor.

The entire circuit is located in an electrical box connected with a computer. The data and the evolution of the test can be seen in real time on the screen and it is registered trough a software edited specifically for the study, fig. 5.13.

Figure 5.13: Designed position for computer and main electrical circuit.

5.2 Calibration

The calibration can be defined as a set of operations done to find the relationship between the electrical output and the corresponding physical quantity. Each sensor has been calibrated following dedicated procedure.

5.2.1 Load sensor calibration

The load sensor calibration has been done imposing a series of predefined load, from 5 N to 20000 N, and measuring them with a reference load cell. Then, the output voltage value obtained by the load sensor (in mV) has been associated with the respectively value of force (in N) measured by the reference load cell.

The experimental data has been fitted with a linear relationship, giving the calibration curve: $y = -247.35x - 335406$, fig.5.14.

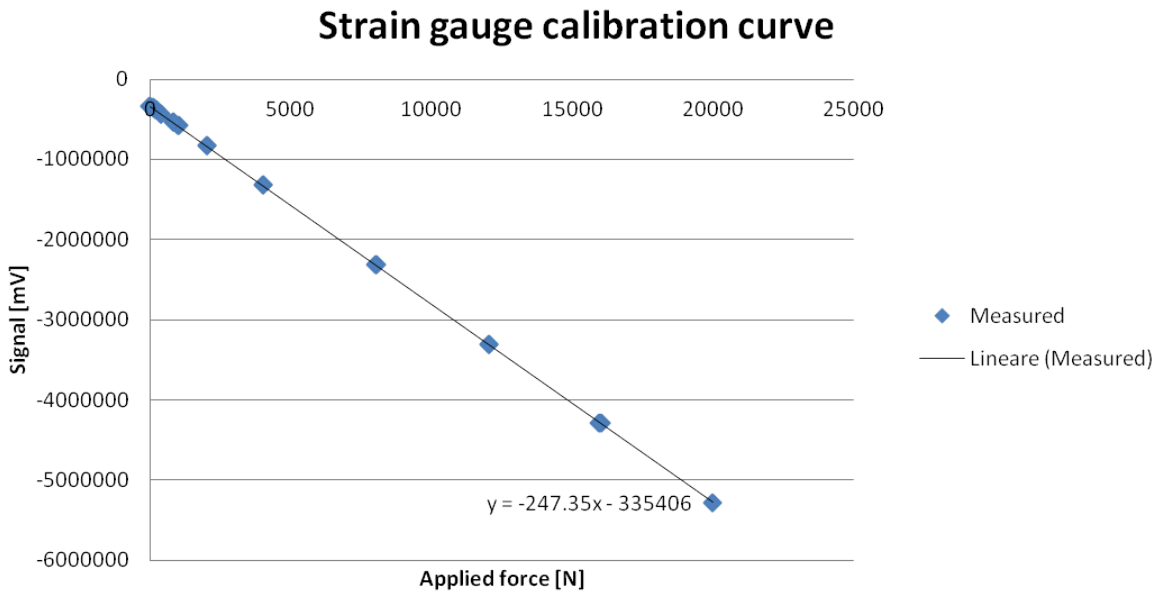

Figure 5.14: load sensor Calibration Curve

The calibration cycle takes into account of the hysteresis effects (load and unload).

5.2.2 Temperature sensor calibration

The calibration is needed to find the correlation between the value of sensor voltage output and the temperature in °C. A reference calibrated PT-100 sensor (Pico Log) has been used as reference sensor. The aim of the test was to measure the temperature which both sensor: in a computer there were the data in mV registered with the ultra-thin thermistor and in another screen we collected the value of temperature in ∘C by the Pico Log sensor.

Firstly, the calibration has been done in water to reproduce the same measurement environment of the real test. The hypothesis at the base of this way of calibration was the simultaneously of the two sensors value. As a first attempt, the calibration has been done inserting both sensors into a plastic bottle filled with liquid water. Then the plastic bottle was inserted in the fridge and the data were collected from both sensor instantaneously. This way of proceeding results to be inaccurate and not precise, so the same test has been done using a rigid container instead of a plastic battle, fig.5.15.

In this case we obtained a good linear trend for the value over 0°C and a more imprecise trend for the last part of the curve corresponding to the interval from 0°C to negative values. This can be explained due to the difference of size and weight of the two sensors. When the water was freezing the most heavier (Pico Log) entered inside the ice while the ultra-thin sensor stayed on the ice surface. This fact causes that the first sensor was collecting temperature data of ice and the second of air, so they were not measuring the same temperature. Moreover another problem has been observed.

The two sensors have different velocity to reach the temperature of equilibrium. While the ultra-thin sensor reached instantaneously a stable value of temperature, the second sensor needed more times to reach equilibrium conditions at the right temperature.
In other words, the two sensors have different time of response to a temperature gradient. Passing from ambient air (28 C in our case) to the fridge temperature, the Pico Log

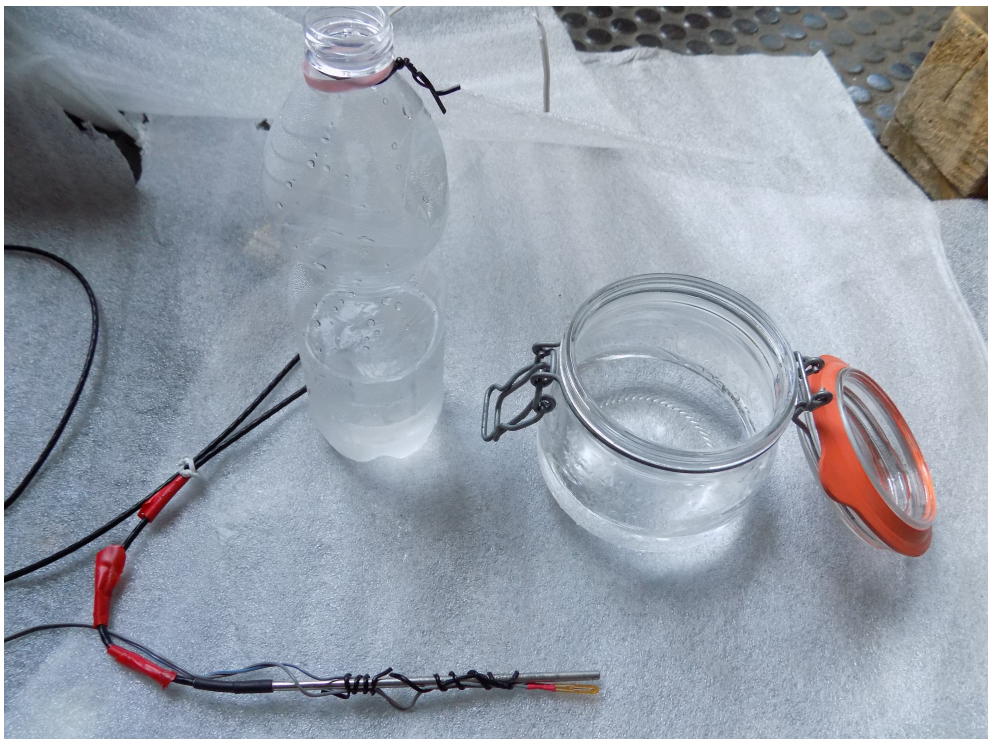

Figure 5.15: First set-up of test for the thermistor'calibration: the plastic and rigid container and the two temperature' s sensors. In the lower part of the figure there are the two sensors: ultra-thin and the heavier steel sensor linked together to be sure that they are measuring the same temperature in the same point.

sensor needs approximately ten minutes to reach the temperature of $-40°C$. Instead, the ultra-thin sensor revealed to be more sensible and it takes only few minutes to reach the temperature of the fridge.

To solve this problem, the procedure was changed. There was the necessity to take points at a situation of equilibrium: when there was a constant value of temperature for a certain time (such as 10 minutes).In this way there was the time for both sensors to reach the right value of external temperature. And so to guarantee that both sensors were measuring the same temperature.

To solve this problem the ambient air temperature has been measured. To have some points corresponding to negative temperature value, some points has been taken at $-40°C$ measuring the temperature in the air of the fridge. The points for the calibration has been

taken at ambient temperature and at $-40°C$ into the fridge. Moreover, some intermediate points has been taken inserting the two sensor into a fridge bag, in way to have constant temperature at values higher than $-40°C$. The points has been fitted by a linear curve: $y = -5e-05x + 179.56$,fig.5.16.

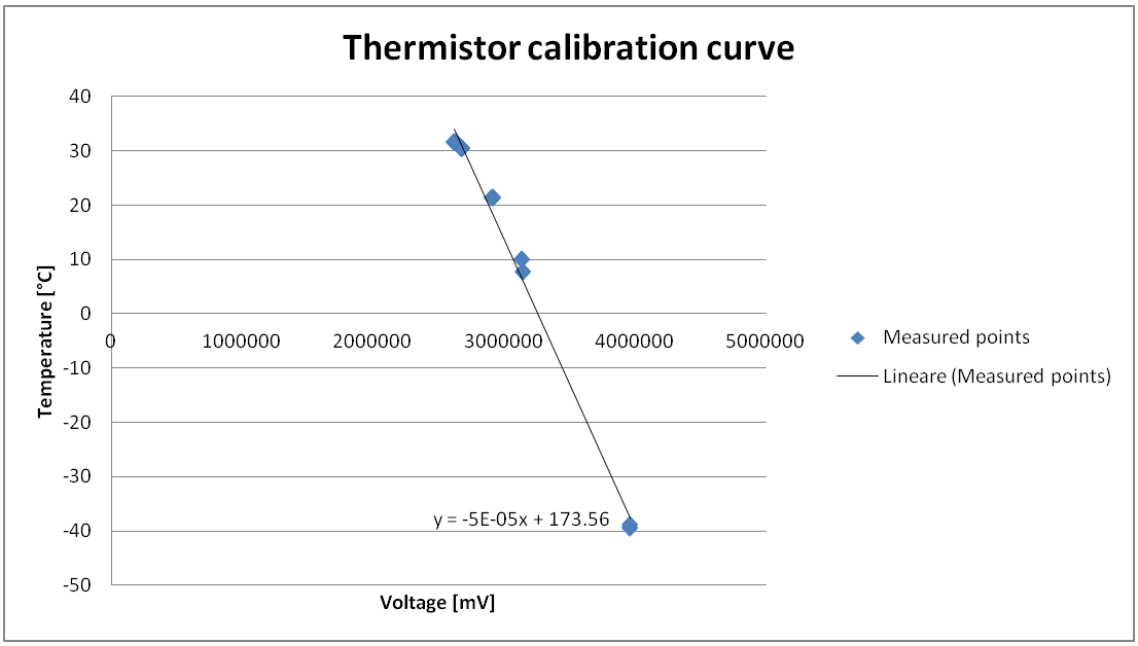

Figure 5.16: Thermistor calibration curve.

5.3 Thermal effects of the confining structure

The general procedure of the experiments consists on inserting the entire structure into the fridge at a temperature of $-40°C$. As the confining structure is entirely made of steel the temperature drop causes deformations due to thermal effect. Some test were done to understand the intensity of force generating by this thermal effect.

During this test only the confining structure has been inserted into the fridge, without the soil sample. The results shows that the rigid structure starts deforming from the first minute of the test. The pressure increases reaching a maximum value of 29.9 kPa (corresponding to a force of 58,6 N) and then decreases, see fig.5.17.

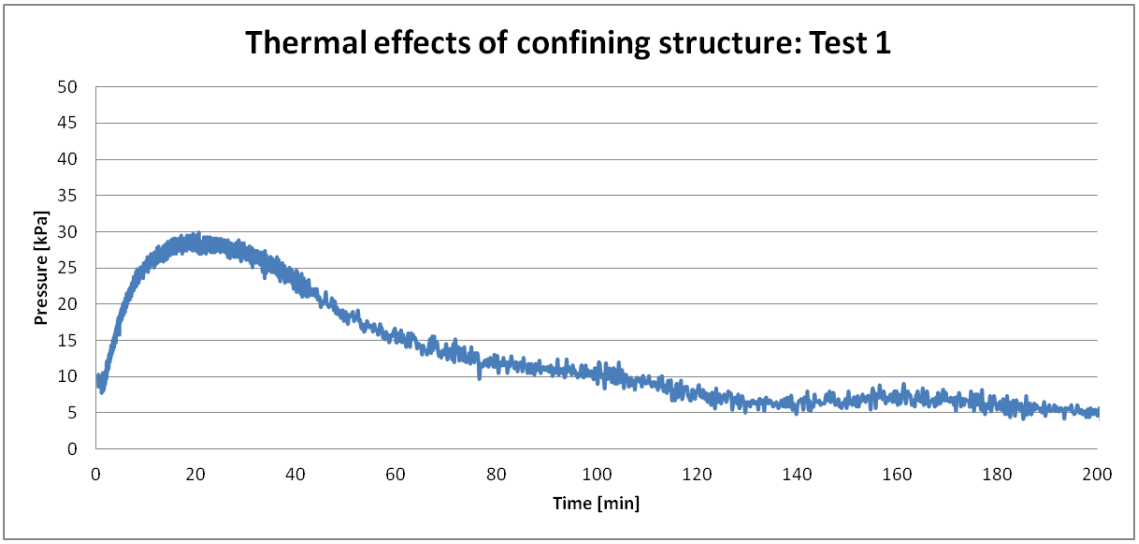

Figure 5.17: Thermal deformation effects of only rigid structure: Test 1.

Another test has been done inserting only the confining structure in the fridge but increasing the initial pressure on the load sensor. In fig.5.18 it can be seen in the same graph the results of both test. As can be seen, in both test it is obtained the same pressure trend. The phenomena is replicable and can also be easily identified because it happens by the first minute of the experiment. After a certain time (120 minutes) for both test the pressure become stable reaching again the initial value imposed.

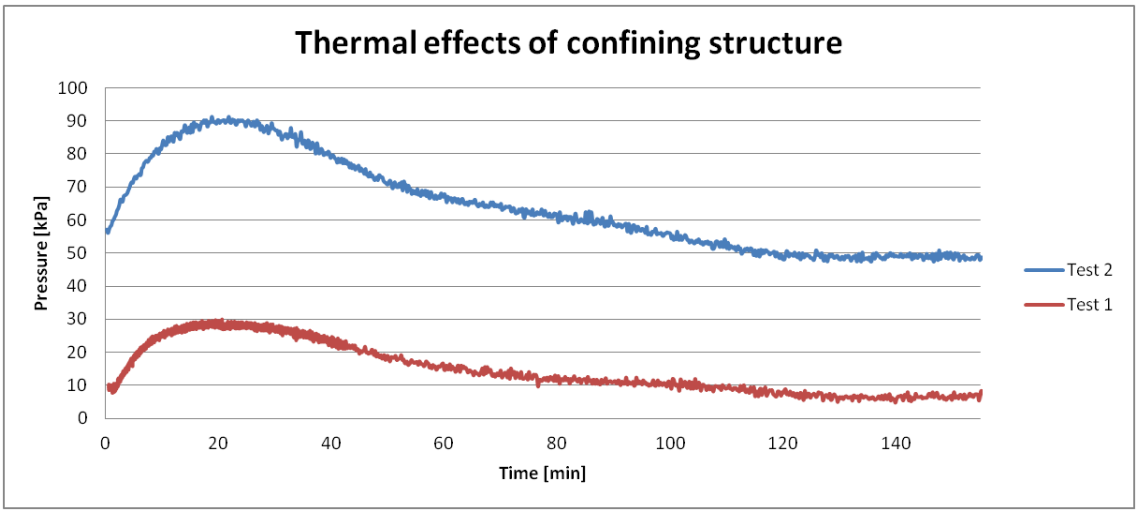

Figure 5.18: Thermal deformation effects of only rigid structure: Test 1 and Test 2.

Moreover, a temperature sensor was positioned over the load sensor to link the force variation to the steel temperature. Looking at the graphic of temperature, it can be seen that the phenomena become stable when the temperature reach the constant value of $-40°C$, fig.5.19.

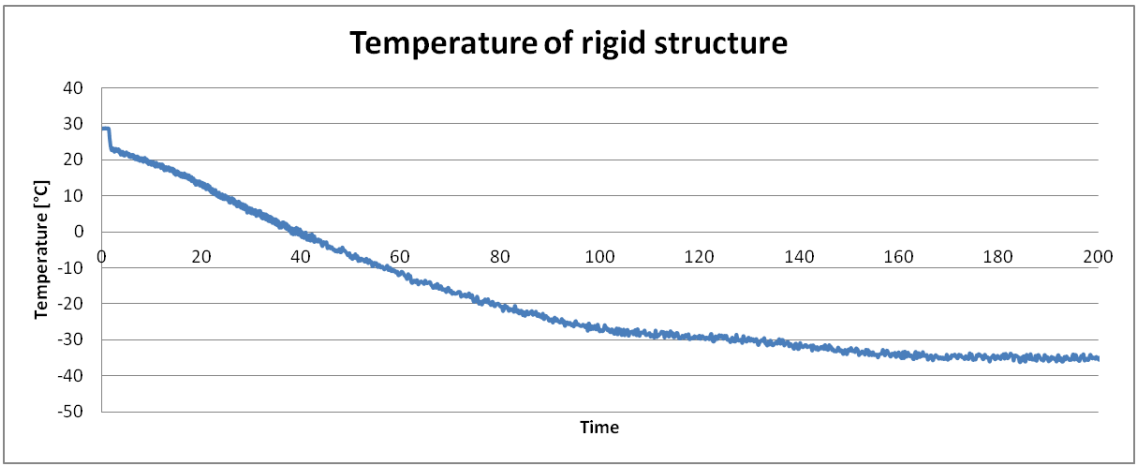

Figure 5.19: Temperature data collected by a sensor positioned in touch with the load sensor.

Taking into account of the thermal effects of the confining structure is important to underling which results are linked to a deformation of steel elements and which are linked to a soil response.

These information are necessary to treat the data of the soil test. Indeed, in all the following test it can be identify the first increasing of pressure due to thermal effects of the structure. So the first part of the curve results will not be considered as a soil response but only as an effects of structure.

5.4 Test with water

5.4.1 Test procedure

1. Sample preparation. The water is inserted between the two disc with O-Ring creating the perfect contact between the water and the disc surface.

2. Positioning into the rigid structure. The mould is placed on the base of the rigid structure.

3. Contact with the load sensor.The contact is made using a piston or placing directly the load sensor in contact with the disc.

4. Initial value of force. A initial value of strenght is imposed on the load cell, screwing the two bolts.

5. Freezing stage. The whole structure is inserted into the fridge.

6. Ending test. After a certain time the test is stopped and the entire structure is bring out of the fridge.

Test 1

The first test considering only water has been done utilizing the water sample between the two discs with O-Ring and the piston over it. The temperature sensor is not positioned in the water because the impermeability of the procedure has to be guarantee and there is no way to put the sensor inside the water without create a hole and so a passage for water. From the graph in fig.5.20, it can be seen an initial increasing of pressure due to thermal effects of the confining structure and then the pressure decrease and stay constant equal to the initial value. The increasing of pressure due to freezing water is not registered. It can be seen only a peak of 6.92 kPa at the 115.4 minute. This is surely linked to the water freezing strength but is a value too low to be considered.

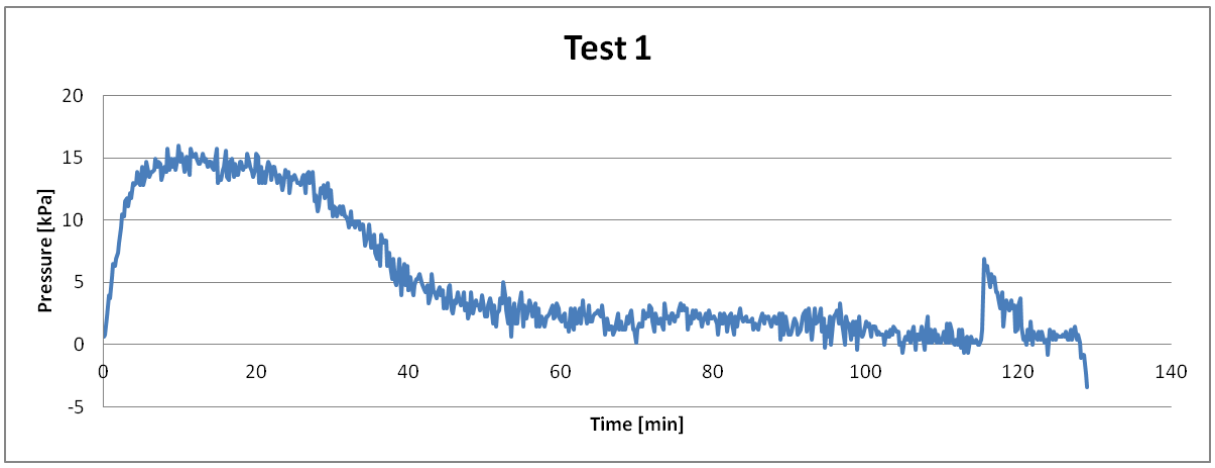

Figure 5.20: Measured pressure with a sample of only water.

The fact that the experiment not registered the increasing of force during freezing can be explained focusing on the contact. Since the water is confined above and in the lower side by the two plastic discs a lot of attention must be payed on the creation of the sample to have a good contact. It is indispensable that the water stays perfectly in contact with the surface of the disc. In this way there is not air and there is not free space for water expanding and the whole force exerted can be registered by the load sensor.

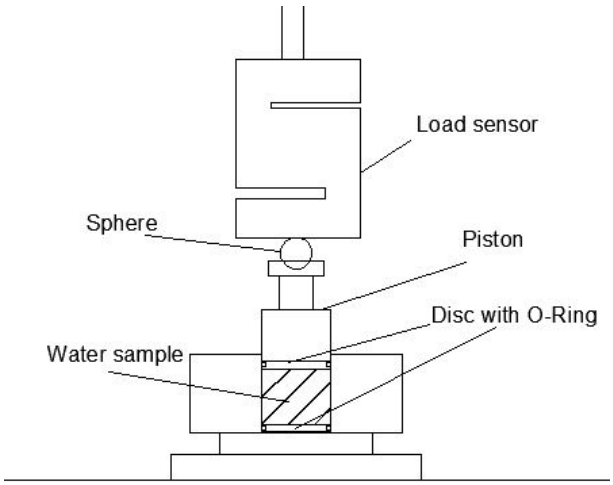

Figure 5.21: Way of contact utilized for Test 1: water sample between the two discs with O-ring and the piston over it.

Test 2

For this test, the water sample is confined by the two discs with O-Ring but the disc in the upper part is positioned in way to be 5 mm higher of the mould surface. A particular procedure of positioning the sample has been followed to assure the perfect contact between water and the disc above, fig.5.22. For this test the piston has not been used, but the load sensor is directly in contact with the plastic disc.

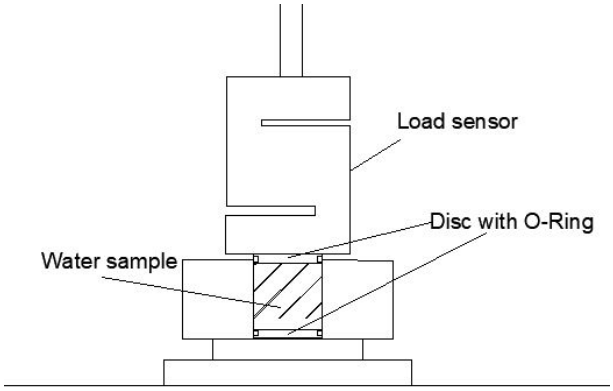

Figure 5.22: Way of contact utilized for Test 2: the load sensor is directly in contact which the plastic disc which is 5 mm above the mould.

Moreover, the procedure of creating the water sample between the two plastic cylinders is done to be sure that there is not air in the cavity and to have a perfect contact between water and the two cylinders In the two photo in fig. 5.23 it can be seen the way of contact used in this test.

Figure 5.23: Photo of the way of contact in Test 2.

The results, fig.5.24, are quietly impressive. The water freezing reaches a strength of 17000 N and so a respectively pressure of 8583.91 kPa. The experiment was stopped and the whole structure was taken out from the fridge because the load sensor utilized can work only till 20000 N and so under a pressure of 10191.08 kPa. The experiment has been stopped abruptly but the linear trend suggest that the pressure would have increase more.

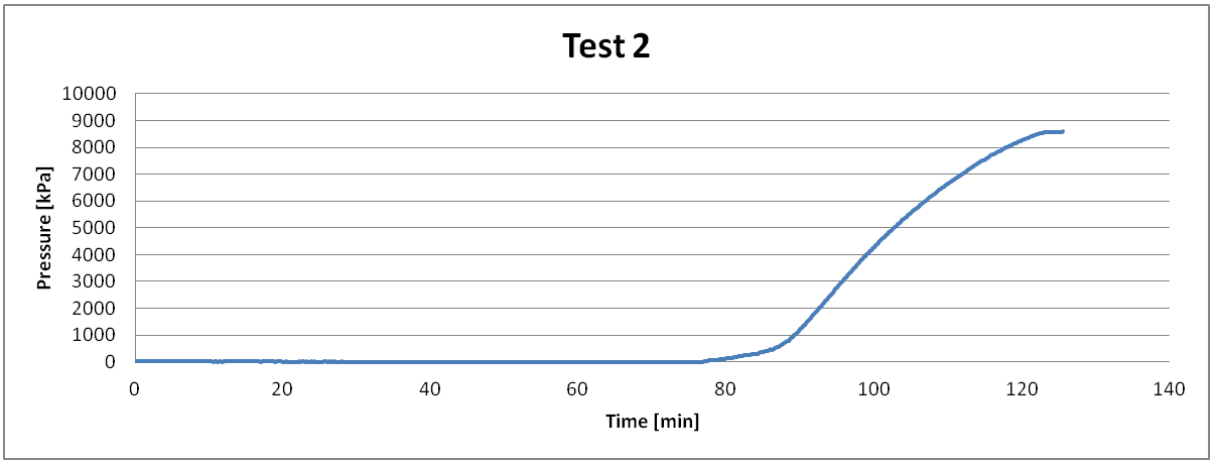

Figure 5.24: Measured pressure with a sample of only water: Test 2.

A particular attention must be done to the structure thermal effects trend at the first part of the graph. Zooming the graph, focusing at the first 80 minutes, before the pressure started increasing, it can be seen the thermal effect of the structure, fig.5.25. This test differs from the previous one because before starting the experiment the whole structure was inserted inside the fridge.

Before this test started, indeed, the only confining structure has been inserted inside the fridge for almost 15 minutes. The aim of this procedure was to reduce the effect of thermal dilatation of the steel structure and to start the test with the already deformed structure. As can be seen from, fig.5.25, the thermal effects of the structure reaches less value of pressure compared to the previous test. Till now we have seen that the effect of thermal dilatation follow a convex trend: a first part of increasing trend, a peak followed by the last part of decreasing trend.

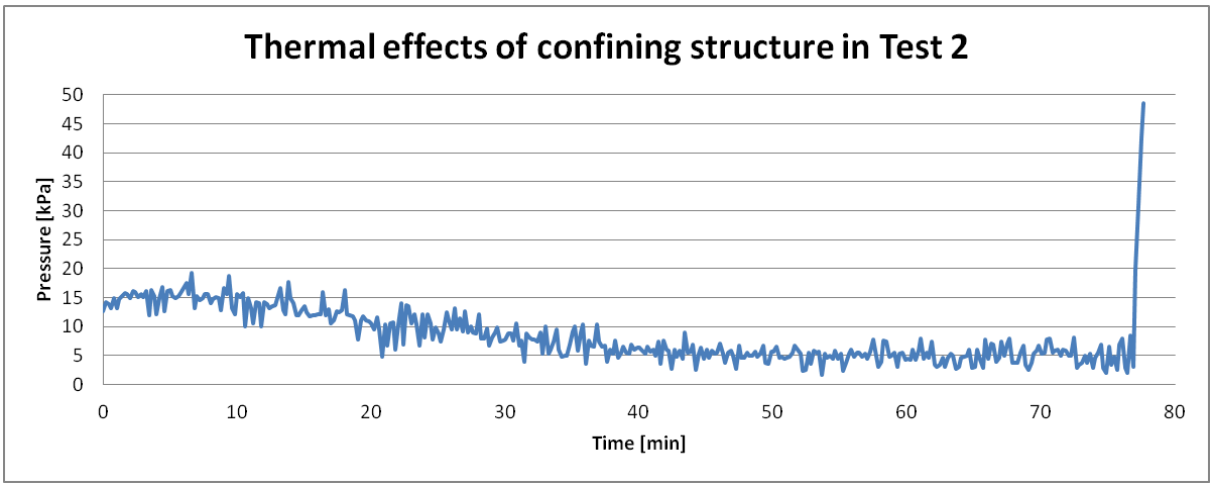

Figure 5.25: Measured pressure with a sample of only water. This graph represents the first 80 minutes of the test, to put the attention on the thermal dilatation effects of the confining structure, that can not be easily seen in the previous graph.

Inserting the only structure in the fridge before starting test has the effect of starting the test in the last part of this curve. This procedure will be followed in the successively test, to reduce the disturb due to freezing of the steel structure.
(The data in fig.5.25 are the same of the fig.5.24, it is only zoomed the first eighty minutes of the experiment).

Test3

The previous experiment has been replicated following the same procedure. This time the experiment has been interrupted when the strength reach a value of 20000 N and not at 17000 N as in the previous one. So, as can be seen from the graph in fig.5.26, the pressure reach a maximum value of 10151.91 kPa. Since there have been obtained the same results of the previous test, the experiment is replicable. The pressure of freezing follows a linear trend, surely it would have increased more if the experiment was not stopped.

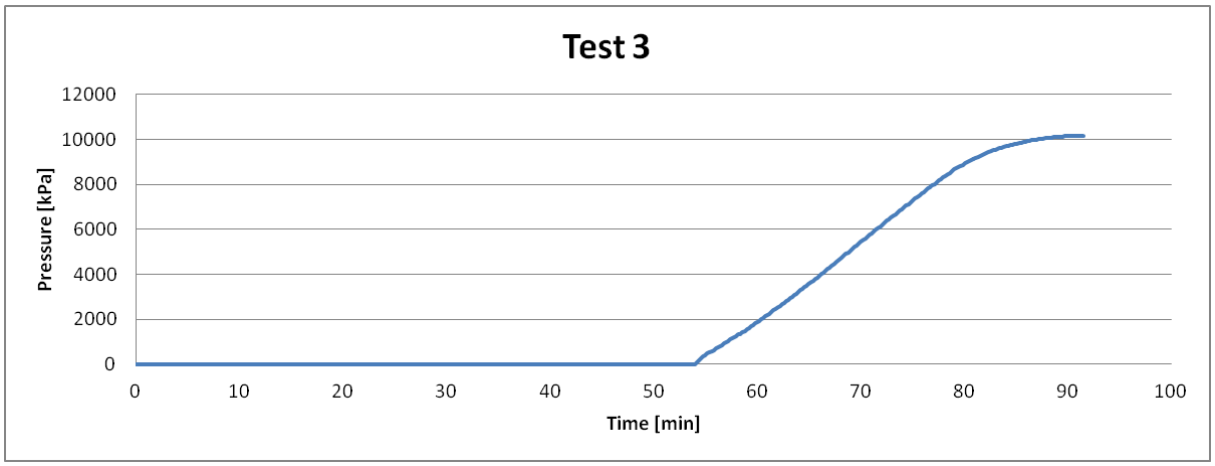

Figure 5.26: Measured pressure with a sample of only water: Test 3.

Also in this case, the structure has been inserted in the fridge for 15-20 minute before the test started. As can be seen from the fig.5.27, the test started in the decreasing part of the curve which characterize the trend of thermal effect of the confining structure.

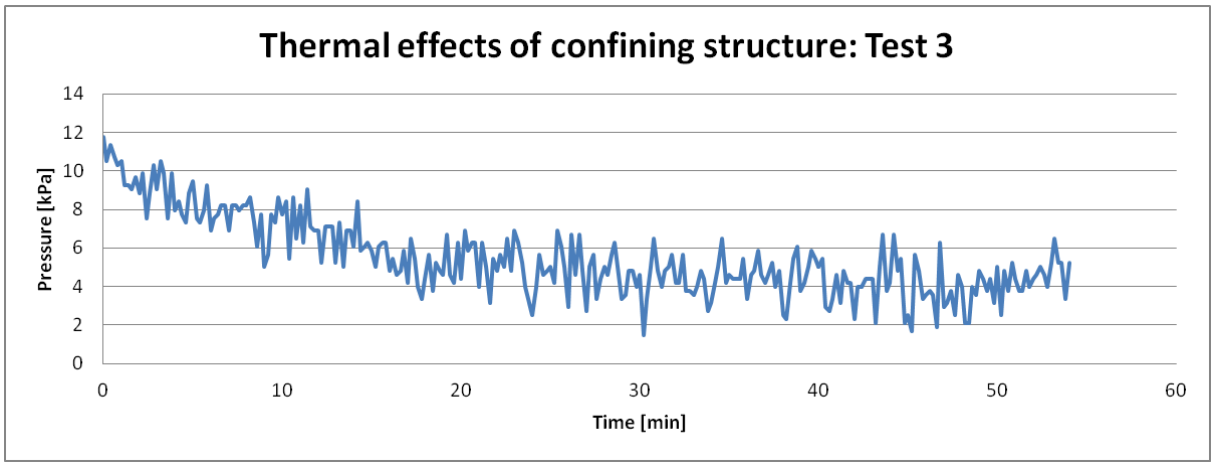

Figure 5.27: Thermal effects registered during the first 60 minute of Test 3.

5.5 Test with soil

5.5.1 Test procedure

The test procedure consisted on different steps:

1. Preparation of soil sample. A saturated soil sample was made using sandy soil. During the preparation of the sample the temperature sensor is inserted inside the core of sample.

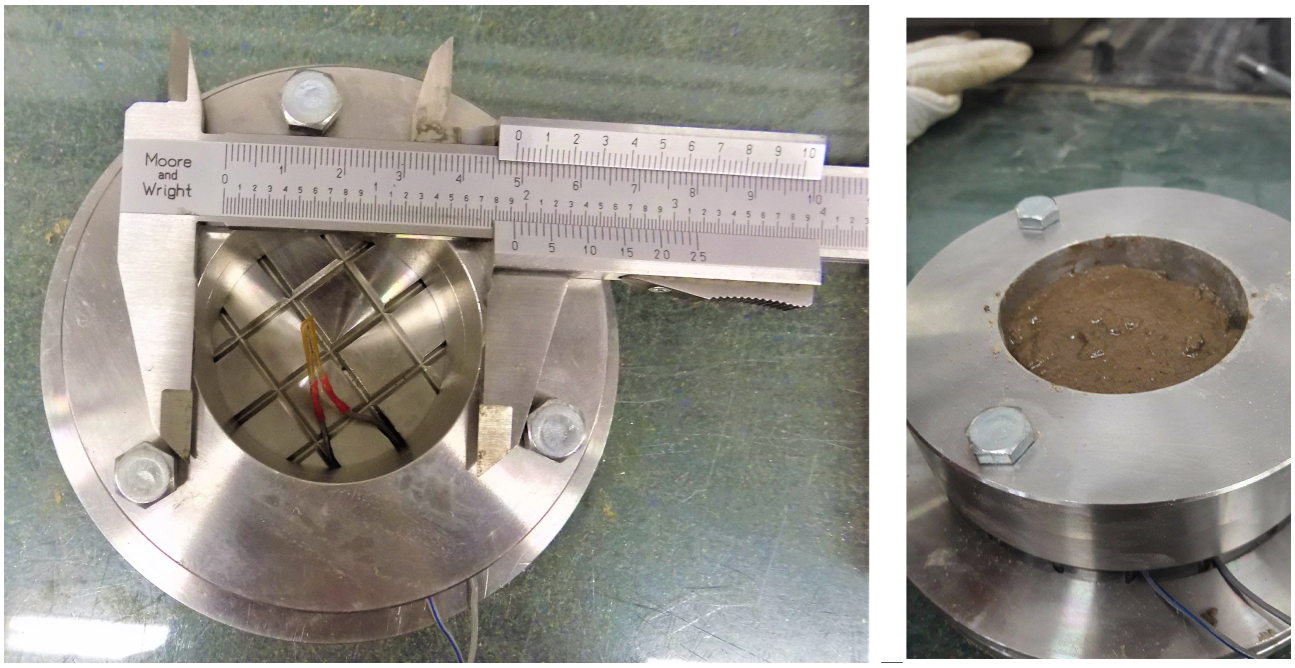

Figure 5.28: Preparation of the soil sample. The temperature sensor is positioned in the end of the mould. Then the mix of soil and water is inserted to cover entirely the sensor. In this way we obtain the temperature data at the soil core.

2. Consolidation. The soil sample is consolidated at different value of force. The sample is consolidated directly inside the mould with the piston over it.

3. The mould with the piston is placed at the base of the rigid structure.

4. Contact with the load sensor. An initial force is applied to the load sensor achieving

the perfect contact between it and the mould. The initial force is applied rotating the two bolts which connected the load sensor to the rigid structure.

5. Freezing stage. The entire structure is positioned inside the fridge which is properly closed. A computer machine recorded instantaneously the pressure and temperature data thanks to the connection with the electrical circuit.

Figure 5.29: Photo of the whole structure positioned inside the fridge.

6. Ending test. After a certain time that the soil core had reach a temperature of $-40°C$ the test is interrupted and the structure is taken out of the fridge.

5.5.2 Test 4

In the test 4 the sample is consolidated at 0.5 kg. Analyzing the results, there is a first increasing of pressure that can be seen from the first moment of inserting the structure

inside the fridge. This increment of pressure is not linked to a soil response but it is due to thermal effects of the confining structure, as already pointed out.

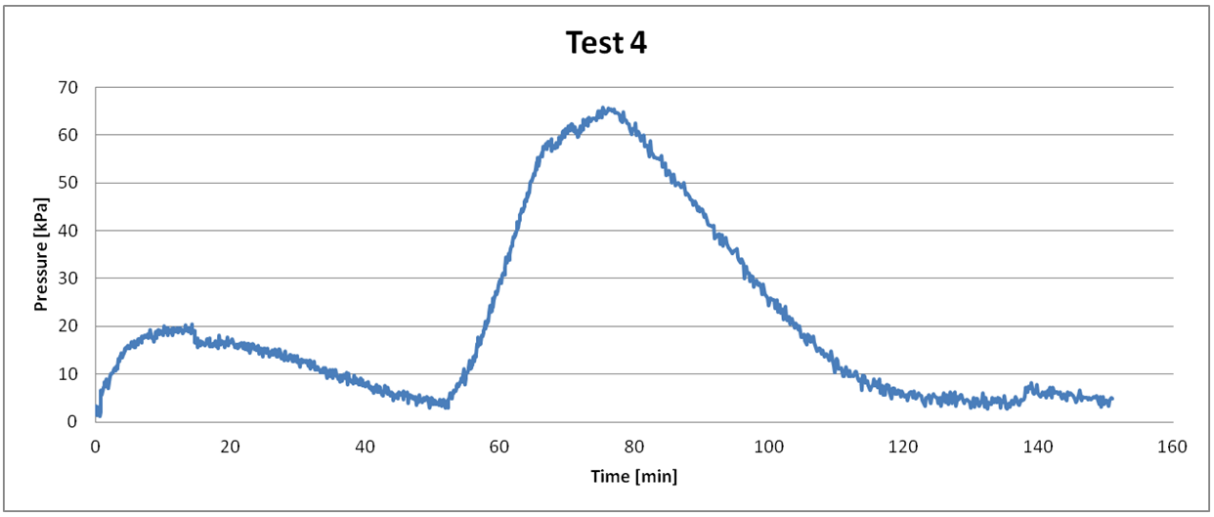

Figure 5.30: Pressure data acquired in Test 4.

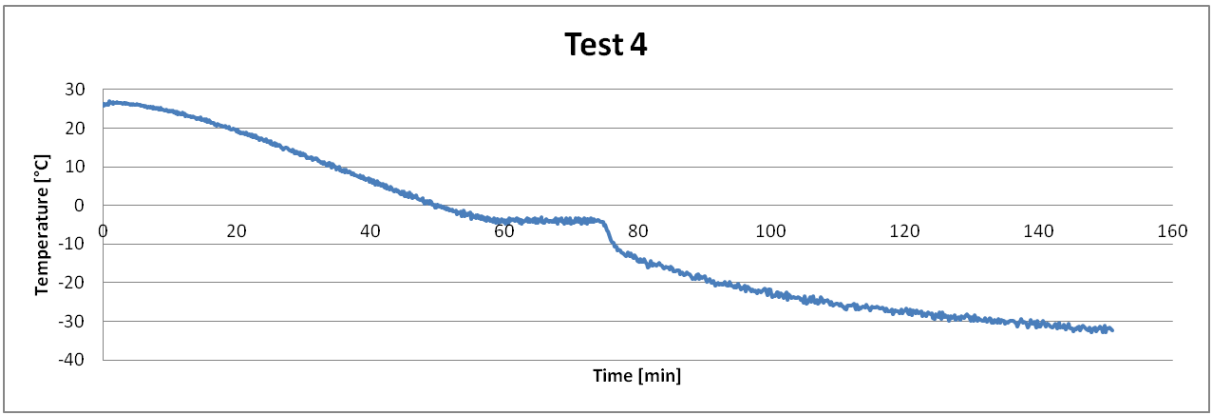

Figure 5.31: Temperature data the soil core acquired in Test 4.

The temperature data corresponds at the values at the core of soil sample. It can be seen a slowly decreasing of temperature till it reach a temperature of $-1°C$. At that moment the values of temperature stays constant, the soil is freezing. In correspondence of this value it can be observed an increasing of pressure reaching a maximum value of 65.84 kPa (129.21 N of force exerted). When the freezing process ends the temperature inside the sample decreases reaching $-30°C$. Looking at the results, it can be seen that

the pressure decreases after having reach a maximum value and in correspondence of the ending of freezing. This behavior is anomalous and it has been studied in successive test.

5.5.3 Test 5

A second test has be done, following the same procedure but consolidating the sample with a force of 25 kg. In this test a major pressure is imposed as initial value on the load sensor.

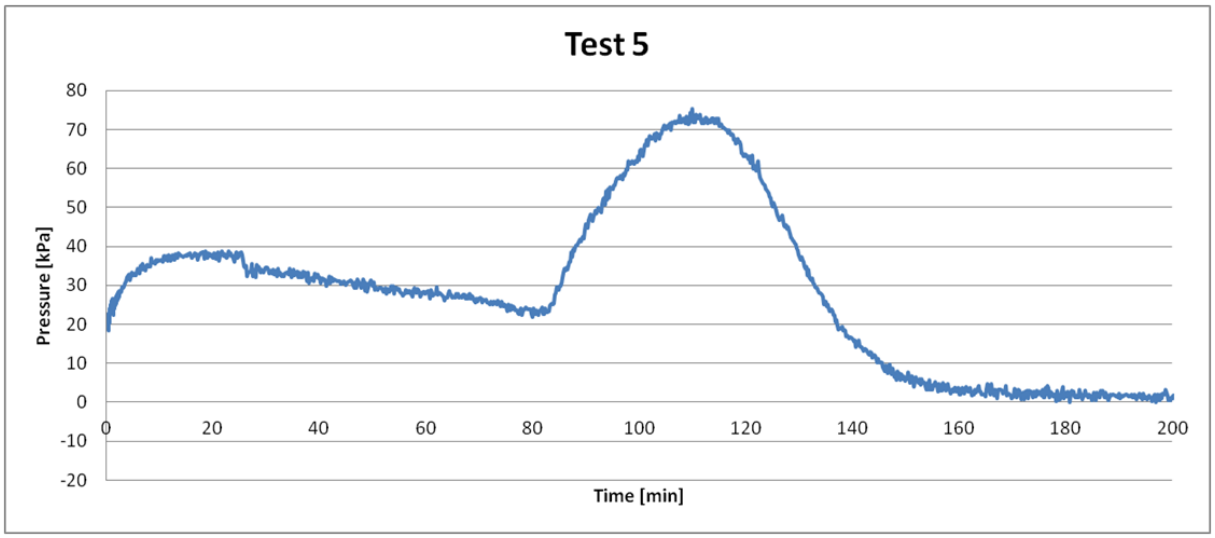

Figure 5.32: Pressure data acquired in Test5.

The results pointed out the same pressure trend obtained in the previous test. The pressure increases when the freezing conditions are reached on the sample. Then it reaches a maximum value and then decreases at the end of freezing process. The decreasing part of the curve is not related to the consolidation force and neither to the initial value of force imposed, which are the parameter modified in this test comparing to the previous one.

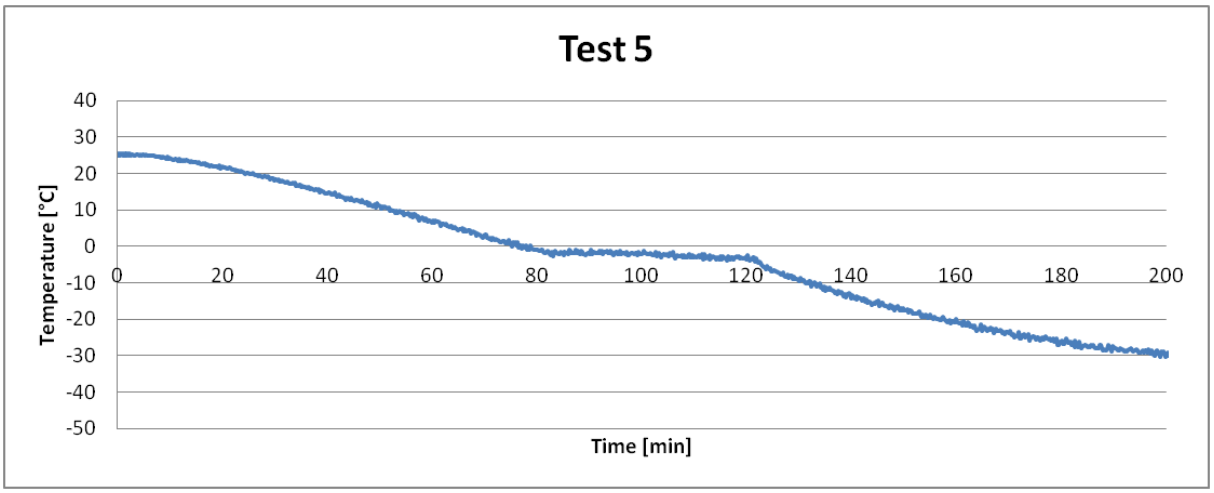

Figure 5.33: Temperature data acquired in Test5

5.6 Test with soil and Disc with O-Ring

The experiment done with water sample make in light the importance of the contact between the various elements of experimental plant. Varying just a little on the configuration the registered value can change of two order of magnitude. In this last series of experiment the way of contact is changed and the decreasing part of the force curve is studied.

5.6.1 Test procedure

1. Initial positioning of the structure in the fridge. The only confining structure is inserted into the fridge for 10-15 minutes.

2. Sample preparation. A sandy soil saturated sample is utilized.

3. Consolidation of soil sample. The sample is consolidated in the mould with a plastic disc with O-Ring over it. The consolidation has be done at a pressure of 49936.30 Pa (10 kg) for both test.

4. Positioning. The confining structure is taken out of the fridge and the mould (with

sample and disc) is positioned over its base.

5. Imposing initial force. The contact of the load sensor and the disc is done screwing the bolts and so, an initial value of force in imposed on the load sensor.

6. Freezing stage. The whole structure is inserted into the fridge.

7. Ending test. After a certain time that equilibrium conditions has been reached the test is stopped and the structure is brought out the fridge.

Test 6

The test started and after 60 minutes the soil sample start freezing and we registered a peak of pressure of 45.64 kPa corresponding to a force of 89.57 N. Then the pressure start decreasing as in the first two test done with soil, fig.5.34.

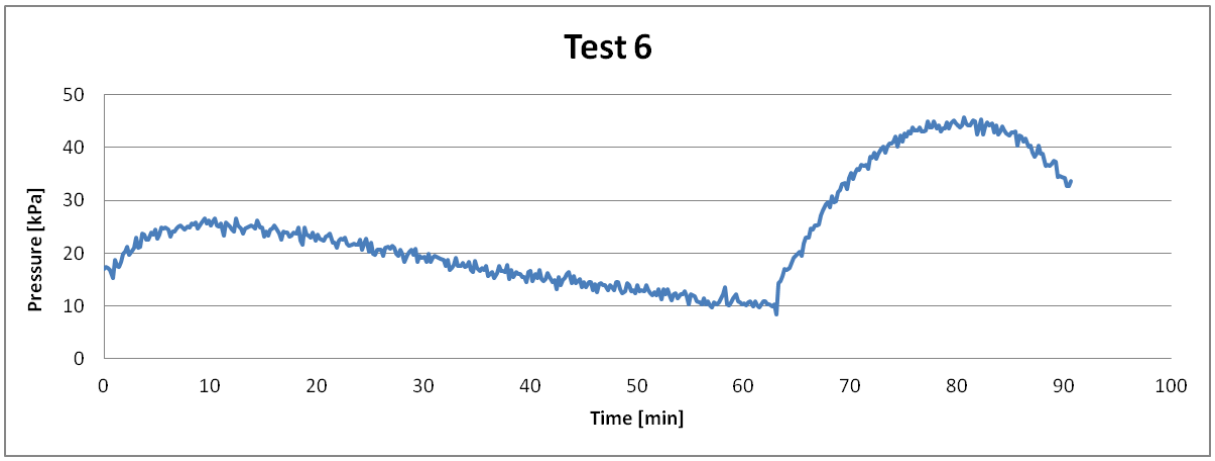

Figure 5.34: Pressure data acquired in Test 6 in the first 90 minutes: soil sample with plastic disc.

This decreasing trend is not what one could expect from these experiments. The freezing soils at the temperature of $-40°C$ should maintain the force and not decreasing the force after freezing. This anomalous behavior can be linked to a soil response or to technical aspects of the physical set-up of the experiment.
To put under light this problem, after 90 minutes, when the force was decreasing the fridge was opened to observe the soil sample condition. Opening the fridge it can be seen that everything was frozen but the bolt on the superior part of the structure was unscrewed. The bolt did not have adherence with the rigid structure, so it was not able to make pressure and so this is surely a cause of the decreasing force registered. At this point, the bolt was screwed and the test started again.

The graph in fig.5.35 shows the measured value of pressure during the entire test. As pointed out, the interval from 90th minute and 99th minute there are not measure because

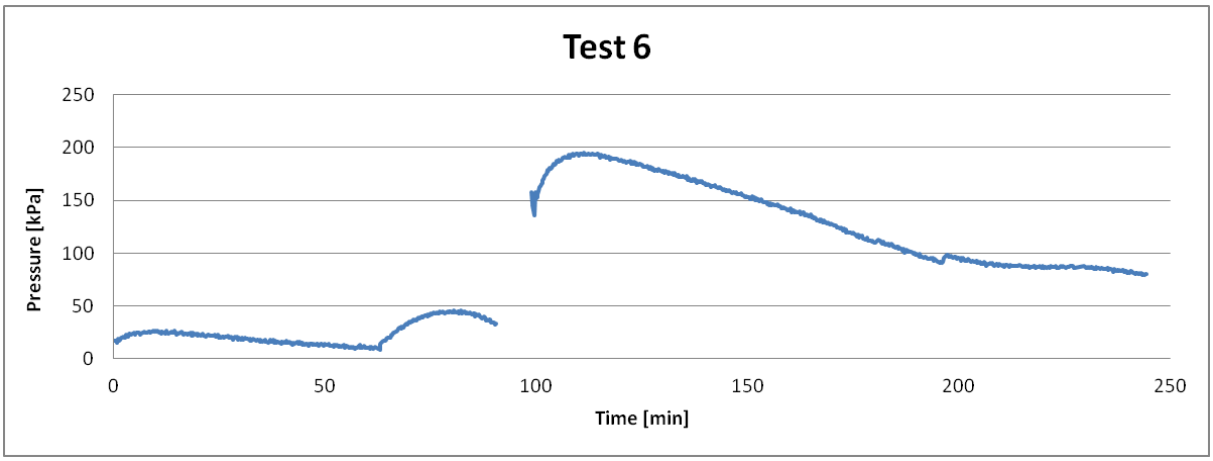

Figure 5.35: Pressure data acquired in Test 6: soil sample with plastic cylinder.

the test was interrupted to do technical operations of fixing bolts. The strength increase reaching 381 N (corresponding to a pressure of 194,81 kPa) and then decreases again, but this time it maintains a constant pressure of almost 90 kPa till the end of experiment. This test was useful to understand the limit of the experiment. Since the behavior of decreasing strength is linked to mechanical problem, in the following test we will not consider the last part of the curve.

Test 7

In the Test 7, the soil probe has been consolidated with a plastic disc on the inferior part. After the consolidation, the second disc has been positioned on the superior part of the soil sample. Also in this case, it was not used the piston and the load sensor was directly in contact with the disc.

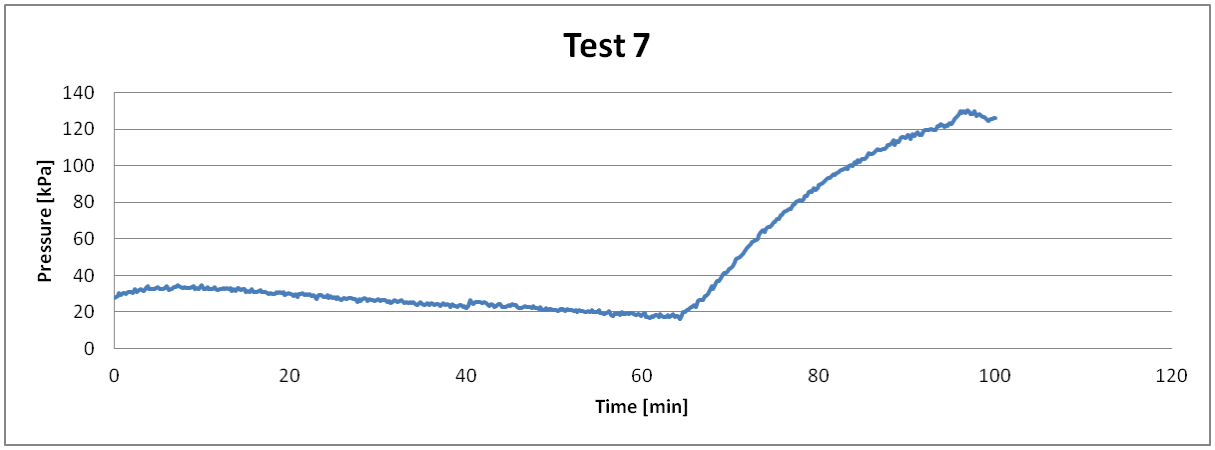

Figure 5.36: Pressure data acquired in Test7: soil sample between the two plastic cylinders.

This strategy wants to eliminate the doubt that the water can leach from the end of the mould. As can be seen from the graph in fig.5.36, the strength reach the value of 255 N and so a pressure of 130.43 kPa. So also this is a good way to proceed.

5.7 Analysis of the results

Analyzing the test results some observations and remarks can be done. During the test, it becomes clear the importance of the way of contact between the various elements. To solve this problem, two plastic cylinder with O-ring has been designed and built. With this new type of contact (collecting the water between the two plastic cylinders and the mould) we were able to measure a strength of 20000 N.
Focusing now on the soils results, in the last test (Test 8) we put the soil sample between the two plastic cylinders and put in contact the load sensor with the superior cylinder. Comparing the soil results using the two way of contact: in Test 8 we registered a force of 255 N. A value greater than the 147.79 N registered in the Test 2 with the piston as contact.
It can be concluded that the contact with the two plastic cylinders is the better one in terms of results.

From the thermal effect of the confining structure point of view, the process of freezing of the entire structure composed by steel and bolts generate some interference on the registered data. This effect is immediate and happens by the first moment of the test. It follows an increasing trend and after reaching a peak it decrease reaching the initial condition of force. A procedure to reduce this interference is found: before starting the test with the sample, the only structure is inserted in the fridge for at least 10-15 minutes. In this way, the real test started with the structure already frozen and deformed. In the test in which this procedure is followed, the thermal effects started in the descending part of the curve.

While the effects of thermal deformation of the entire structure can be easily identify on the results, the interaction between the various steel components made a strong influence on the contact between the load sensor and the rigid structure. The test with the soils sample highlight one of the most important drawback of the set-up of the experiment.

As can be seen from the graph showing the force trend in soil sample, it increase as the sample is freezing, then there is a decreasing part of the curve. To study this anomalous behavior, the test has been interrupted during the decreasing part of the curve. The fridge was opened to check the state of sample and of the structure to understand the possibly reason. Everything was frozen, but the bolt in the superior part of the structure was completely unscrewed. The bolt, as already explained, as a relevant role for the contact. Screwing the bolt we impose a tension on the load sensor and this constraint permits to registered the strength data. The decreasing part of the curve in strength measurement is surely linked to this lose of contact. The possibly explanation is that putting the whole structure at $-40°$C generates a series of dilatation of every element which lead to unscrew the bolt.

From the theoretical point of view, some observations can be done. The temperature registered follows the trend that one can expected after the study of the literature. It decrease till it reach the temperature of freezing and then stays constant for all the process of freezing. In correspondence of the start of the phase change, the strength abruptly increase. Moreover, we registered a temperature of freezing less than $0°$C , the soil freezes at a series of point as $-1°$C. This behavior has been discussed in the theorectical part and it is described by the Clapeyron equation.

Secondly, as explained in the first chapter, the frost heaving process is caused both by the water thermal expansion and both by a flux of water caused by a phenomena similar to capillarity, cryostatic suction. Since the set-up of the experiment do not permit the simulation of presence of an aquifer from which the water can be recalled, the force registered is only due to phase change. So, with the experimental part we want to focus on the force generating only from the water freezing. Focusing at the pore dimension and considering only the water we obtain a peak of 20000 N, which is a very significant force if one think that at this force has to be added the contribute of cryostatic suction.

The analysis of the literature, highlight that most of the models neglect the phase change phenomena: not only the mechanical aspects but also doing strong approximations on the Clapeyron equation (for instance considering the density of water and ice equal in the equation). This result is very significant also because it can be a proof that the force due to water expansion can reach very huge value to not be considered negligible.

For future developments, the set-up can be improved to obtain better results and also to increase the type of experiment that can be done. The better solution can be to freeze only the sample surface using, for example, dry ice surrounding only the sample circumference. This will avoid the problems linked to the thermal dilatation of the structure and screwing bolts. With this new set-up we will be able also to provide a quantity of liquid water in contact with the inferior part of the sample to study also the force generated by cryostatic suction. Another way to improve the experiment should be to try different way of contact for soils sample to be sure to register the right intensity of the force.

Chapter 6

Comsol simulation

COMSOL Multiphysics is a cross-platform finite element analysis, solver and multiphysics simulation software. It allows to solve and simulate problem for electrical, mechanical, fluid, and chemical application. COMSOL provides some conventional physics-based interface and the possibility of write coupled systems of partial differential equations (PDEs). The user interface permits the user to recreate the scenario utilizing some predefined physical equation and made multiphisics link between different physics.

In this chapter, will be presented the simulation of temperature and pressure trend focusing on the single pore and so considering only the freezing water behavior. From the temperature point of view, we focused on the study of the energy equation and the change of phase process. There are presented two simulation which differs from the temperature boundary conditions. In the first simulation, an instantaneous boundary condition of $-40°C$ is imposed in the superior side of the sample. In the second case, a smoothly temperature gradient is imposed using a temperature function that varies from 20 to $-40°C$. The output of these simulations are: the temperature variation and the mass of water transformed into ice (and the opposite) at any time and at any depth.

The simulation of pressure exerted by the freezing sample is modeled considering the

sample as a solid body following the elastic law. A temperature gradient is imposed and through the thermal expansion coefficient the pressure increasing is modeled.

These simulations, focused at the single pore size, are the basis to built a more complex model that can simulate the frost heave process in the soil.

6.1 COMSOL simulation: Temperature field

Focusing on the pore size, the aim of the COMSOL simulation is to recreate the dynamics of temperature and pressure obtained in the laboratory experiments, considering only water sample. It will be present the result considering the two type of boundary conditions: instantaneous and not instantaneous.

6.1.1 Equations

To solve the energy conservation equation and the phase change process, has been used two modules of the physics presented in COMSOL. The Heat tranfer in porous media has been coupled with the phase change module.

Considering local thermal equilibrium, the equation presented on COMSOL is:

$$(\rho C_p)_{eff}\frac{\partial T}{\partial t} + (\rho_w C_p v)\nabla T - \nabla \cdot (\lambda_{eff}\nabla T) = Q \tag{6.1}$$

Where ρ is the fluid density, C_p the fluid heat capacity and Q is the heat source (or sink). The third term can also be express as $\mathbf{q}$ and is the conductive heat flux equal to: $\mathbf{q} = -\lambda_{eff}\nabla T$. The parameter λ_{eff} is the effective thermal conductivity.

$$(\rho C_p)_{eff} = \theta^s \rho^s C_p^s + \varepsilon \rho C_p \tag{6.2}$$

The thermal conductivity is obtained as:

$$\lambda_{eff} = \theta^s \lambda^s + \varepsilon \lambda \tag{6.3}$$

Where λ^s is the conductivity of the solid, λ is the conductivity of the fluid phase.

Then the Heat Transfer with Phase Change node is utilized to solve the heat equation after specifying the proprieties of phase change, according to the Apparent Heat Capacity

formulation.

Instead of adding a latent heat L_f in the energy balance equation exactly when the material reaches its phase change temperature $T_{f/m}$, it is assumed that the transformation occurs in a temperature interval between $T_{f/m} - \triangle T\backslash 2$ and $T_{f/m} + \triangle T\backslash 2$. In this interval, the material phase is modeled by a smoothed function, θ, representing the fraction of phase before transition, which is equal to 1 before $T_{f/m} - \triangle T\backslash 2$ and to 0 after $T_{f/m} + \triangle T\backslash 2$.

The C_p coefficient is considered as the sum of two terms: the equivalent heat capacity C_{eq}^p and the distribution of latent heat C_L.

$$C_{eq} = \frac{1}{\rho}(\theta_1 \rho_{ph1} C_{ph1}^p + \theta_2 \rho_{ph2} C_{ph2}^p) \tag{6.4}$$

And

$$C_L(T) = (H_{ph2} - H_{ph1}) \frac{d\alpha_m}{dt} \tag{6.5}$$

And so it is equal to:

$$C_p = \frac{1}{\rho}(\theta_1 \rho_{ph1} C_{ph1}^p + \theta_2 \rho_{ph2} C_{ph2}^p) + (H_{ph2} - H_{ph1}) \frac{d\alpha_m}{dt} \tag{6.6}$$

Where the indices $ph1$ and $ph2$ indicate a material in phase 1 or in phase 2, respectively. The terms θ_1 and θ_2 are equal to θ and $1 - \theta$.

The mass fraction α_m, is defined as:

$$\alpha_m = \frac{1}{2} \frac{\theta_2 \rho_{ph2} - \theta_1 \rho_{ph1}}{\rho} \tag{6.7}$$

It is equal to $-1/2$ before transformation and $1/2$ after transformation. The latent heat distribution C_L is approximated by:

$$C_L(T) = L_f \frac{d\alpha_m}{dt} \tag{6.8}$$

so that the total heat per unit volume released during the phase transformation coincides with the latent heat:

$$\int_{T_{f/m}+\triangle T/2}^{T_{f/m}-\triangle T/2} C_L(T)dT = \int_{T_{f/m}+\triangle T/2}^{T_{f/m}-\triangle T/2} L_f \frac{d\alpha_m}{dt} dT = L_f \tag{6.9}$$

The effective thermal conducibility reduces to:

$$\lambda = \theta_1 \lambda_{ph1} + \theta_2 \lambda_{ph2} \tag{6.10}$$

The density, ρ, and the specific enthalpy, H, are expressed by:

$$\rho = \theta_1 \rho_{ph1} + \theta_2 \rho_{ph2} \tag{6.11}$$

So, the equation modeled in Comsol are:

$$(\rho C_p)_{eff} \frac{\partial T}{\partial t} + (\rho_w C_p v)\nabla T - \nabla \cdot (\lambda_{eff} \nabla T) = Q \tag{6.12}$$

Where:

$(\rho C_p)_{eff} = \theta^s \rho^s C_p^s + \varepsilon(\theta_1 \rho_{ph1} C_{ph1}^p + \theta_2 \rho_{ph2} C_{ph2}^p) + L_f \frac{d\alpha_m}{dt}$

Comparing with the system of equation applied for saturated case reported in the chapter 2 , it can be seen that the equation has the same form. (The system is written in terms of saturation of both phase which is equal to the volumetric content divided the porosity).

6.1.2 Geometry and mesh

The geometry utilized on the simulation is a rectangular of 5 cm of diameter and 2,5 cm of height, fig.6.1. The geometry'dimensions are the same of the water sample used in the laboratory test.

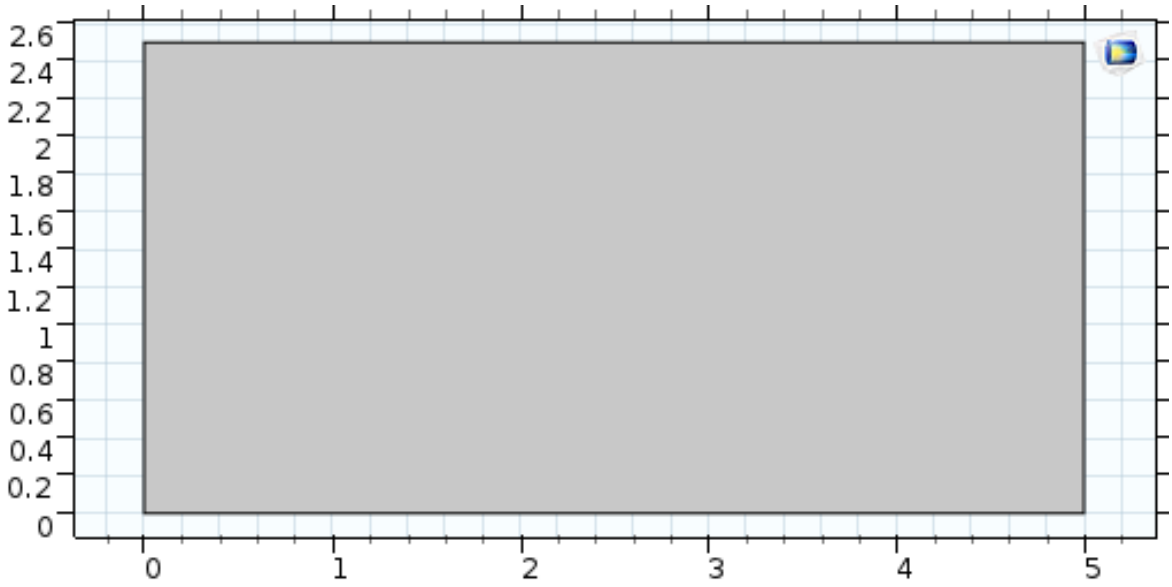

Figure 6.1: Geometry of water sample.

In the software is it possible to insert a probe in the domain to register the variation of a specific variable in a specific point. In the simulation,a probe was placed in the center on the inferior part of the geometry, fig.6.2. The aim is to compare the temperature trend obtained by the simulation with the temperature data registered by the temperature sensor in the experimental test.

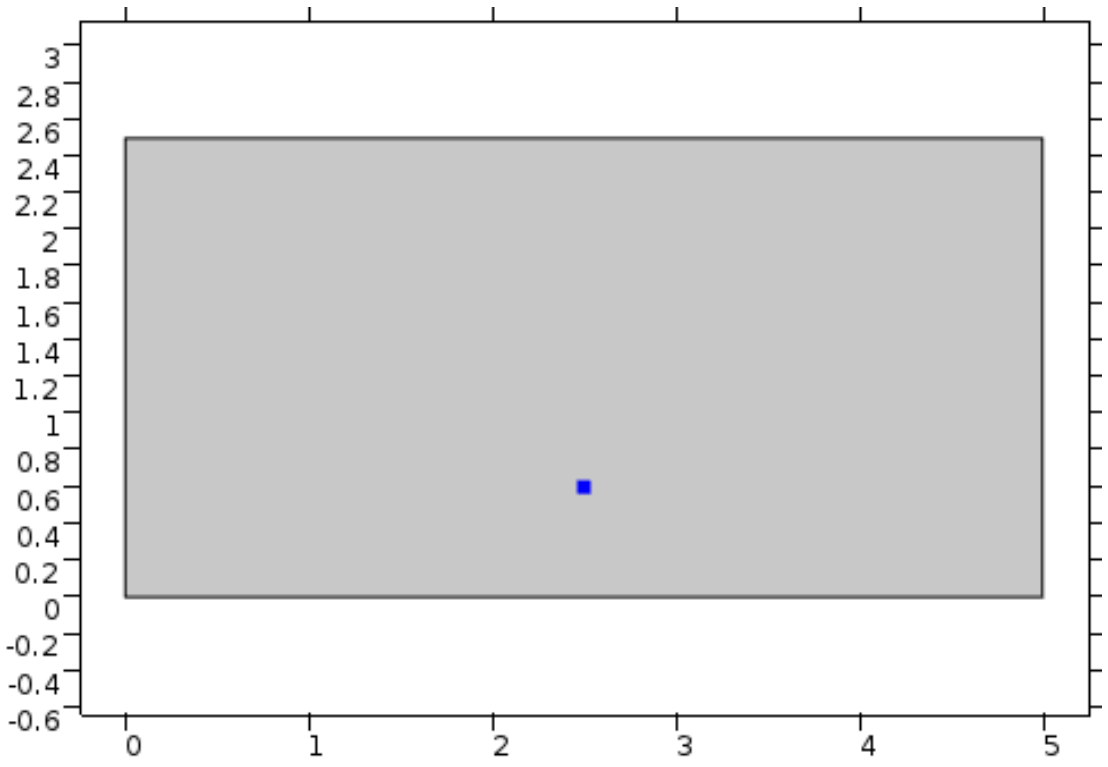

Figure 6.2: Probe to register temperature data in a point of the geometry.

The mesh has a relevant importance on the simulation results. Depending on the size and type of the element of the mesh, the results can have more or less numerical instabilities. This can be seen in the scheme on figure 6.3.

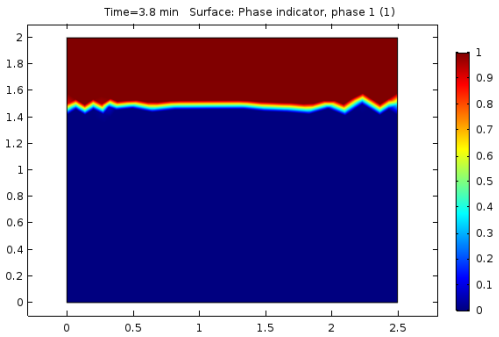

(a) Numerical instabilities on mass exchange results using the mesh 1.

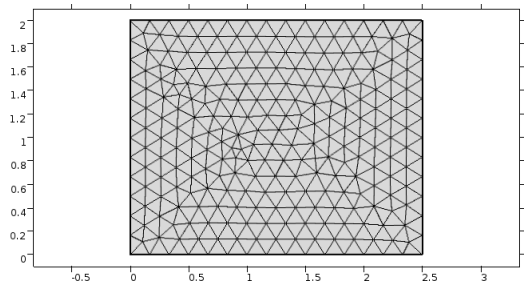

(b) Mesh 1.

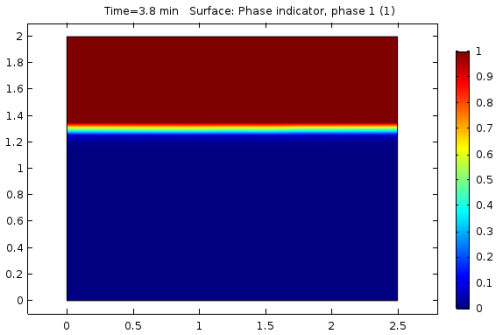

(c) Mass exchange results using a regular and symmetric mesh (mesh2).

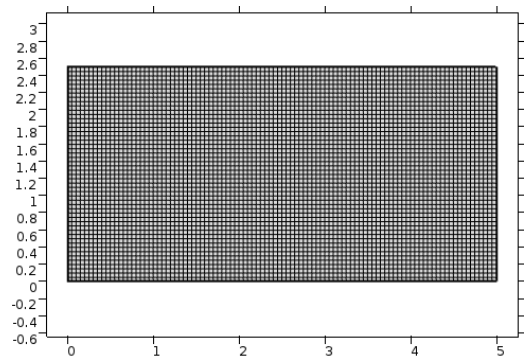

(d) Mesh 2.

Figure 6.3: Example of numerical instabilities variation in the results depending on the mesh.

The mesh utilized for the simulation is regular, symmetric and composed by very fine elements, fig.6.4.

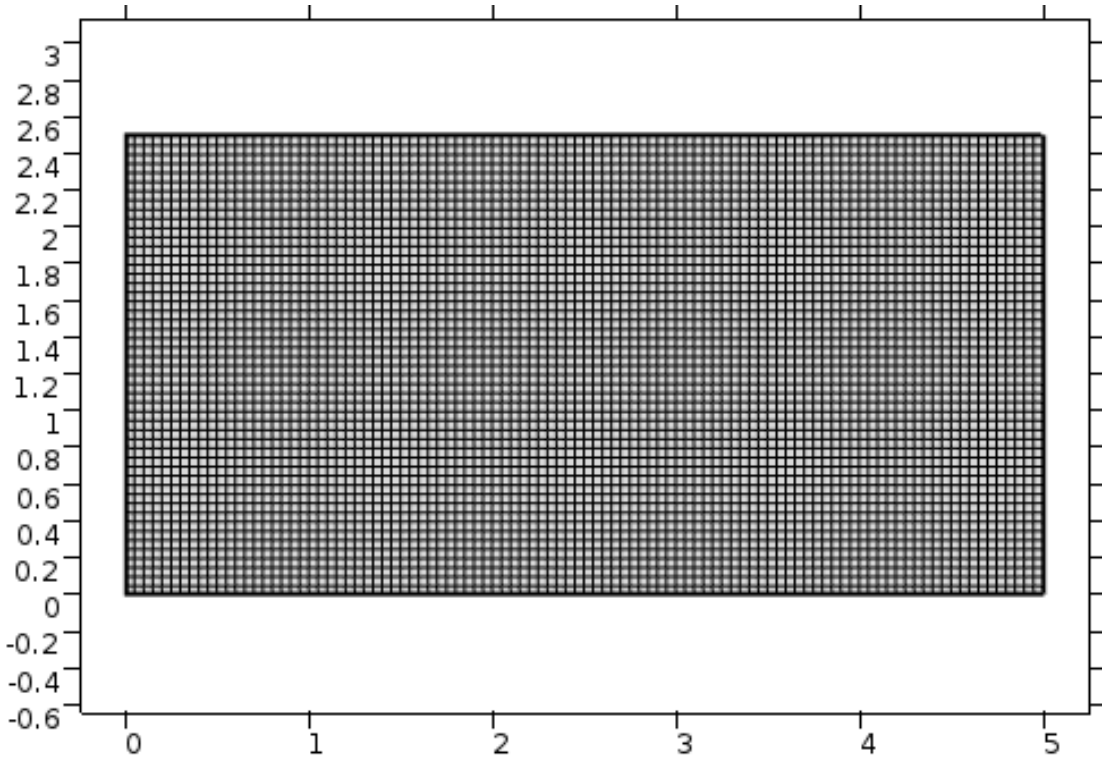

Figure 6.4: Mesh used for the simulations.

6.1.3 Simulation of a water sample

Boundary and initial conditions

Considering only a water sample, the equations solved are the same already presented but obviously there are not the thermal coefficient relative to the terrain. The sample of water is considered to be at ambient temperature, 20°C, at the initial time of simulation, fig.6.5.

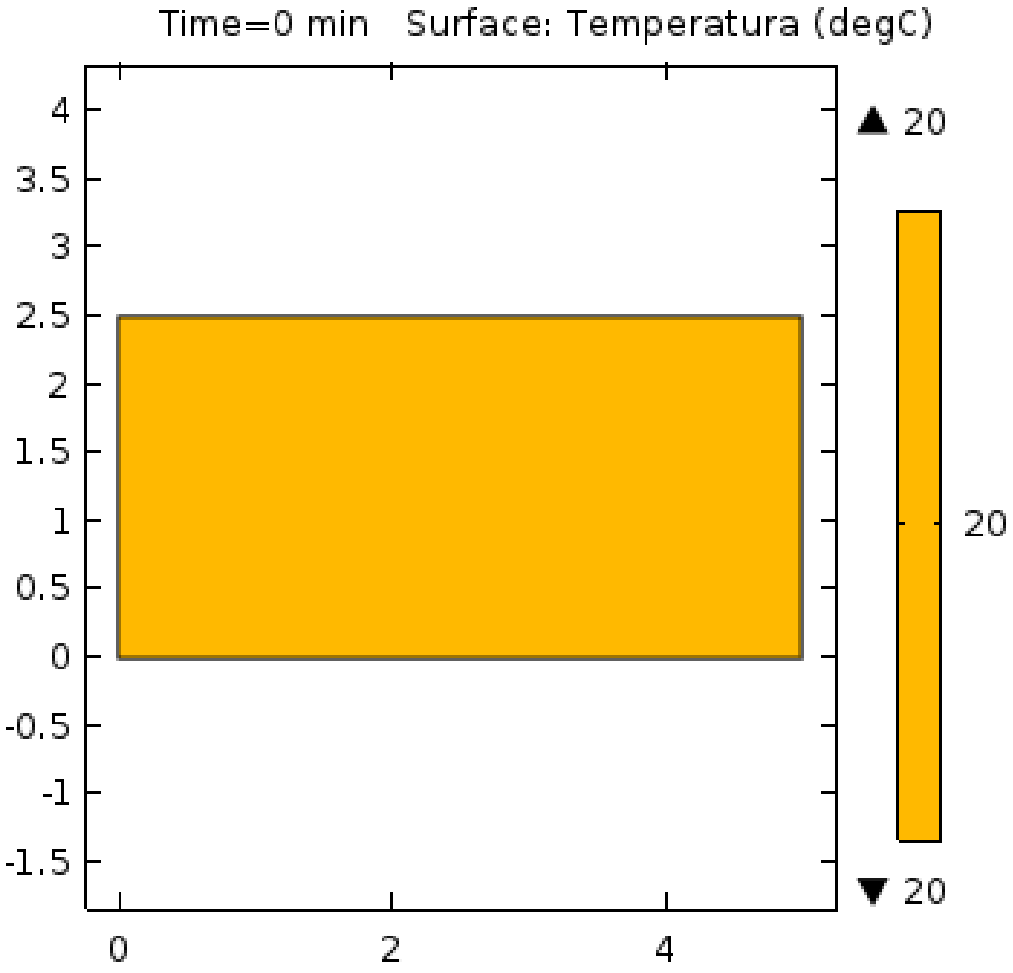

Figure 6.5: Initial values of temperature.

The software permits to impose temperature boundary condition on the various side. In the following pages are presented two simulations. The first one has a instantaneous

boundary condition of $-40°C$ in the upper side of the sample, while in the second one a stepped function is imposed to obtain a gradually variation of the temperature.

This function, called T_{right}, varies from $20°C$ to $-40°C$, fig.6.6. This function is imposed as boundary condition on the superior part of the probe and thermal insulation in the remain sides.

function.png

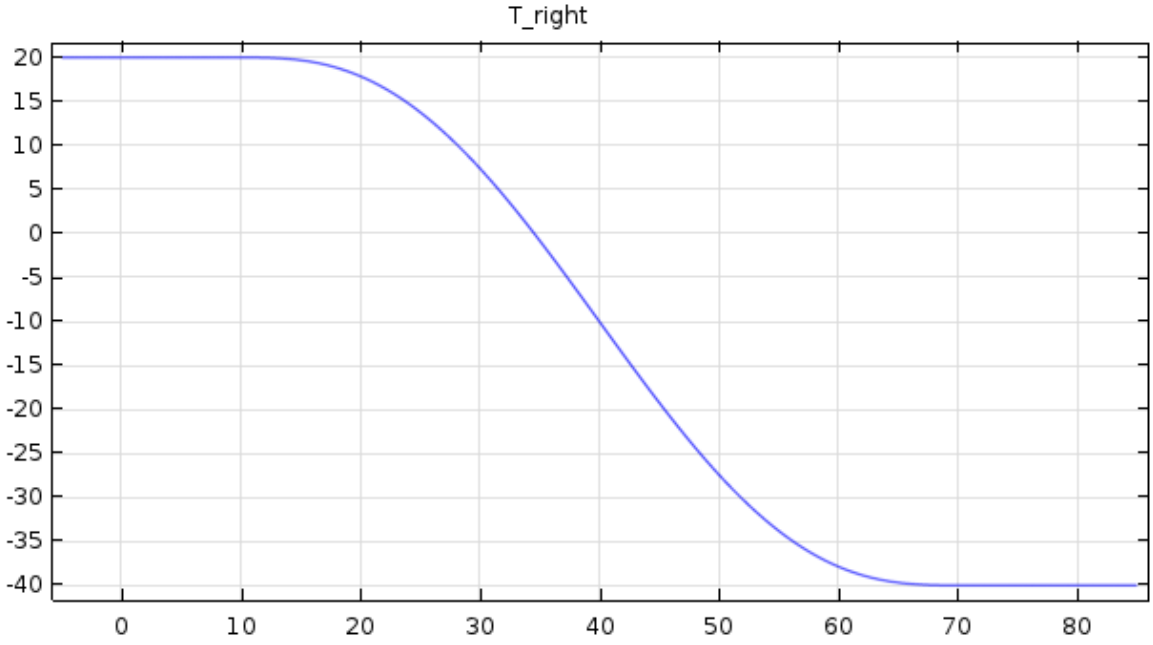

Figure 6.6: Temperature function as boundary condition on the superior side of the sample.

The COMSOL software has a physics to simulate the heat transmission on fluid and the phase change. As a results of the energy conservation equation the software gives as output the quantity of ice formed during the freezing process. The grade of saturation of the two phase are presented in the graph results as "phase indicator": the phase 1 is the ice phase and the phase 2 is the water phase.

Since this is an output of the energy equation we can not impose the initial condition of the saturation. As it will be seen in the results, the phase indicator 2 (water saturation) is equal to 1 till the freezing process started. At the end of the simulation the phase

indicator 2 is equal to 0, fig.6.7. The results presented are in terms of water saturation; the ice saturation can be calculated from the simple equation: $phaseindicator1 = 1 - phaseindicator2$.

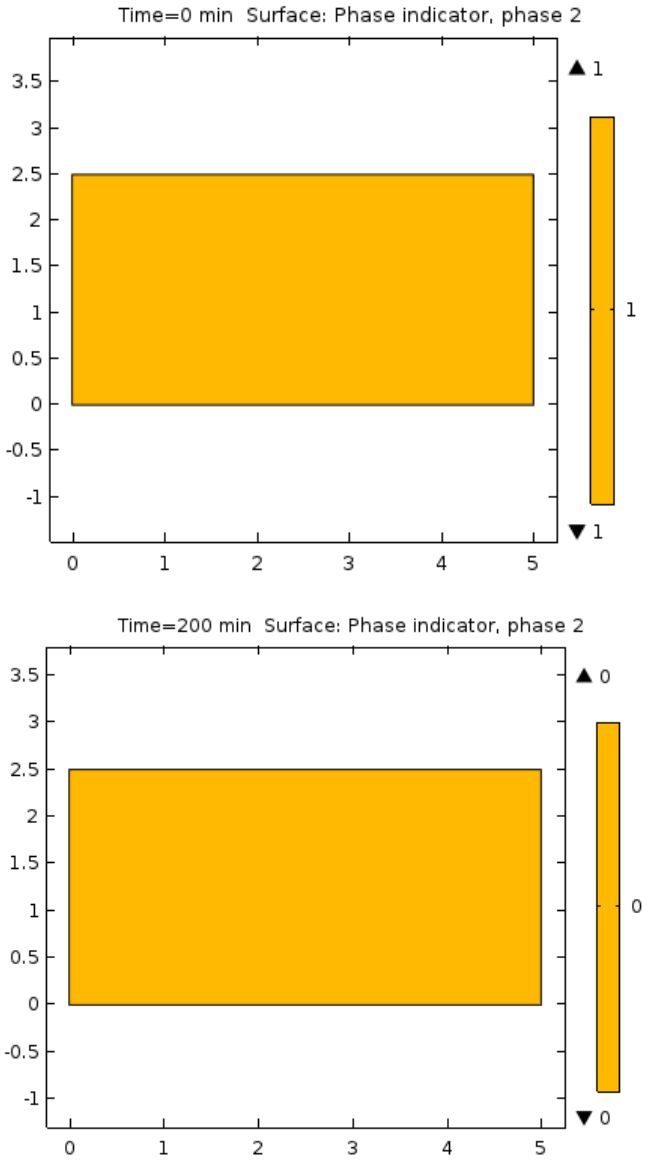

Figure 6.7: Water change of mass (phase indicator 2) at the initial time and last time of simulation.

Parameters and steps of simulation

The software COMSOL permits to proceed for different steps, called Studies. The simulation of temperature fields follows these steps.

1. Study 1. A stationary condition of temperature is imposed, applying only the initial temperature value. This is the initial condition of the sample.

2. Study 2. On the base of the previous test results the boundary condition temperature is enabled.

The parameter utilized on the simulation are summarized in the following table.

Symbols	Parameters	Value	Units
C_p^w	Water heat capacity	4179	$J/(kgK)$
λ^w	Water thermal conductivity	0.613	$W/(mK)$
ρ^w	Water density	997	$kg/(m^3)$
C_p^i	Ice heat capacity	2052	$J/(kgK)$
λ^i	Ice thermal conductivity	2.31	$W/(mK)$
ρ^i	Ice density	918	$kg/(m^3)$
L_f	Latent heat	333.5	kJ/kg

Results with instantaneous boundary conditions

As a first attempt, the first simulation were done imposing an instantaneous boundary condition of $-40°C$ at the superior side. Running a simulation of 200 minute we obtain as results the trend of temperature in the sample, fig.6.8.

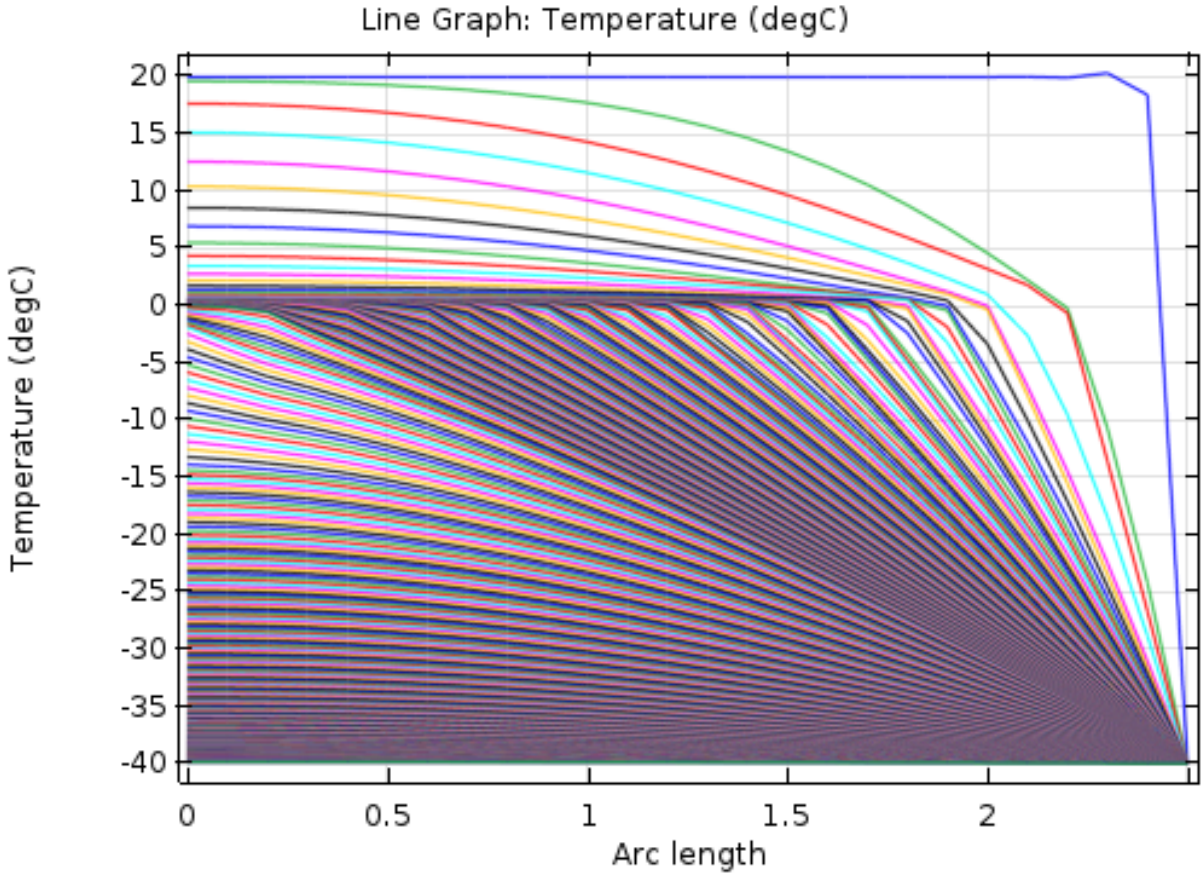

Figure 6.8: Temperature data taken every 0.2 minute of simulation.

In the x axis there is the depth of sample and in the ordinate there are the temperature value at the various time of the simulation. The time increase from the top to the downside of the graph. At the start everything is at a temperature of $20°C$ and then after more then 200 minutes it reach $-40°C$.

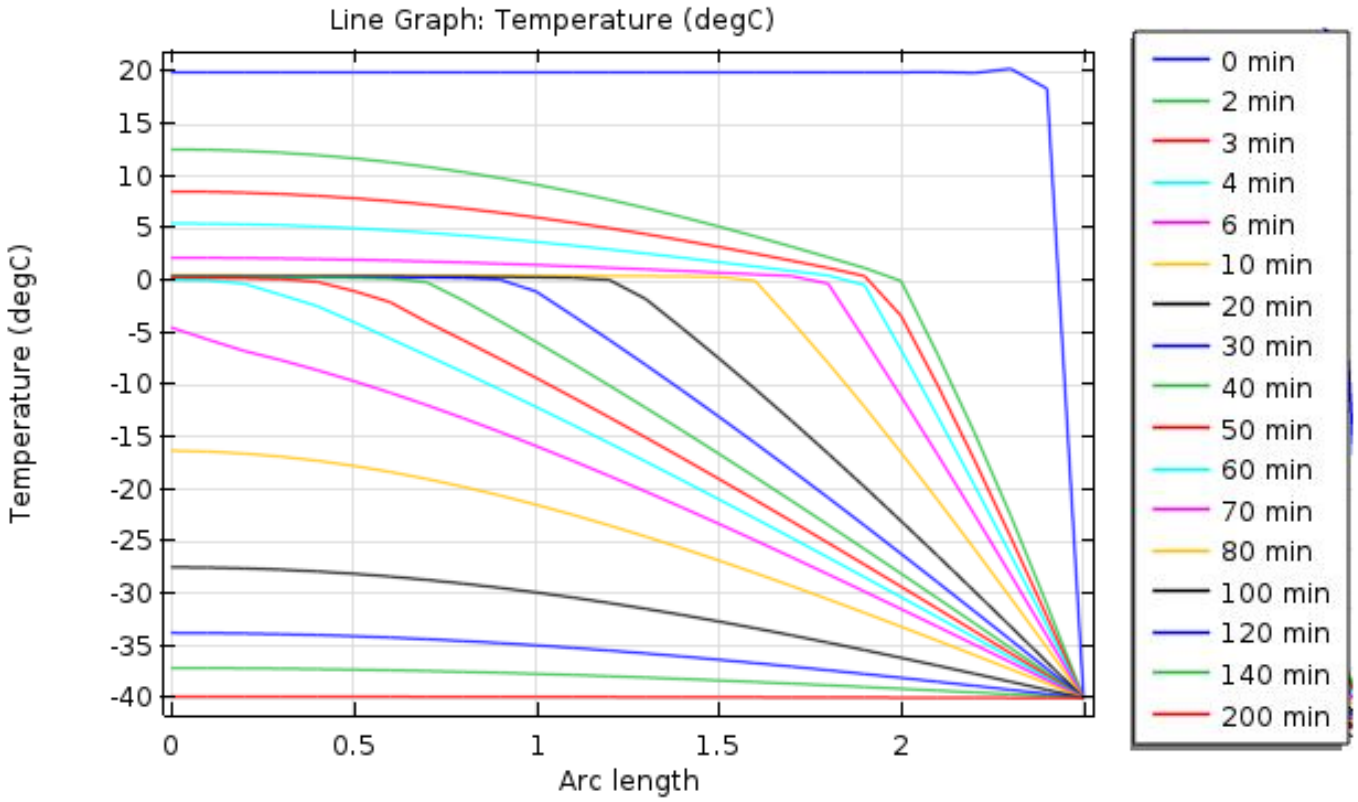

Figure 6.9: Temperature data at various depth collected at specific time of the simulation.

In the fig.6.9 there are the same temperature data but taken at specific time, to have a better view of the results. Every line correspond to a time of the simulation, the time is in crescent order from the top of the graph. From both graph it can be seen that the temperature stay constant at 0°C for a certain time. After 70 minutes the whole sample is frozen because the temperature is at every depth less than zero. It takes 200 minute to reach the temperature of -40°C in the whole sample.

The COMSOL software permits to insert a probe in the domain, to have as results the temperature trend in a specific point of the domain. Looking at the temperature variation in a point at the center of sample we obtain the behavior already observed in the experimental results, see fig.6.19(p).

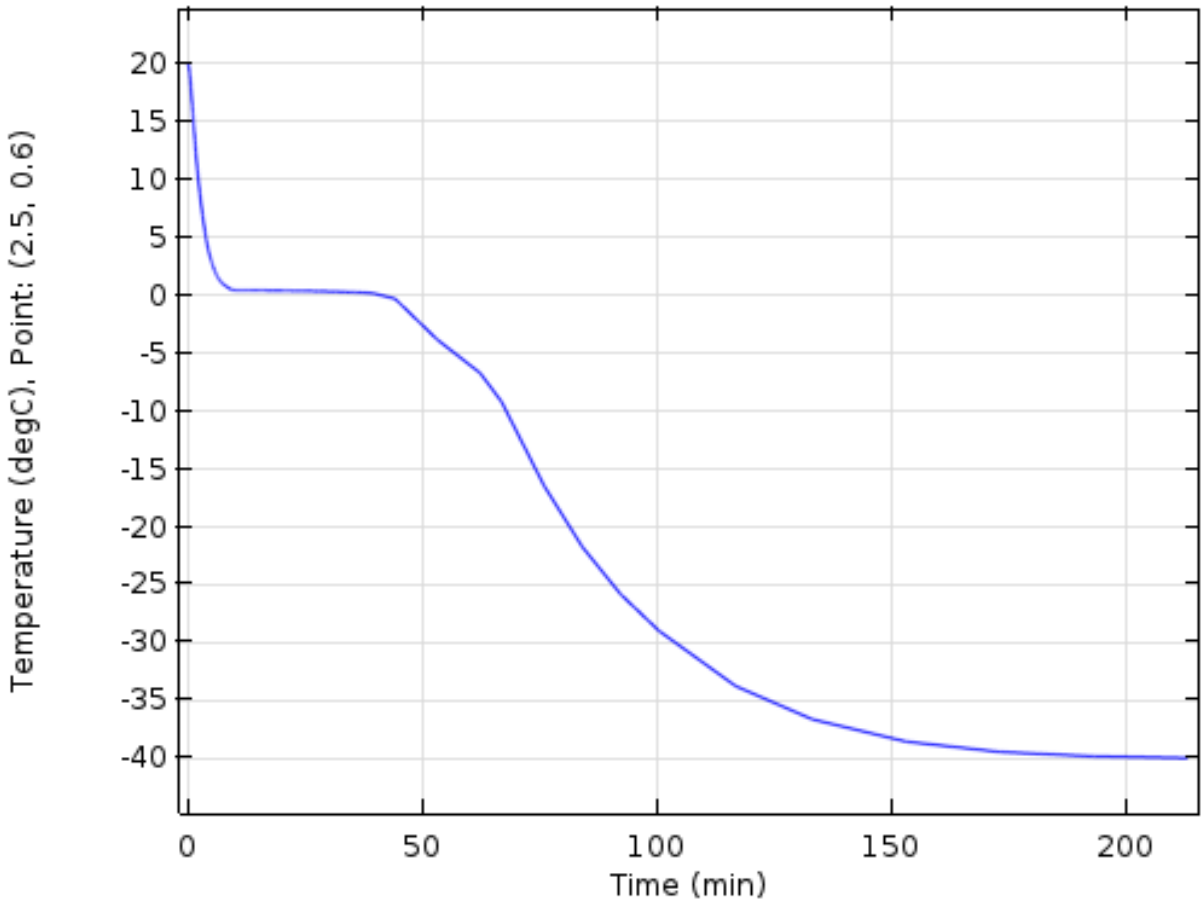

Figure 6.10: Temperature trend in a point of the domain.

The temperature decreases till it reaches a value of almost 0°C, then during the freezing process the temperature stays constant. After the freezing process is concluded the temperature continue to decreases.

As an output of the simulation we have also the variation of ice and water content during the time. It can be seen from fig.6.12 the trend of water content (phase indicator 2). It varies from 0 to 1 and in the last time it is equal to 0 (fig.6.12,6.11).

In this graph, fig.6.11, it can be seen the trend of the water phase indicator at the various time, this variable represents the exchange of mass due to phase-change. Every line correspond to the value of water content at a specific time. The time increase from the right to the left side of the graph.

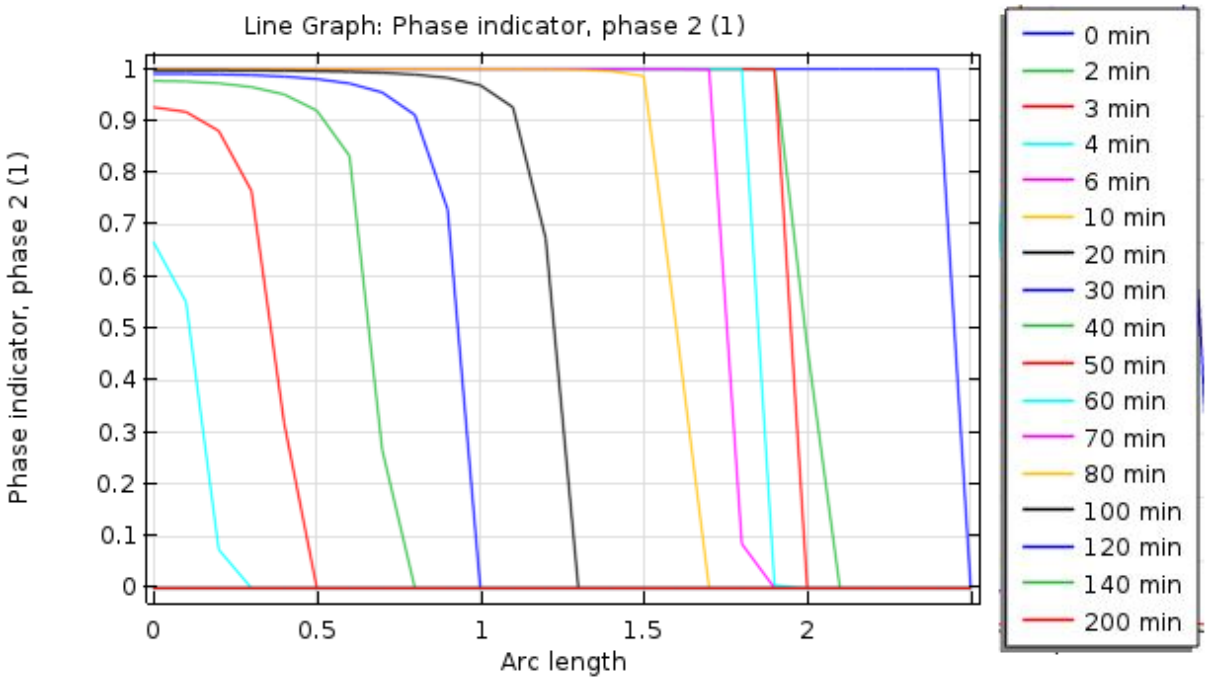

Figure 6.11: Water content trend at selected time.

At the superior side (height: 2.5 cm) the first line start from 0 because we are imposing an instantaneous temperature of $-40°C$, so that point is considered already frozen and the water phase indicator is equal to zero. Then after 70 minutes the curve are equal to zero for every depth of sample. The freezing process is finished and the phase indicator stays at the value of zero for the rest of the simulation time. In the next figure, fig.6.12, it can be seen the trend of water phase indicator considering all the simulation time.

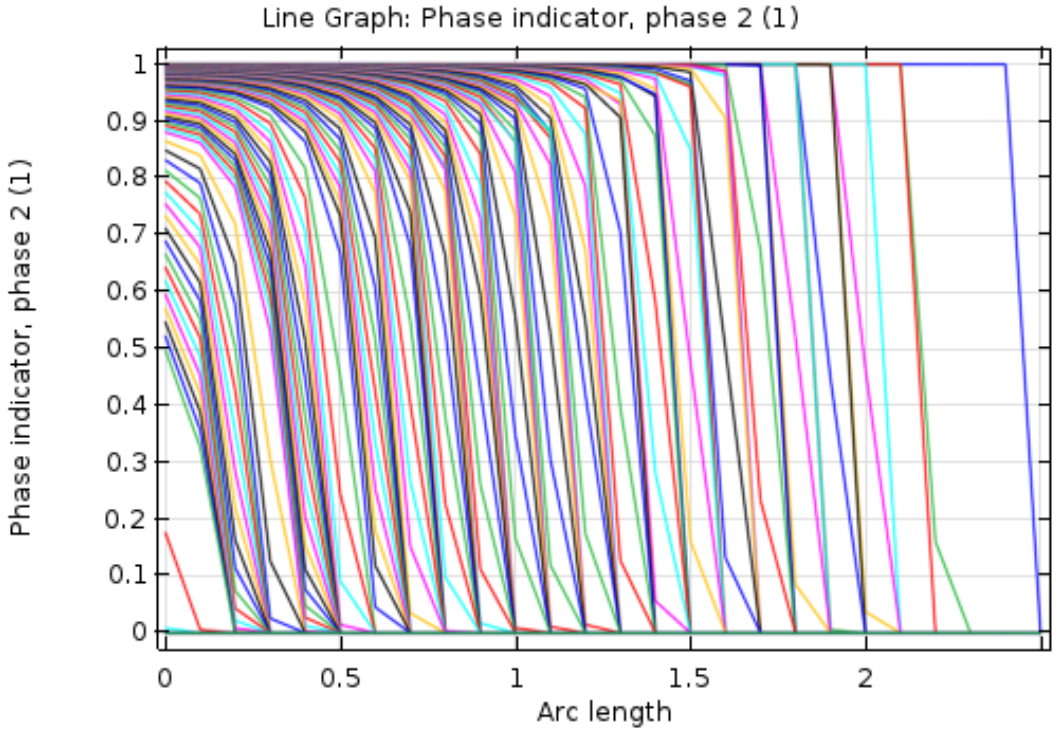

Figure 6.12: Water content trend at various time of the simulation, data measured every 0.2 minute.

In the following pages it will be showed the trend of temperature and then of the phase indicator in the whole sample for different time.

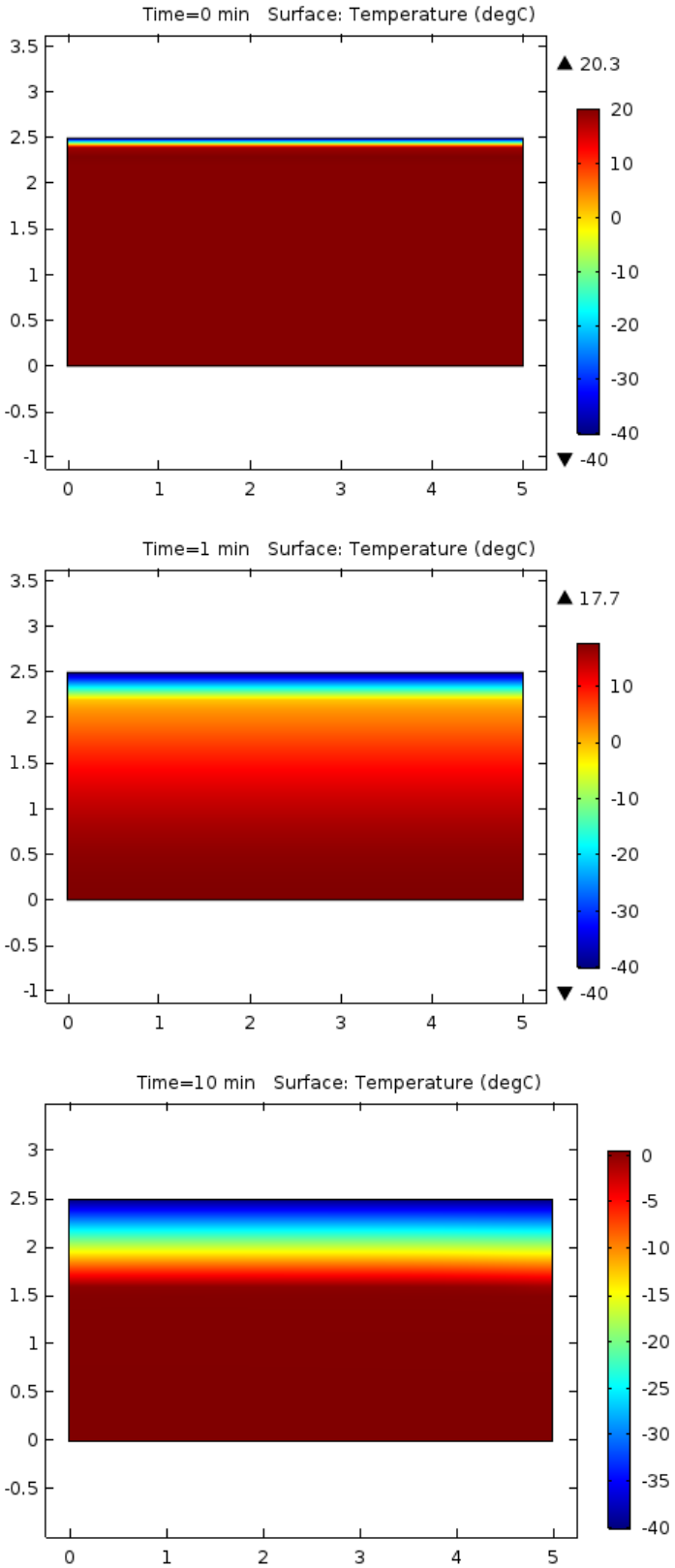
Time=0 min Surface: Temperature (degC)
▲ 20.3
20
10
0
-10
-20
-30
-40
▼ -40
Time=1 min Surface: Temperature (degC)
▲ 17.7
10
0
-10
-20
-30
-40
▼ -40
Time=10 min Surface: Temperature (degC)
0
-5
-10
-15
-20
-25
-30
-35
-40

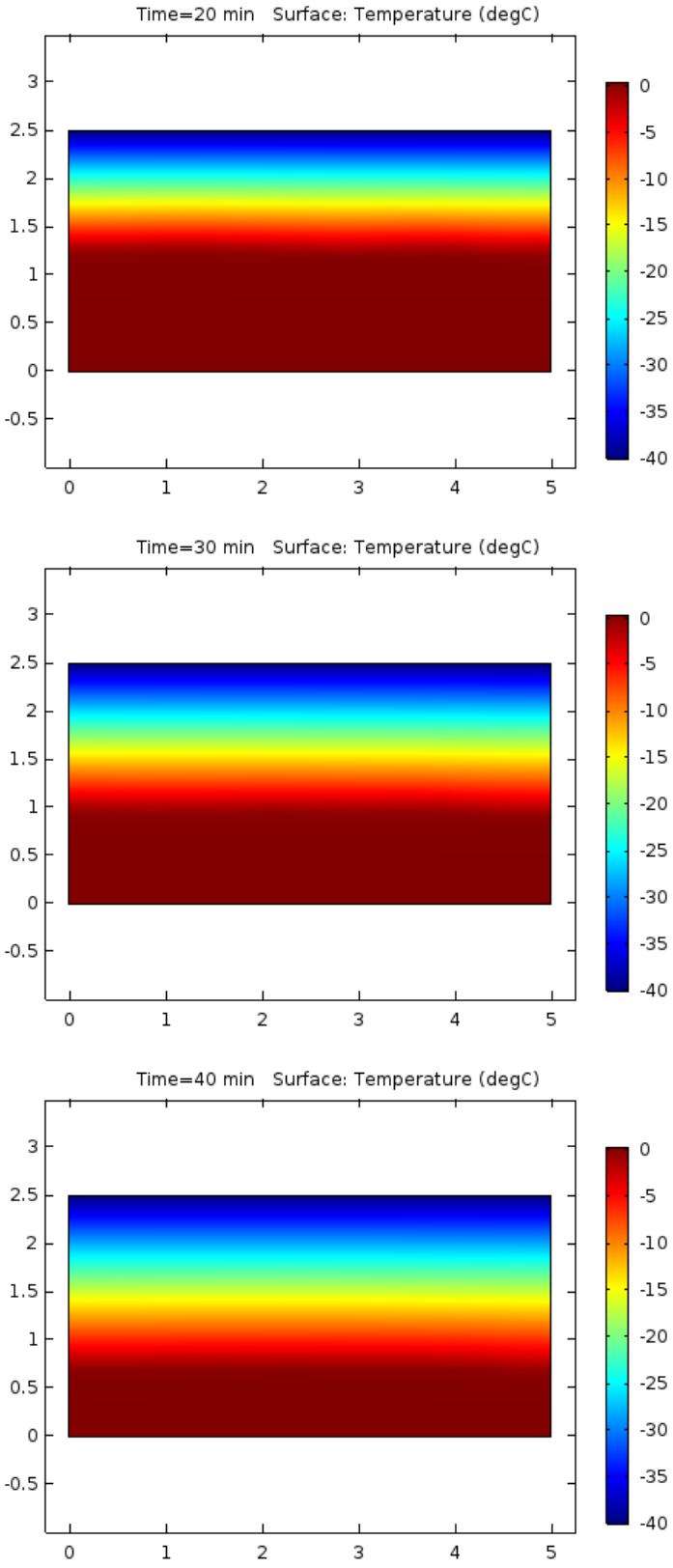
Time=20 min Surface: Temperature (degC)
3
2.5
2
1.5
1
0.5
0
-0.5
0
1
2
3
4
5
0
-5
-10
-15
-20
-25
-30
-35
-40
Time=30 min Surface: Temperature (degC)
3
2.5
2
1.5
1
0.5
0
-0.5
0
1
2
3
4
5
0
-5
-10
-15
-20
-25
-30
-35
-40
Time=40 min Surface: Temperature (degC)
3
2.5
2
1.5
1
0.5
0
-0.5
0
1
2
3
4
5
0
-5
-10
-15
-20
-25
-30
-35
-40

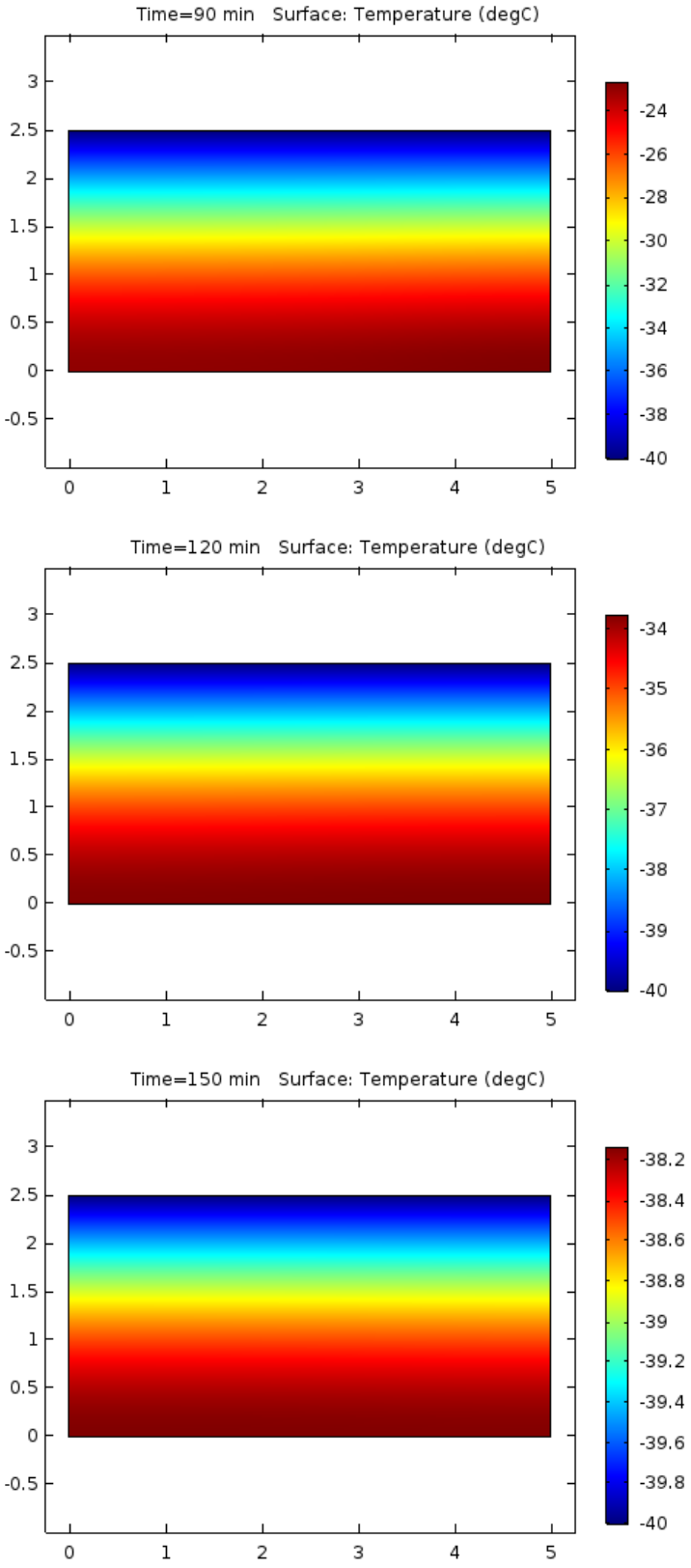
Time=90 min Surface: Temperature (degC)
-24
-26
-28
-30
-32
-34
-36
-38
-40
Time=120 min Surface: Temperature (degC)
-34
-35
-36
-37
-38
-39
-40
Time=150 min Surface: Temperature (degC)
-38.2
-38.4
-38.6
-38.8
-39
-39.2
-39.4
-39.6
-39.8
-40

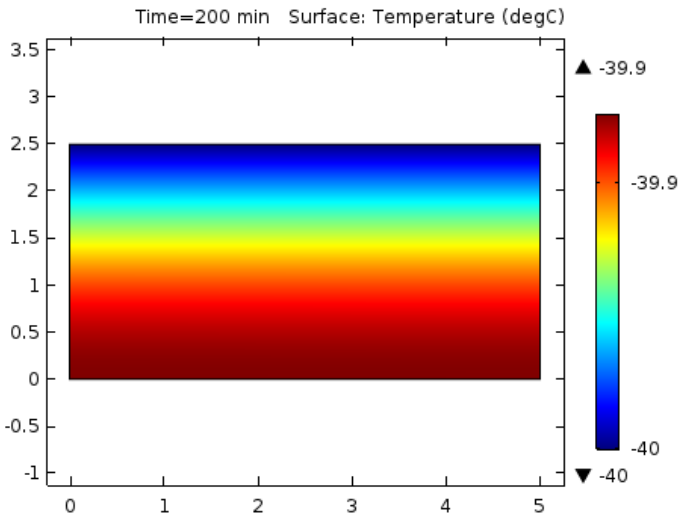
Time=200 min Surface: Temperature (degC)
3.5
3
2.5
2
1.5
1
0.5
0
-0.5
-1
0
1
2
3
4
5
▲ -39.9
-39.9
-40
▼ -40

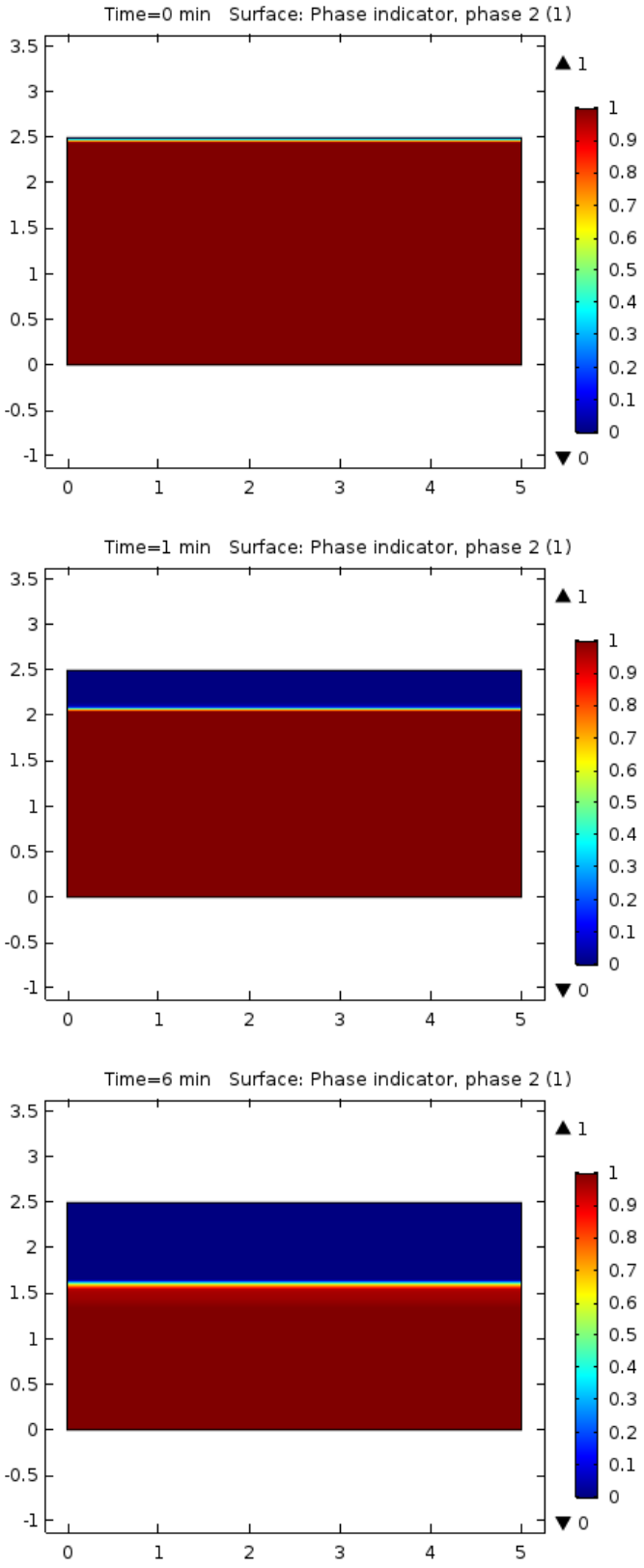
Time=0 min Surface: Phase indicator, phase 2 (1)
Time=1 min Surface: Phase indicator, phase 2 (1)
Time=6 min Surface: Phase indicator, phase 2 (1)
▲ 1
▼ 0
1
0.9
0.8
0.7
0.6
0.5
0.4
0.3
0.2
0.1
0
3.5
3
2.5
2
1.5
1
0.5
0
-0.5
-1
0
1
2
3
4
5

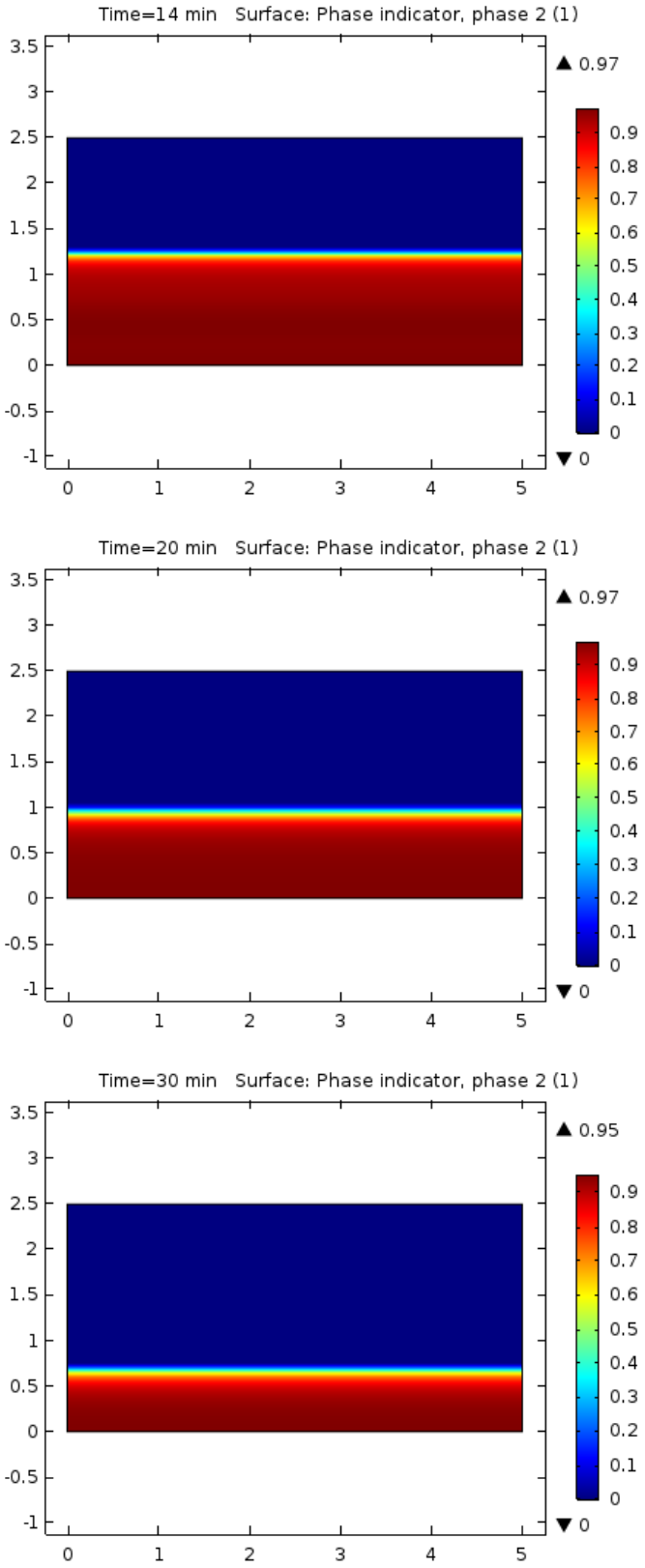
Time=14 min Surface: Phase indicator, phase 2 (1)
▲ 0.97
0.9
0.8
0.7
0.6
0.5
0.4
0.3
0.2
0.1
0
▼ 0
3.5
3
2.5
2
1.5
1
0.5
0
-0.5
-1
0
1
2
3
4
5
Time=20 min Surface: Phase indicator, phase 2 (1)
▲ 0.97
0.9
0.8
0.7
0.6
0.5
0.4
0.3
0.2
0.1
0
▼ 0
3.5
3
2.5
2
1.5
1
0.5
0
-0.5
-1
0
1
2
3
4
5
Time=30 min Surface: Phase indicator, phase 2 (1)
▲ 0.95
0.9
0.8
0.7
0.6
0.5
0.4
0.3
0.2
0.1
0
▼ 0
3.5
3
2.5
2
1.5
1
0.5
0
-0.5
-1
0
1
2
3
4
5

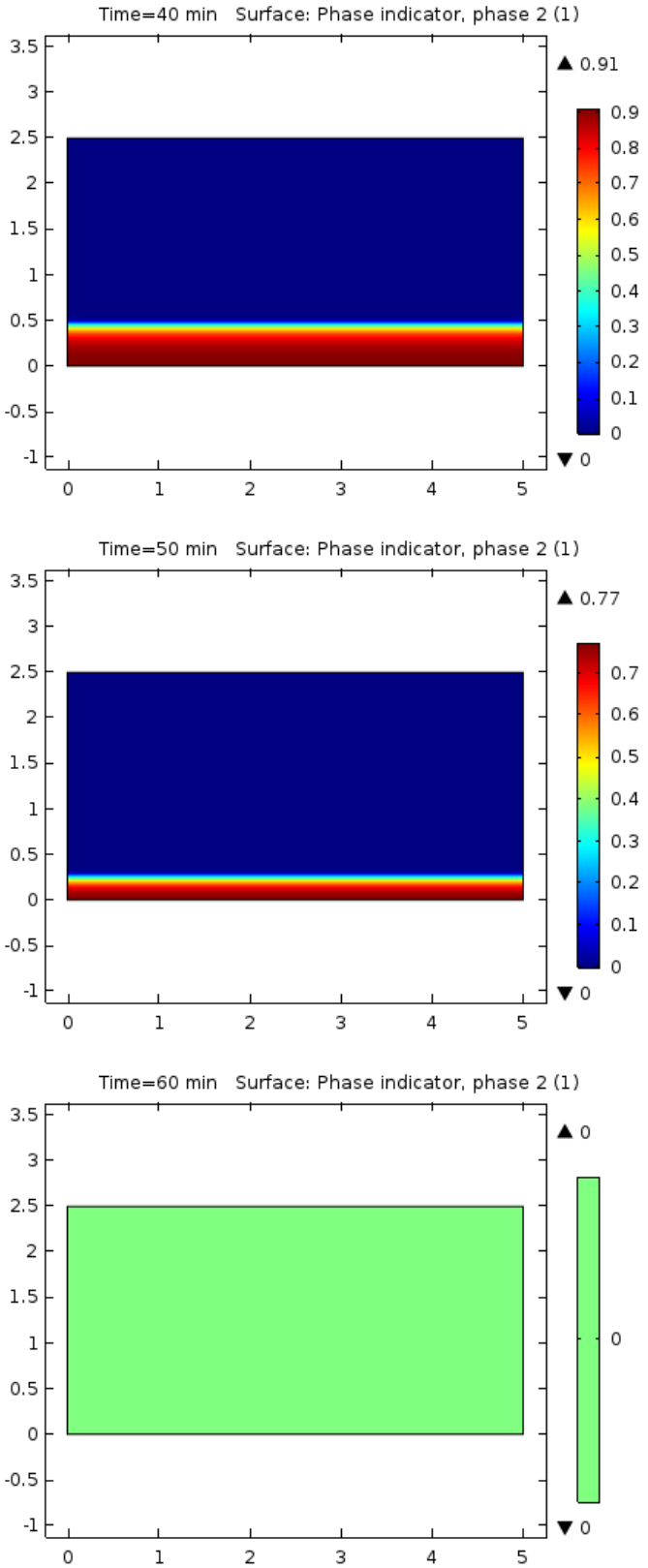
Time=40 min Surface: Phase indicator, phase 2 (1)
▲ 0.91
0.9
0.8
0.7
0.6
0.5
0.4
0.3
0.2
0.1
0
▼ 0
3.5
3
2.5
2
1.5
1
0.5
0
-0.5
-1
0
1
2
3
4
5
Time=50 min Surface: Phase indicator, phase 2 (1)
▲ 0.77
0.7
0.6
0.5
0.4
0.3
0.2
0.1
0
▼ 0
Time=60 min Surface: Phase indicator, phase 2 (1)
▲ 0
0
▼ 0

Results with temperature function

The simulation has been done considering a temperature function as boundary condition, see fig.6.6 at the begin of this chapter. Here will be presented the results.

Analyzing the temperature trend in a point of the domain (fig.6.13), it can be seen that in this simulation the first region of the curve is more representative of the real conditions. Indeed, considering the experimental set-up the temperature gradient is not instantaneous. In the experiment, the water sample is in contact with steel elements which need some time to reach the fridge's temperature. So, a gradually decreasing of temperature in the first minutes of simulation is more representative of the real situation.

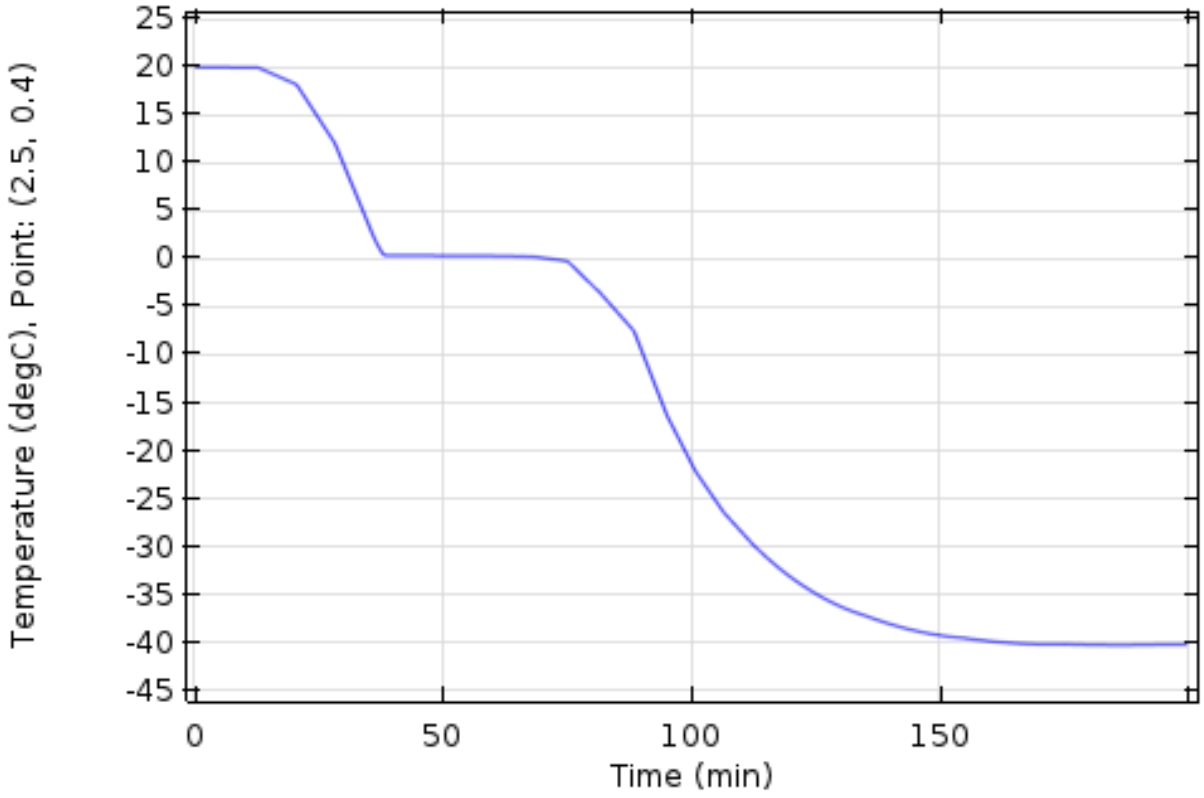

Figure 6.13: Temperature trend in a point of the domain considering a non instantaneous boundary condition.

The graph in fig.6.14 is the variation of the temperature in a section passing through the center of the sample. In the x-axis there is the sample depth, varying from 0 to 2.5 cm; and in correspondence of every depth the respective temperature values for the time considered. In the fig.6.14 , some specific time are seletioned to have a better view of the results. We can see that at the first time the temperature is at 20C and at the last time at $-40°C$ in all the sample. Moreover, the temperature stayed constant ad $0°C$, when the freezing process is happening. Comparing the results with the previous simulation, in this case the freezing process ended after 120 minutes.

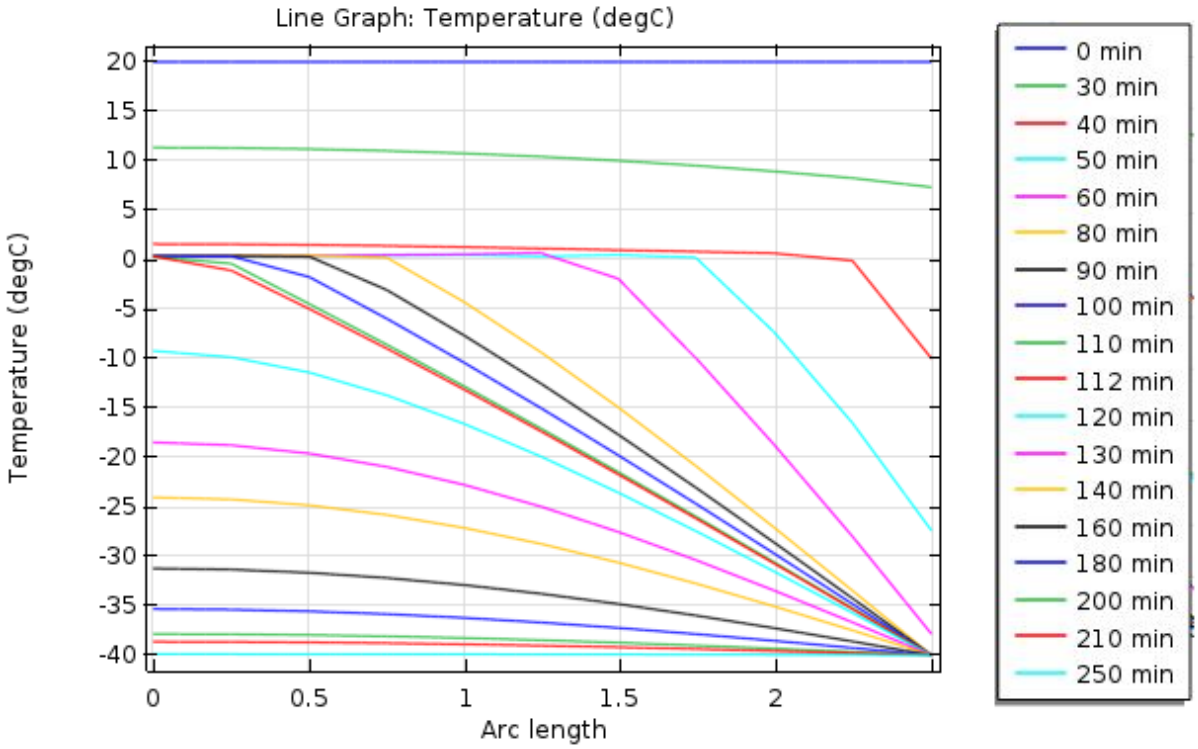

Figure 6.14: emperature data at various depth collected at specific time of the simulation.

In fig.6.15 is presented the trend collected every 6 minutes of simulation. The time increase from the top to the downside of the graph.

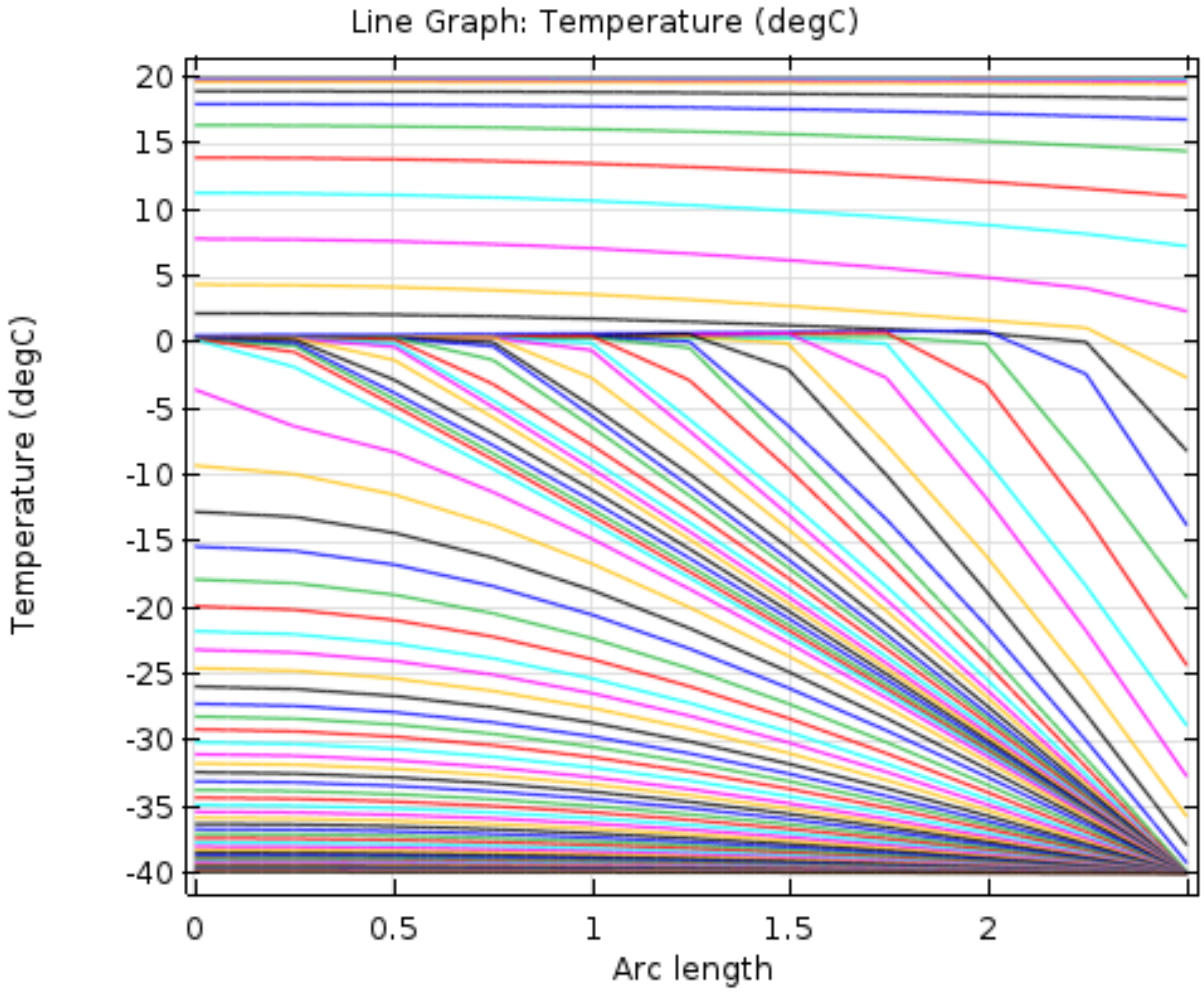

Figure 6.15: Temperature data at various depth collected every 6 minutes of simulation.

In the following pages will be presented the variation of temperature at every depth for selected time. Comparing with the previous results, it can be seen as the temperature varies more gradually in the whole sample.

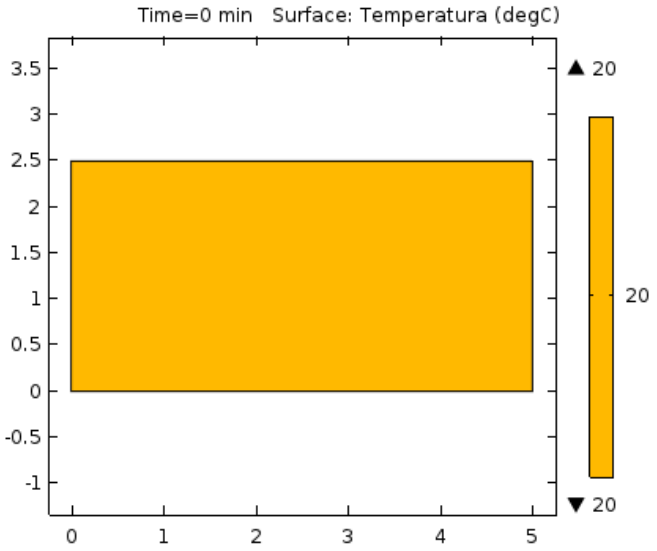
Time=0 min Surface: Temperatura (degC)
▲ 20
20
▼ 20
3.5
3
2.5
2
1.5
1
0.5
0
-0.5
-1
0
1
2
3
4
5

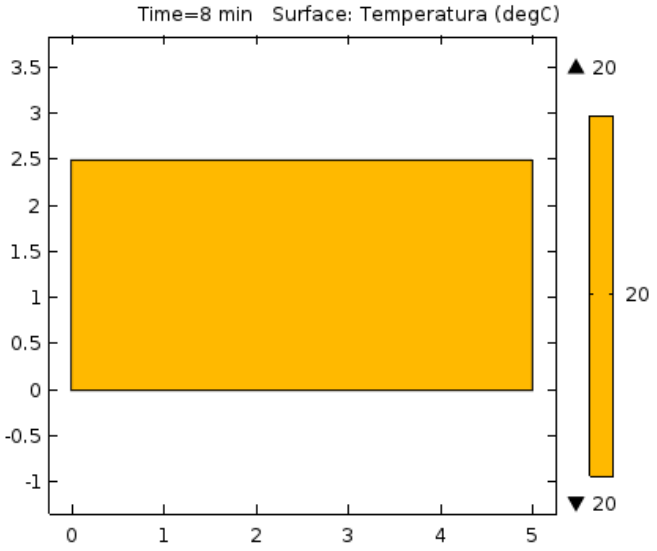
Time=8 min Surface: Temperatura (degC)
▲ 20
20
▼ 20
3.5
3
2.5
2
1.5
1
0.5
0
-0.5
-1
0
1
2
3
4
5

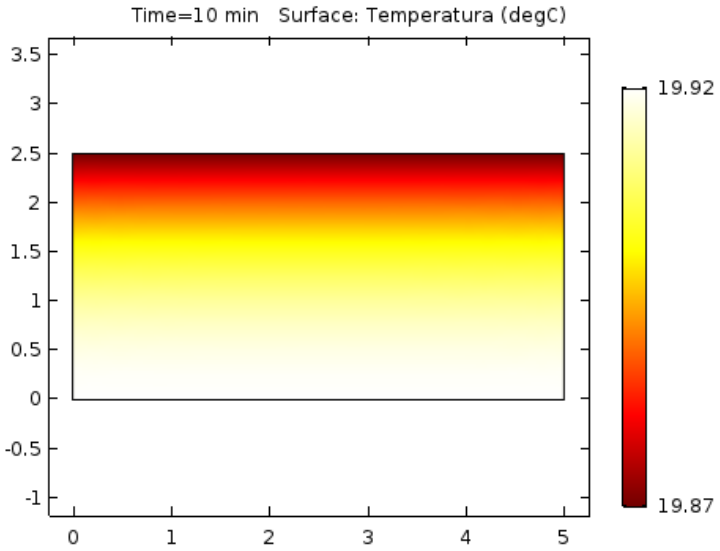
Time=10 min Surface: Temperatura (degC)
19.92
19.87
3.5
3
2.5
2
1.5
1
0.5
0
-0.5
-1
0
1
2
3
4
5

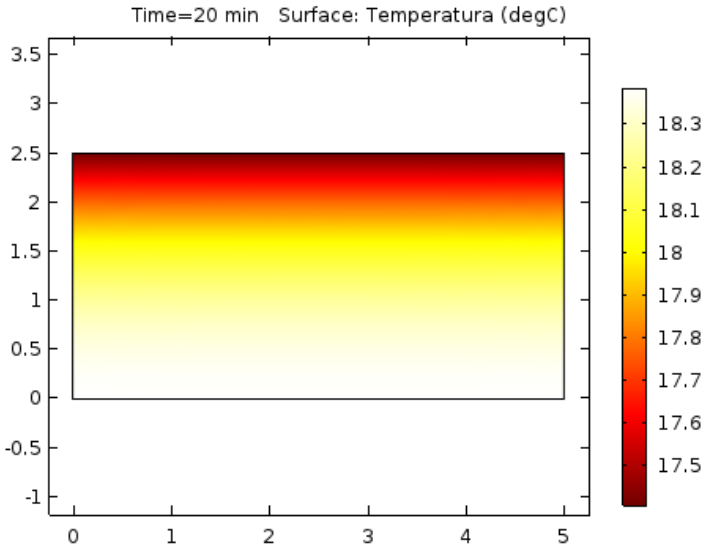
Time=20 min Surface: Temperatura (degC)
3.5
3
2.5
2
1.5
1
0.5
0
-0.5
-1
0
1
2
3
4
5
18.3
18.2
18.1
18
17.9
17.8
17.7
17.6
17.5

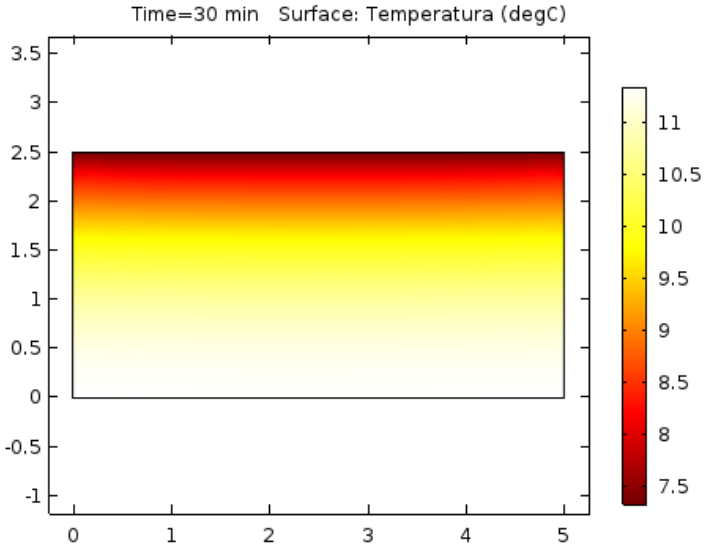
Time=30 min Surface: Temperatura (degC)
3.5
3
2.5
2
1.5
1
0.5
0
-0.5
-1
0
1
2
3
4
5
11
10.5
10
9.5
9
8.5
8
7.5

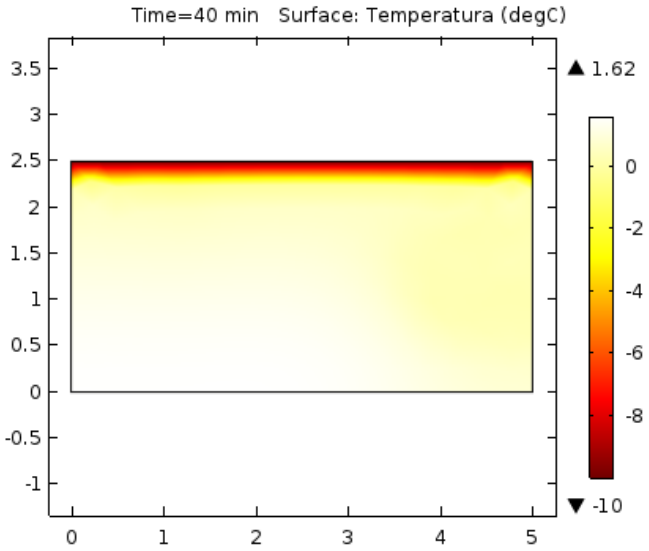
Time=40 min Surface: Temperatura (degC)
3.5
3
2.5
2
1.5
1
0.5
0
-0.5
-1
0
1
2
3
4
5
▲ 1.62
0
-2
-4
-6
-8
▼ -10

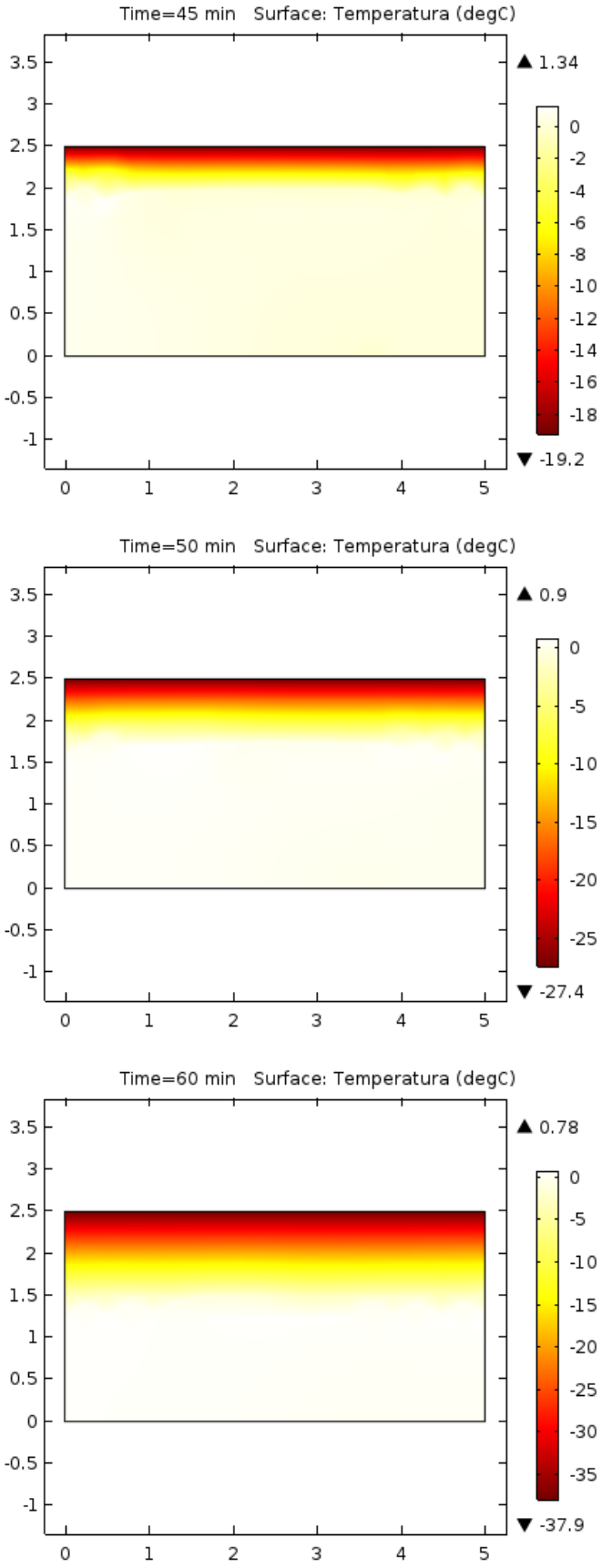
Time=45 min Surface: Temperatura (degC)
▲ 1.34
0
-2
-4
-6
-8
-10
-12
-14
-16
-18
▼ -19.2
Time=50 min Surface: Temperatura (degC)
▲ 0.9
0
-5
-10
-15
-20
-25
▼ -27.4
Time=60 min Surface: Temperatura (degC)
▲ 0.78
0
-5
-10
-15
-20
-25
-30
-35
▼ -37.9

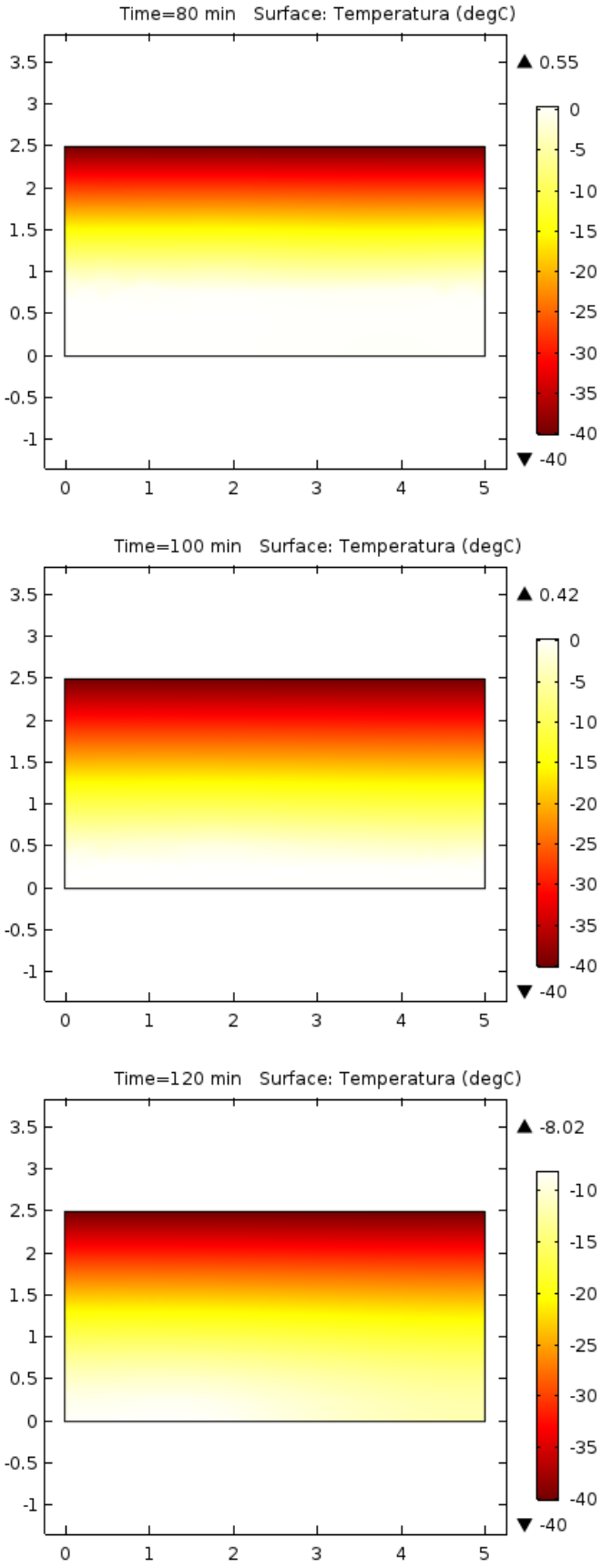
Time=80 min Surface: Temperatura (degC)
▲ 0.55
0
-5
-10
-15
-20
-25
-30
-35
-40
▼ -40
3.5
3
2.5
2
1.5
1
0.5
0
-0.5
-1
0
1
2
3
4
5
Time=100 min Surface: Temperatura (degC)
▲ 0.42
0
-5
-10
-15
-20
-25
-30
-35
-40
▼ -40
3.5
3
2.5
2
1.5
1
0.5
0
-0.5
-1
0
1
2
3
4
5
Time=120 min Surface: Temperatura (degC)
▲ -8.02
-10
-15
-20
-25
-30
-35
-40
▼ -40
3.5
3
2.5
2
1.5
1
0.5
0
-0.5
-1
0
1
2
3
4
5

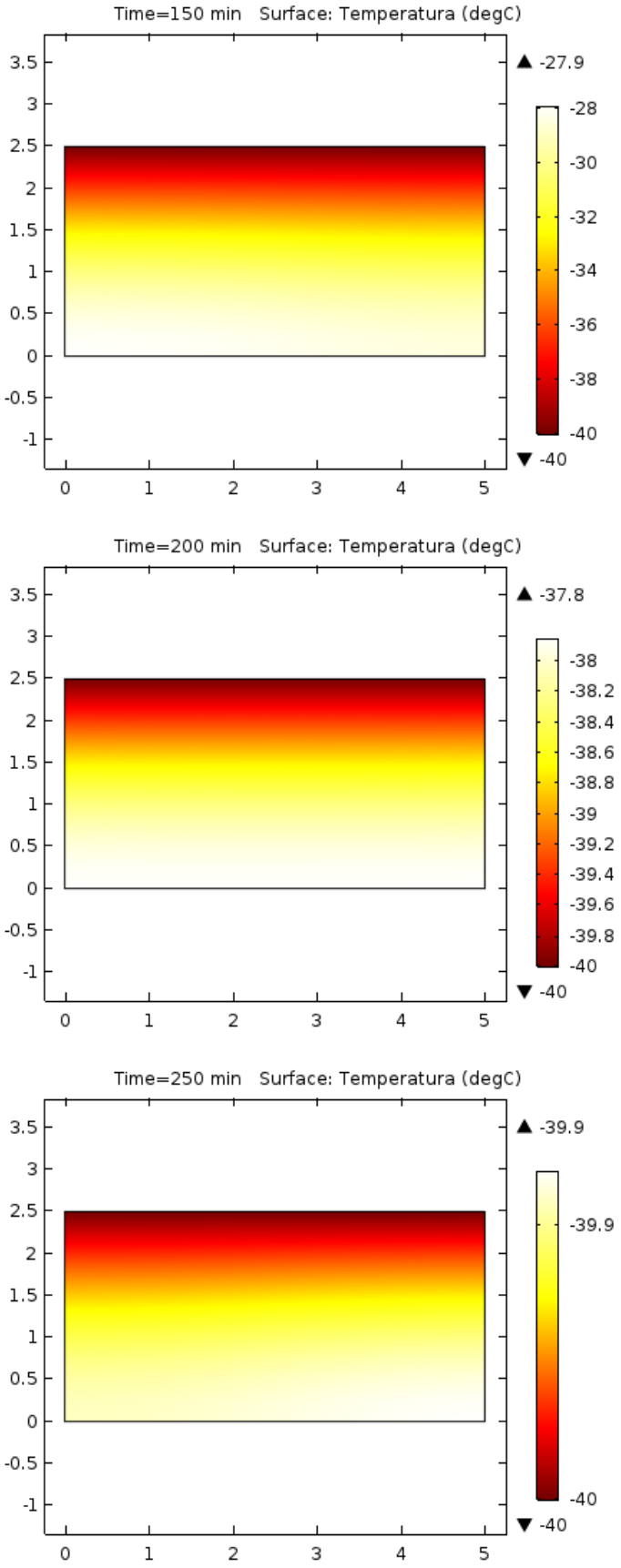

Figure 6.15: Temperature variation on water sample at different time of simulation

In the figure 6.16 it can be seen the trend of water content (phase indicator 2) at various depth and at specific time. It can be seen that before 30 minutes the freezing process is not started so the water phase indicator is equal to zero. The sample than start freezing and after 120 minutes the process ended. From that moment the sample is totally made of ice and so the water phase indicator is equal to zero.

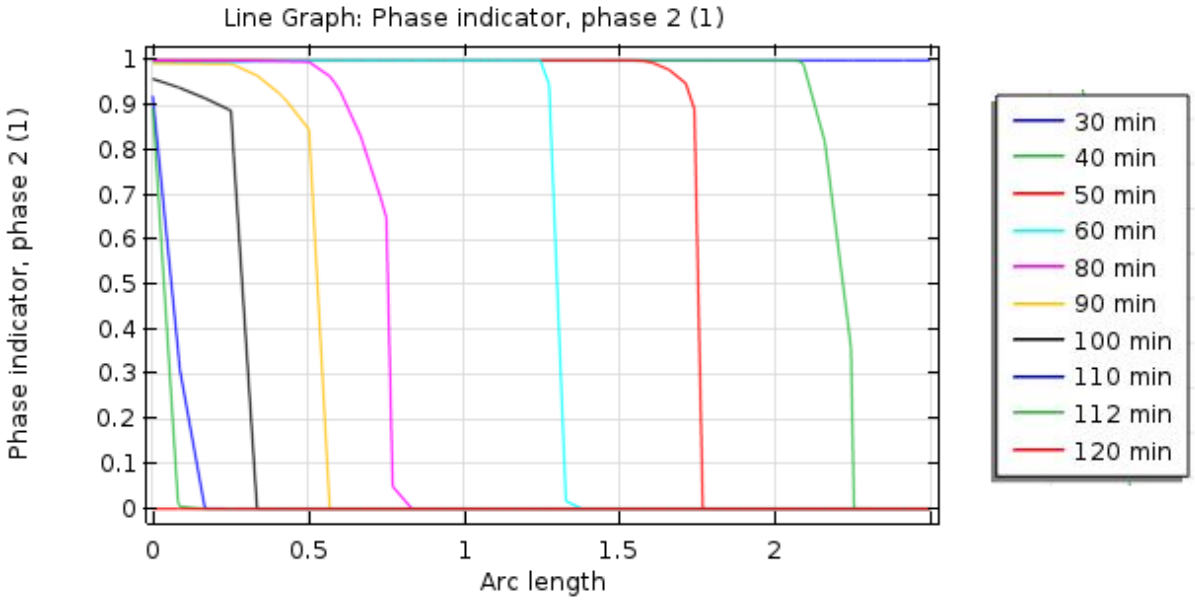

Figure 6.16: Water content variation due to change of phase at selected time.

To visualize better the trend, the water phase indicator at the minute 60 is reported in fig.6.17. It can be seen the S-shape trend, in the superior part of the sample it is equal to 0 , so it is already frozen. In correspondence of the first cm of the sample is it equal to 0.95, it is in major part still all water. The S-shape describe the process of freezing that is happening.

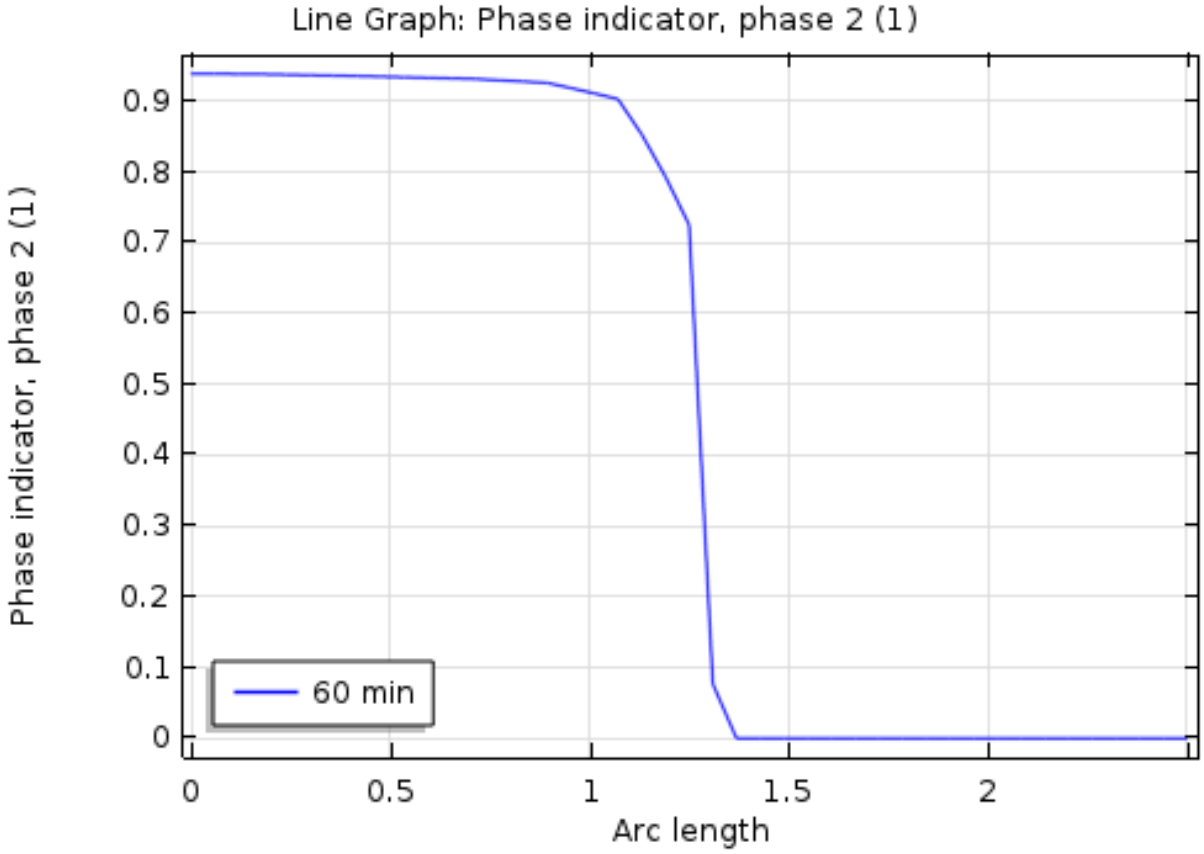

Figure 6.17: Water content variation at the various sample height at 60 minute.

In the figure 6.18, we can see the trend at every time of simulation.

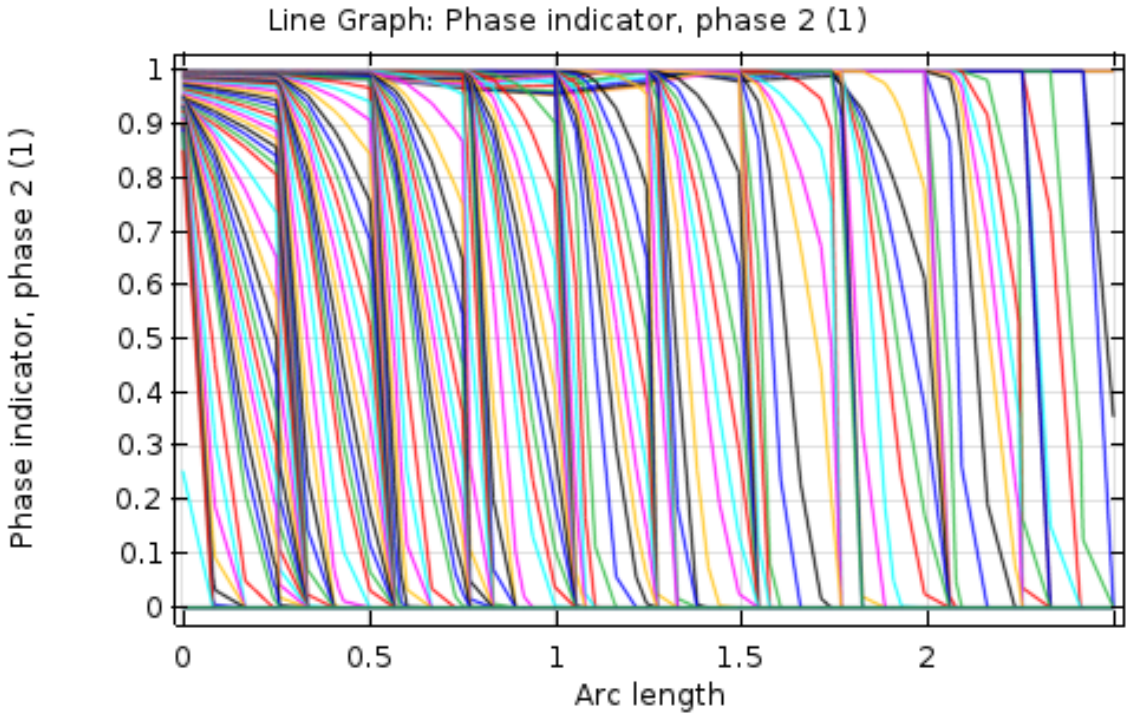

Figure 6.18: Water content trend due to change of phase at every time of simulation.

In the following pages, it can be seen the variation of water phase indicator in the whole sample at specific time.

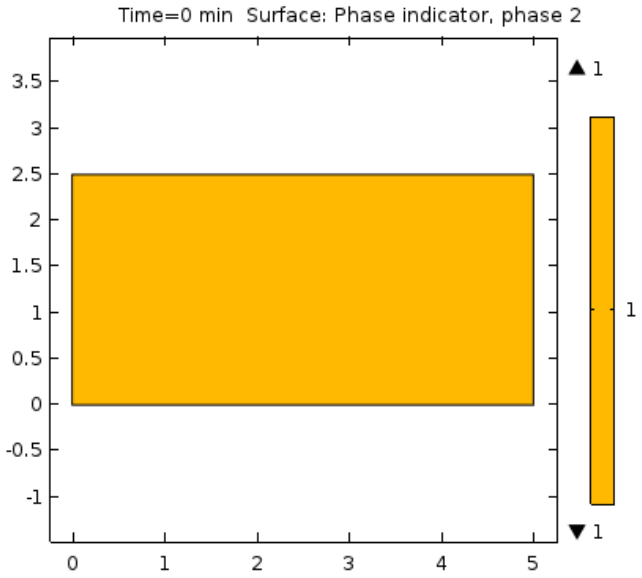
Time=0 min Surface: Phase indicator, phase 2
3.5
3
2.5
2
1.5
1
0.5
0
-0.5
-1
0
1
2
3
4
5
▲ 1
1
▼ 1

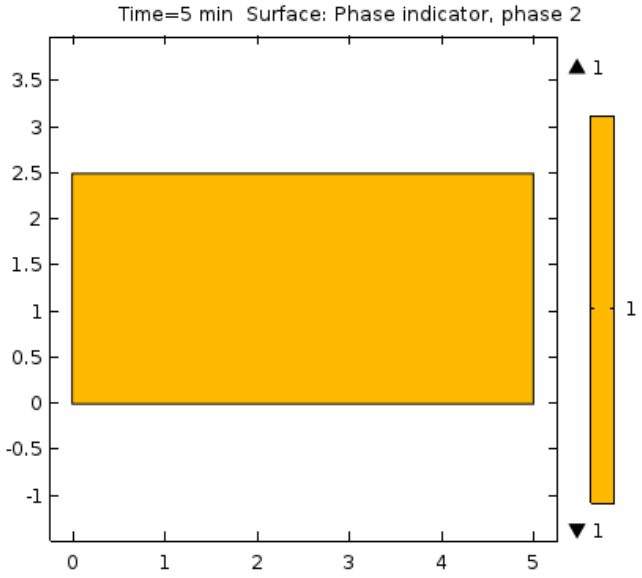
Time=5 min Surface: Phase indicator, phase 2
3.5
3
2.5
2
1.5
1
0.5
0
-0.5
-1
0
1
2
3
4
5
▲ 1
1
▼ 1

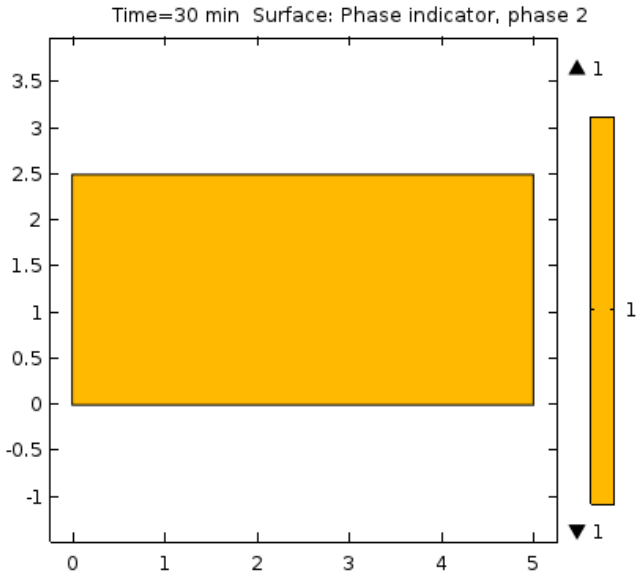
Time=30 min Surface: Phase indicator, phase 2
3.5
3
2.5
2
1.5
1
0.5
0
-0.5
-1
0
1
2
3
4
5
▲ 1
1
▼ 1

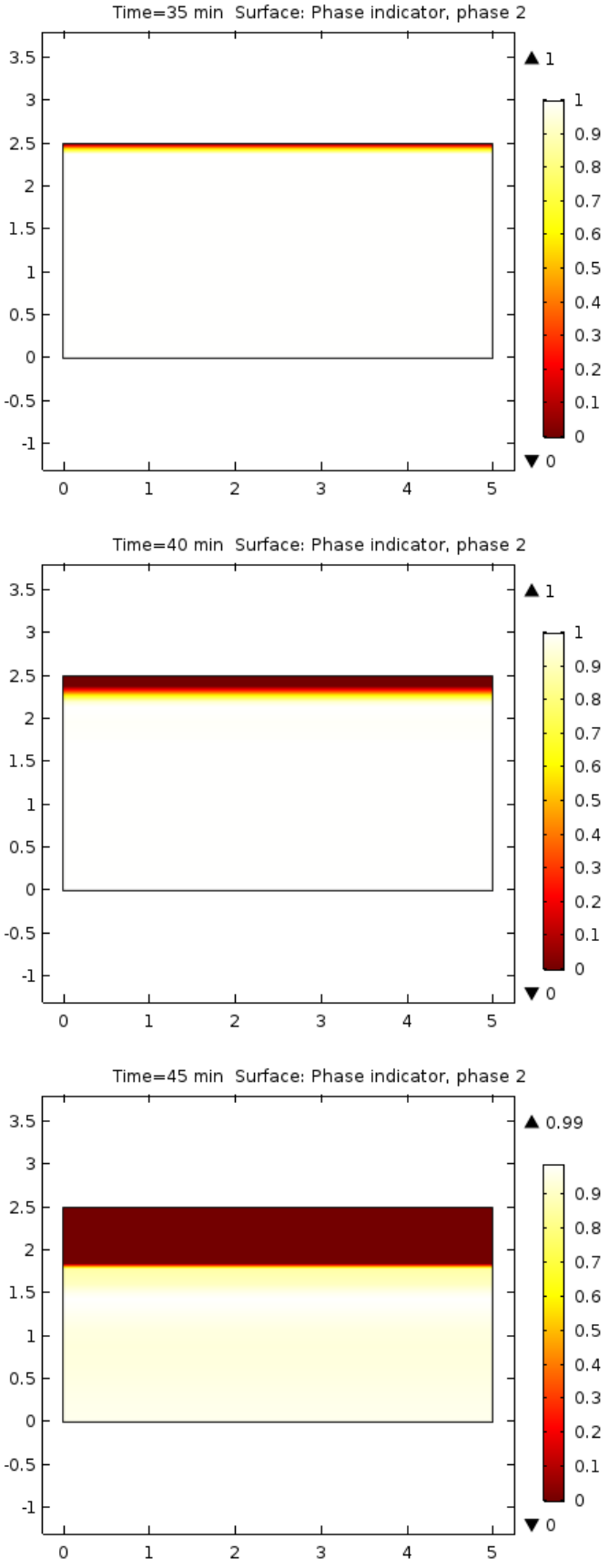
Time=35 min Surface: Phase indicator, phase 2
Time=40 min Surface: Phase indicator, phase 2
Time=45 min Surface: Phase indicator, phase 2
▲ 1
▼ 0
▲ 0.99
3.5
3
2.5
2
1.5
1
0.5
0
-0.5
-1
0
1
2
3
4
5
0.9
0.8
0.7
0.6
0.5
0.4
0.3
0.2
0.1

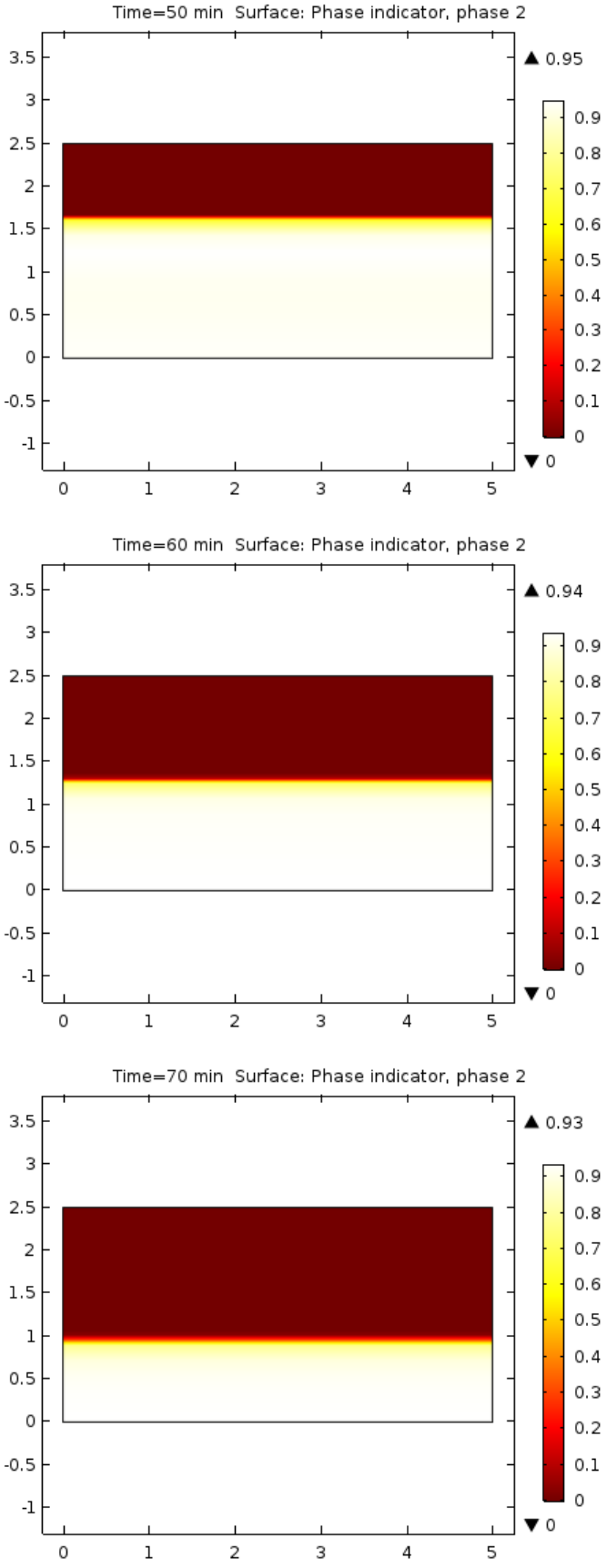
Time=50 min Surface: Phase indicator, phase 2
▲ 0.95
0.9
0.8
0.7
0.6
0.5
0.4
0.3
0.2
0.1
0
▼ 0
3.5
3
2.5
2
1.5
1
0.5
0
-0.5
-1
0
1
2
3
4
5
Time=60 min Surface: Phase indicator, phase 2
▲ 0.94
0.9
0.8
0.7
0.6
0.5
0.4
0.3
0.2
0.1
0
▼ 0
3.5
3
2.5
2
1.5
1
0.5
0
-0.5
-1
0
1
2
3
4
5
Time=70 min Surface: Phase indicator, phase 2
▲ 0.93
0.9
0.8
0.7
0.6
0.5
0.4
0.3
0.2
0.1
0
▼ 0
3.5
3
2.5
2
1.5
1
0.5
0
-0.5
-1
0
1
2
3
4
5

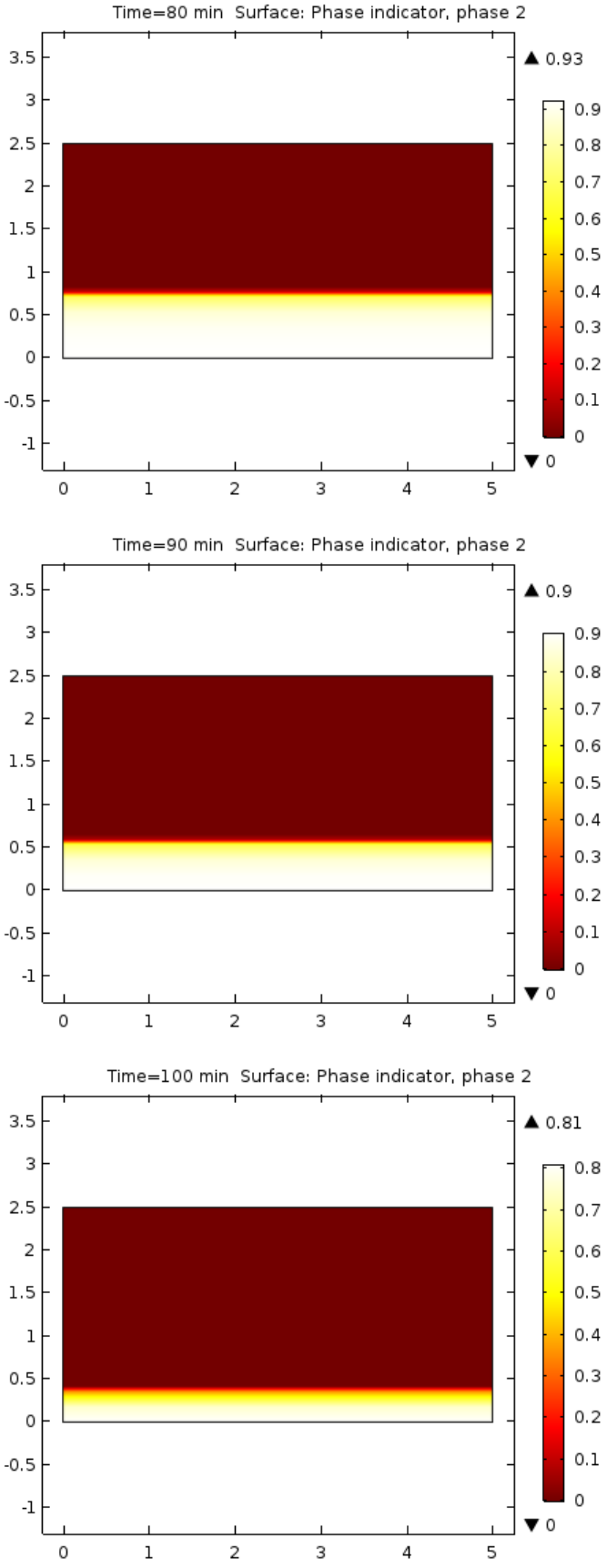
Time=80 min Surface: Phase indicator, phase 2
▲ 0.93
0.9
0.8
0.7
0.6
0.5
0.4
0.3
0.2
0.1
0
▼ 0
3.5
3
2.5
2
1.5
1
0.5
0
-0.5
-1
0
1
2
3
4
5
Time=90 min Surface: Phase indicator, phase 2
▲ 0.9
0.9
0.8
0.7
0.6
0.5
0.4
0.3
0.2
0.1
0
▼ 0
3.5
3
2.5
2
1.5
1
0.5
0
-0.5
-1
0
1
2
3
4
5
Time=100 min Surface: Phase indicator, phase 2
▲ 0.81
0.8
0.7
0.6
0.5
0.4
0.3
0.2
0.1
0
▼ 0
3.5
3
2.5
2
1.5
1
0.5
0
-0.5
-1
0
1
2
3
4
5

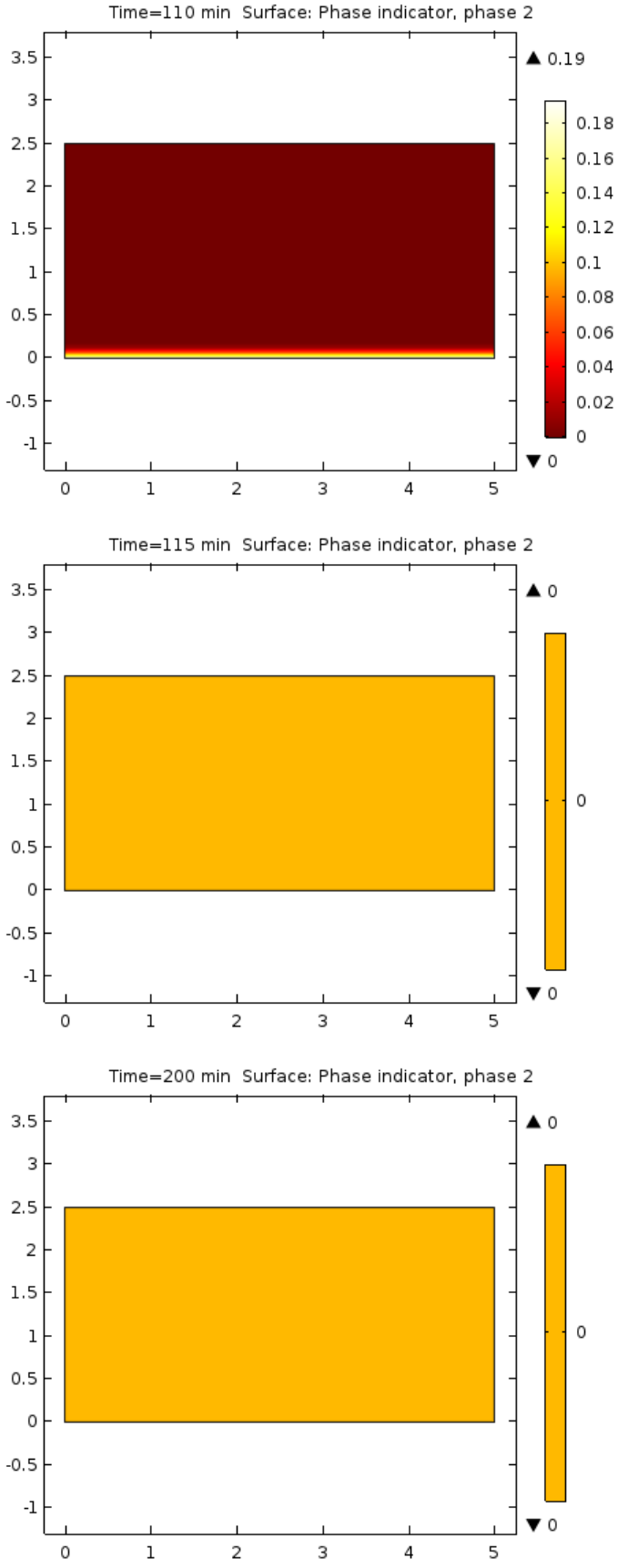

Figure 6.18: Water content variation in the soil probe at specific time of simulation.

Observations

Comparing the results of this two simulation, the temperature trend using a not instantaneous boundary conditions gives better results. Looking at the temperature variation in a point of the domain it can be seen the difference of the first part of the curve. In the first case it decreases rapidly, passing from 20 to 0 C in a few second (fig.6.19(p)). In the second case that part of the curve has a parabolic shape similar to the experimental results in the terrain (fig.6.19(q)).

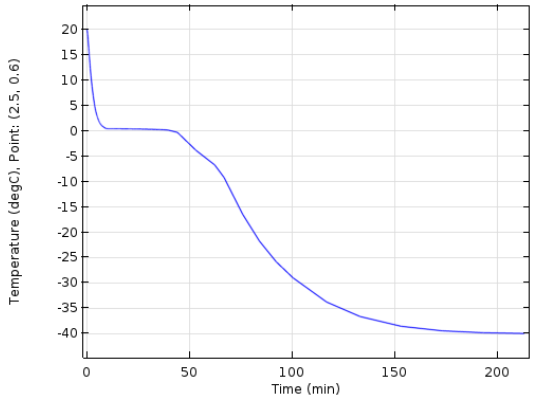

(p) Temperature trend in a point of the domain with instantaneous boundary condition.

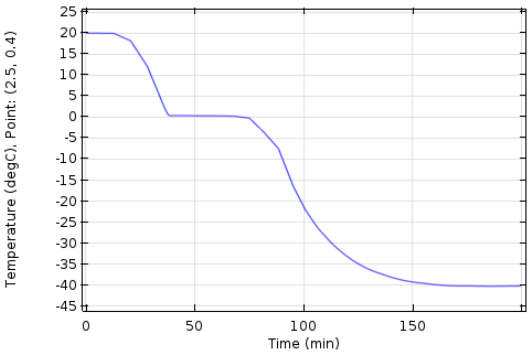

(q) Temperature of a point of the domain with non instantaneous boundary condition.

Figure 6.19: Comparing results with instantaneous and not temperature boundary condition.

Moreover, it is clear from the simulation that the moment of starting freezing and the duration of freezing is a lot influenced by the position of the probe. Taking a point nearer the superior part of the sample, the duration of freezing is less because is tended to freeze in less time.

6.1.4 Simulation of a soil sample

A silty soil sample is considered. The sample geometry is the same of water simulation: 2,5 cm height and 5 cm of diameter. The energy conservation equation is solved and the results are compared with the experimental test results.

Boundary and initial conditions

To compare the simulation and experimental results, it is necessary to simulate in COMSOL also the temperature variation obtained by the freezing of the mould. Indeed, the sample is not directly in contact with the fridge temperature but it has to be taken into account the freezing time of the steel structure around it. This is simulated as a temperature boundary condition on the superior side of the sample. The boundary condition follows the trend found experimentally by the the temperature sensor in touch with the load cell.

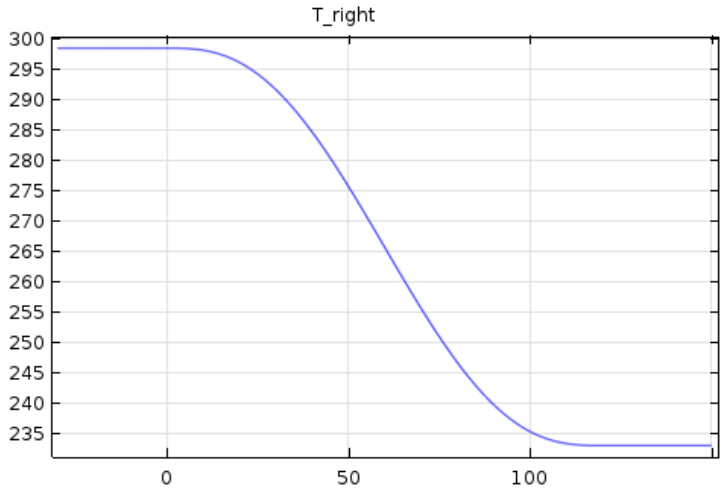

Figure 6.20: Temperature function imposed as boundary condition on the superior side of the sample, in Kelvin.

Looking at the curve in fig.5.19 presented in Chapter 5, it can be seen a temperature variation from 25 C (298 K) to -38 C (235 K) in a interval of 100 minutes, and a change of

concavity at almost 50 minutes. This trend is inserted in COMSOL using a Step function (fig.6.20) which as been called T_{right}. As initial condition a temperature of 25 C is imposed in the sample.

Results

In the figure 6.21 it can be seen the temperature trend in two point of the domain. In the figure the results of simulation are compared with the experimental data obtained in Test 4 (see page 80). The two data simulated with COMSOL has been taken at two points in the center of domain, trying to simulate the position of the temperature probe in the experiment.

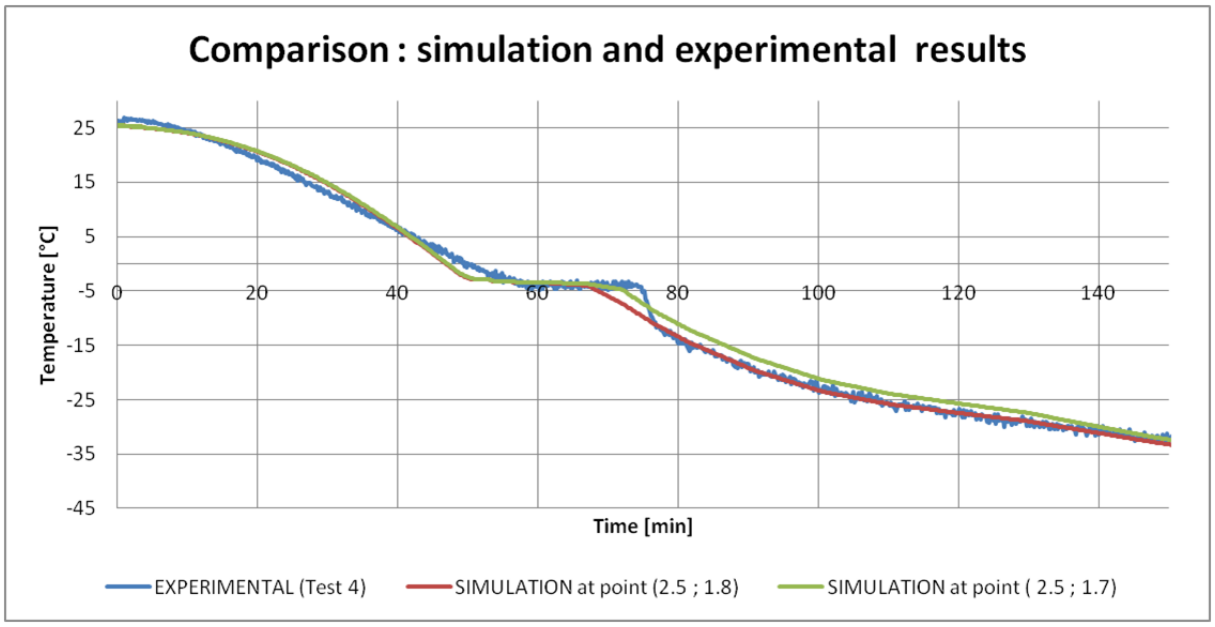

Figure 6.21: Soil sample simulation: temperature trend in a point of the domain. Comparison between data experimental results (Test 4) and numerical simulations.

Comparing the temperature trend obtained by the simulation with the experimental results, it can be seen that the model is able to simulate the temperature trend with a certain precision.

Moreover, analyzing the temperature trend on a point of domain nearer to the upper side of the sample the freezing time is less respect to a point more distant by the superior boundary conditions. Looking at the simulation results at another point (2.5; 1), so in inferior position respect the two already presented; it can be seen that the time of freezing is longer. The data can be compared to the temperature experimental data obtained in Test 5.

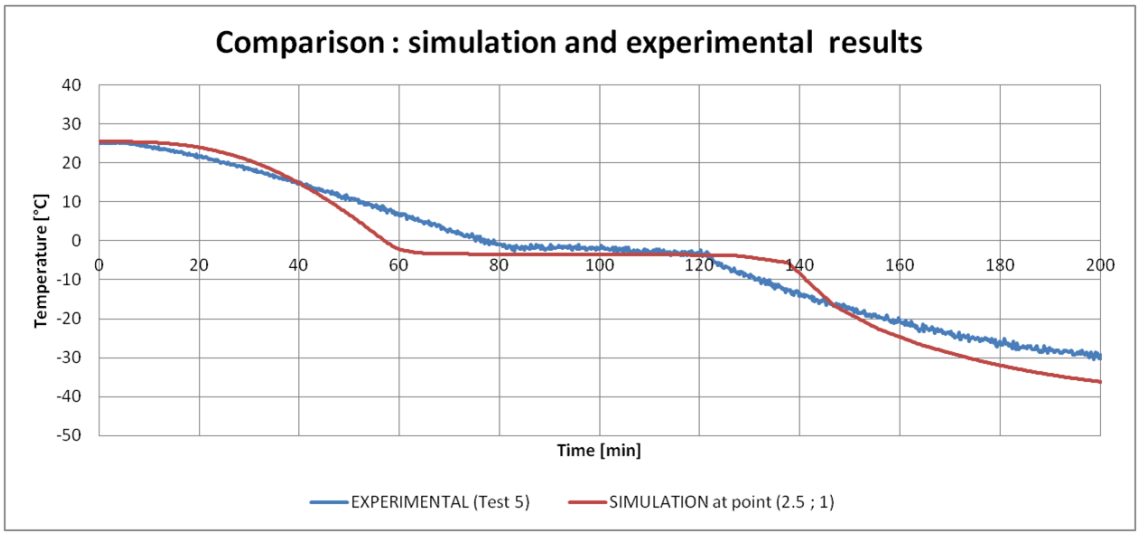

Figure 6.22: Soil sample simulation: temperature trend in a point of the domain. Comparison between data experimental results (Test 5) and numerical simulations.

The experimental results obtained by two different experimental Test (Test 4 and Test 5) can be quietly good represents by the same COMSOL simulation, considering two different position of the point probe. The difference of the time of freezing in the temperature data registered in the two Test can be explained by the position of the temperature sensor. In Test 4 it was surely in a upper position respect to the Test 5.

In the following pages it will be presented the trend of water phase indicator (named phase indicator, phase 2 in the graph) and the temperature trend in a section passing from the sample center, fig.6.23.

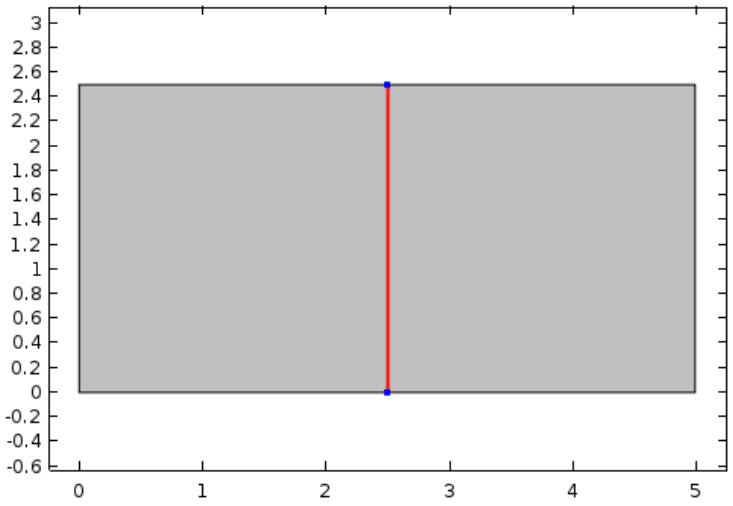

Figure 6.23: Section of the geometry

In fig.6.24 it can be seen the temperature and water phase indicator data at specific time, taken in a section passing through the center of the sample. In the x-axis there is the sample depth, it varies from 0 (the inferior side of sample) and 2.5 (the sample height).

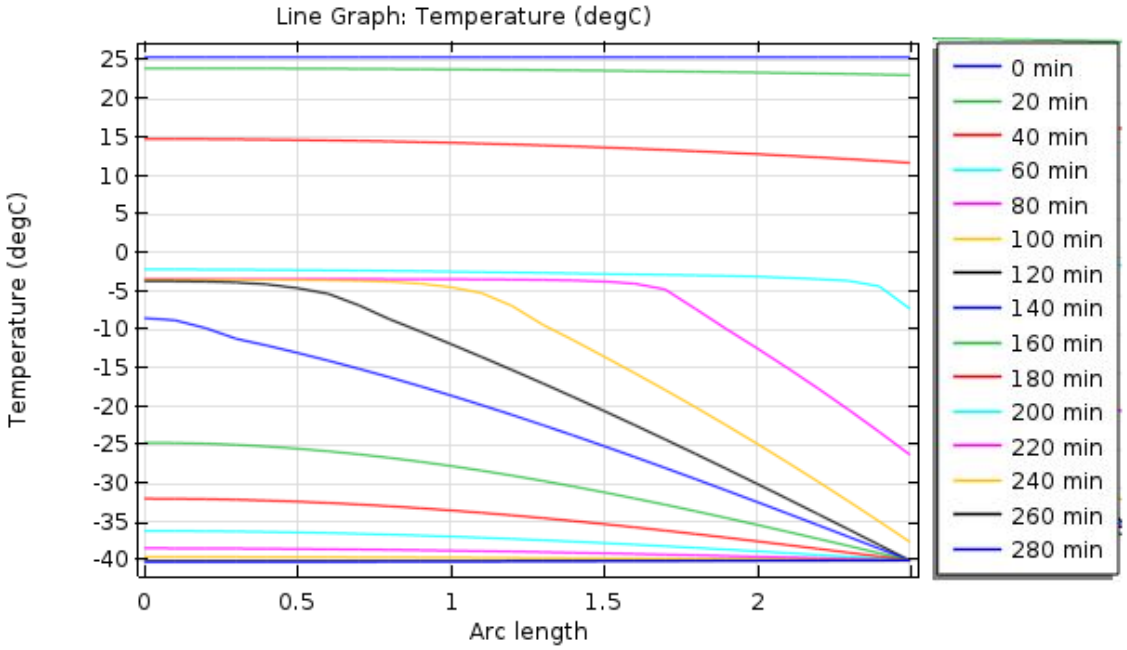

(a) Temperature trend in depth at specific time.

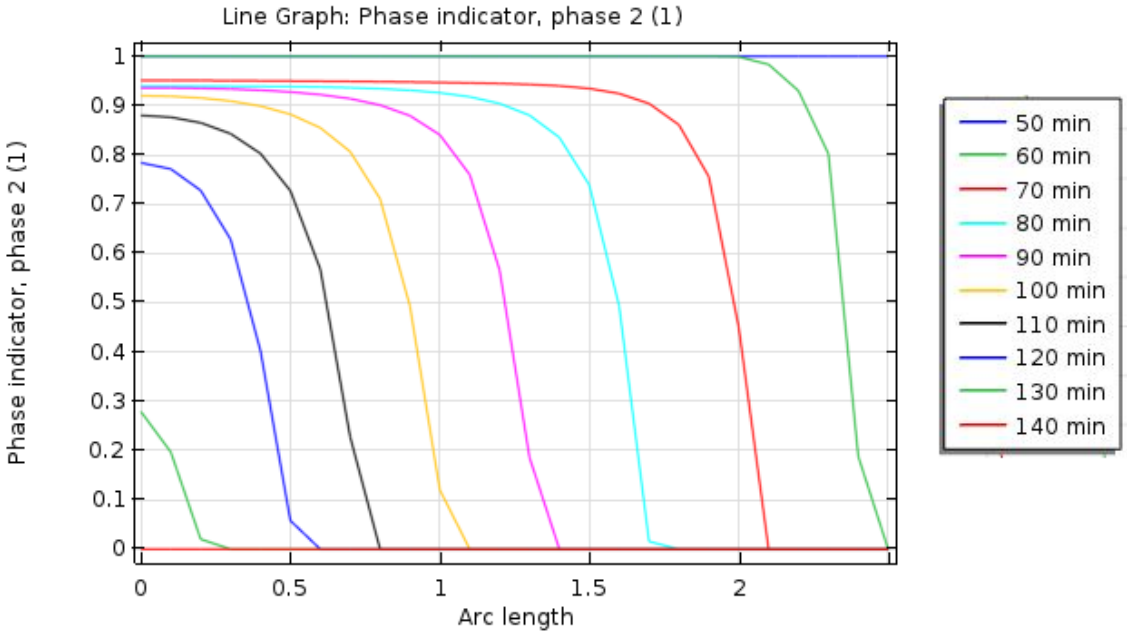

(b) Water phase indicator trend in depth at specific time.

Figure 6.24: COMSOL simulation results at a section passing through the center of the soil sample.

In the next pages are presented a series of graphs showing the temperature evolution (fig.6.25) and water phase indicator variation (fig.6.26) during time.

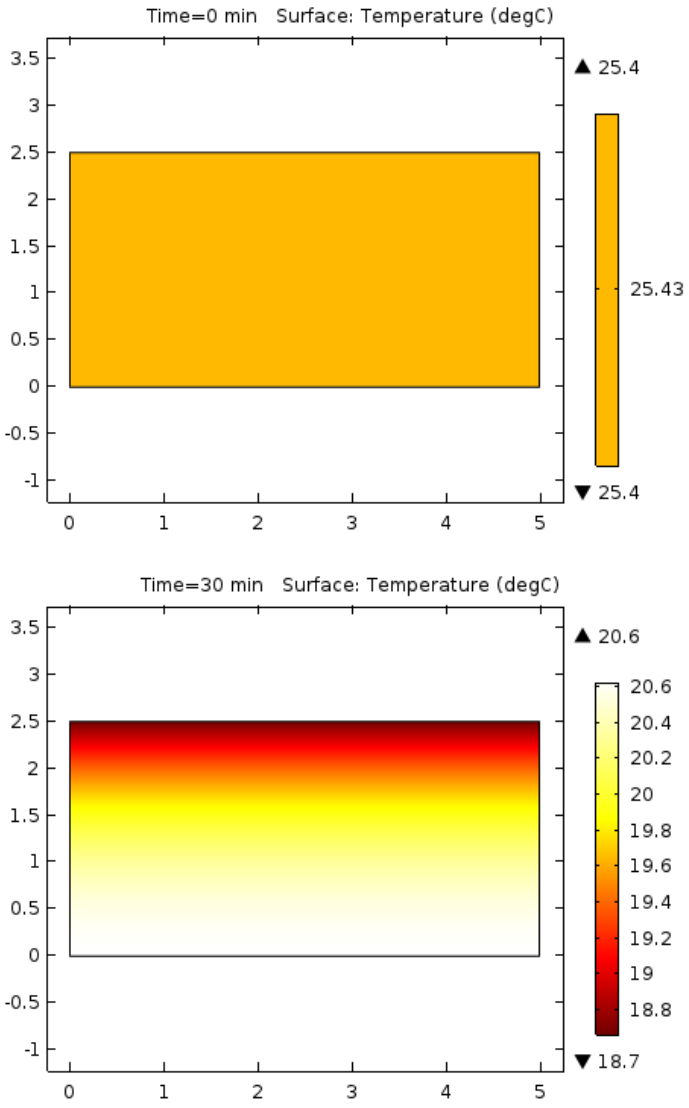

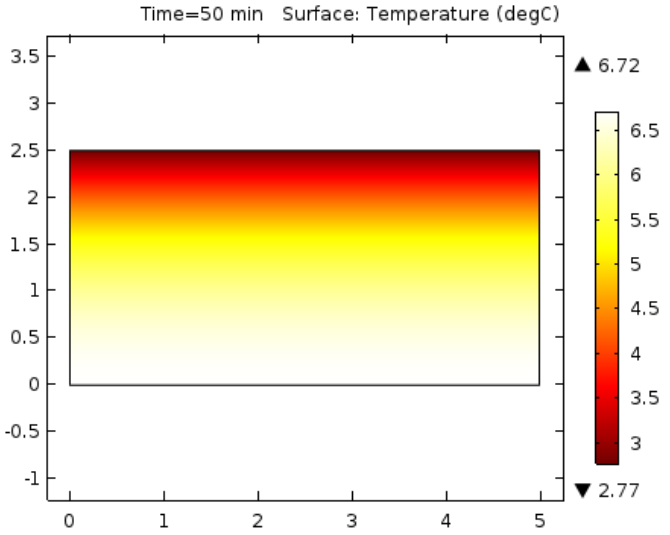
Time=50 min Surface: Temperature (degC)
▲ 6.72
6.5
6
5.5
5
4.5
4
3.5
3
▼ 2.77
3.5
3
2.5
2
1.5
1
0.5
0
-0.5
-1
0
1
2
3
4
5

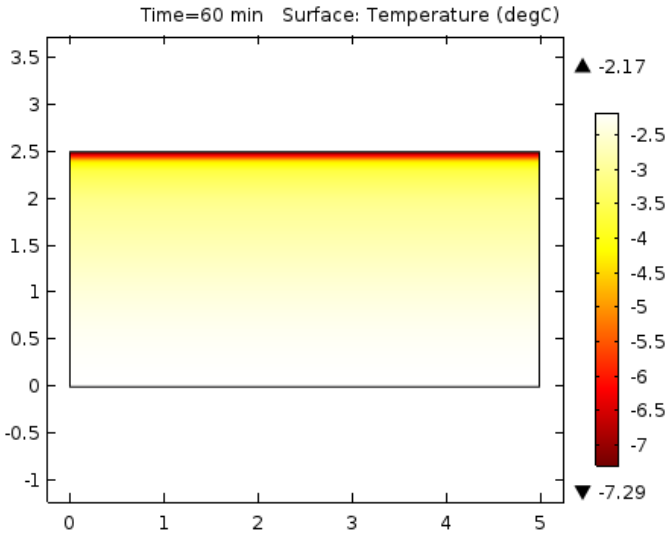
Time=60 min Surface: Temperature (degC)
▲ -2.17
-2.5
-3
-3.5
-4
-4.5
-5
-5.5
-6
-6.5
-7
▼ -7.29
3.5
3
2.5
2
1.5
1
0.5
0
-0.5
-1
0
1
2
3
4
5

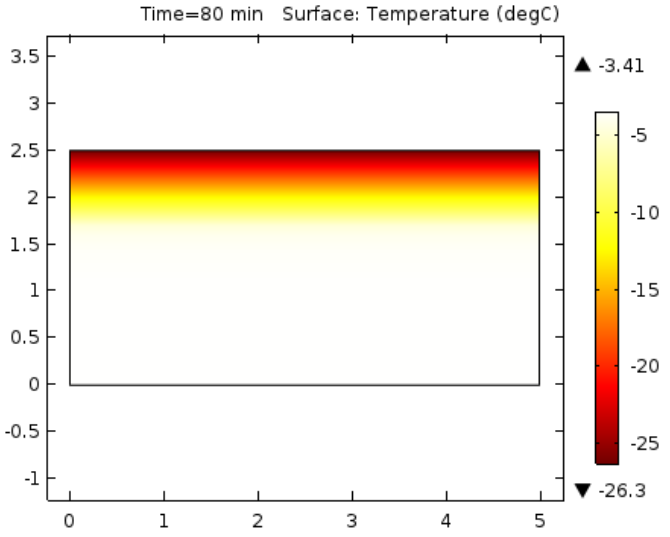
Time=80 min Surface: Temperature (degC)
▲ -3.41
-5
-10
-15
-20
-25
▼ -26.3
3.5
3
2.5
2
1.5
1
0.5
0
-0.5
-1
0
1
2
3
4
5

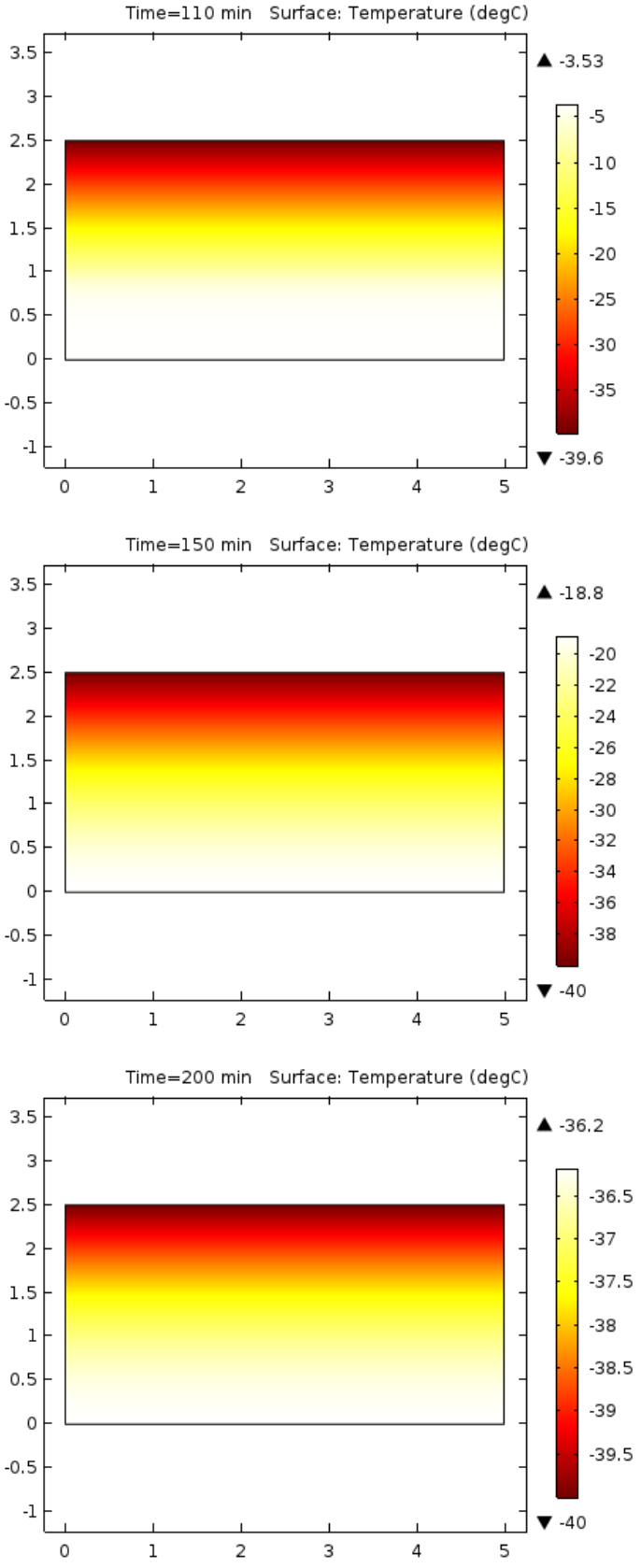
Time=110 min Surface: Temperature (degC)
▲ -3.53
-5
-10
-15
-20
-25
-30
-35
▼ -39.6
Time=150 min Surface: Temperature (degC)
▲ -18.8
-20
-22
-24
-26
-28
-30
-32
-34
-36
-38
▼ -40
Time=200 min Surface: Temperature (degC)
▲ -36.2
-36.5
-37
-37.5
-38
-38.5
-39
-39.5
▼ -40

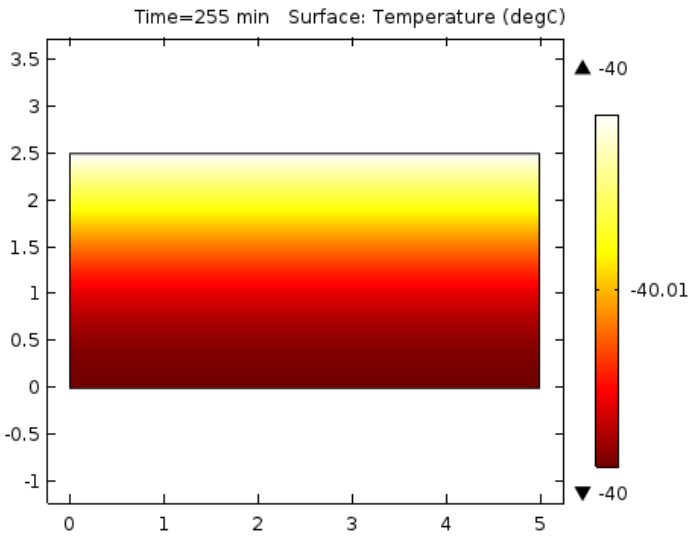

Figure 6.25: Temperature variation on soils sample during time

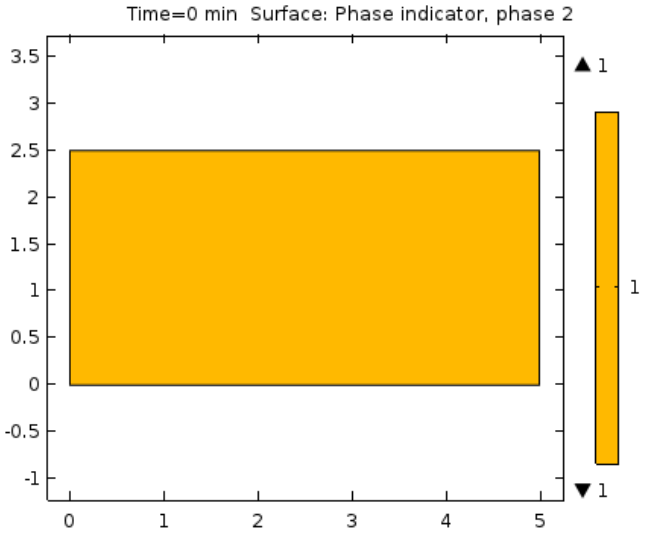
Time=0 min Surface: Phase indicator, phase 2
3.5
3
2.5
2
1.5
1
0.5
0
-0.5
-1
0
1
2
3
4
5
▲ 1
1
▼ 1

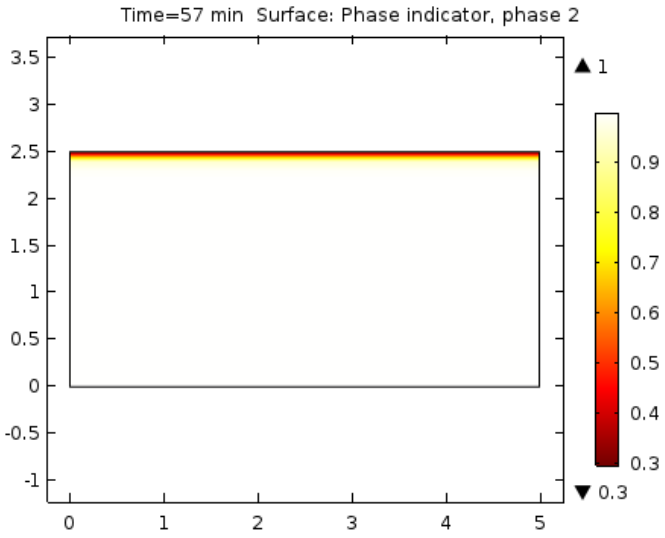
Time=57 min Surface: Phase indicator, phase 2
3.5
3
2.5
2
1.5
1
0.5
0
-0.5
-1
0
1
2
3
4
5
▲ 1
0.9
0.8
0.7
0.6
0.5
0.4
0.3
▼ 0.3

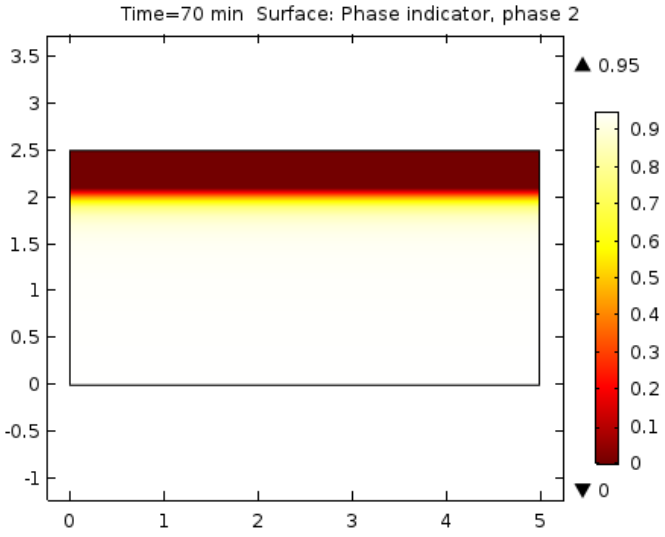
Time=70 min Surface: Phase indicator, phase 2
3.5
3
2.5
2
1.5
1
0.5
0
-0.5
-1
0
1
2
3
4
5
▲ 0.95
0.9
0.8
0.7
0.6
0.5
0.4
0.3
0.2
0.1
0
▼ 0

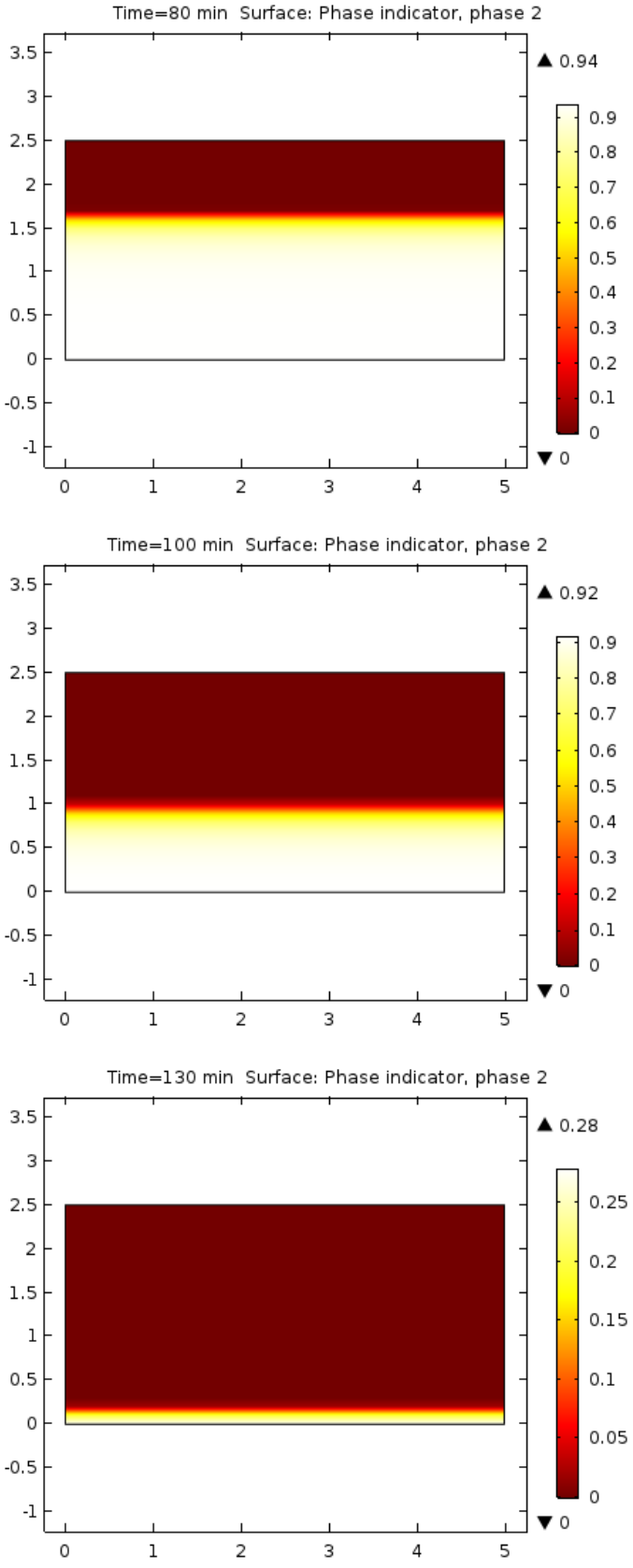
Time=80 min Surface: Phase indicator, phase 2
▲ 0.94
0.9
0.8
0.7
0.6
0.5
0.4
0.3
0.2
0.1
0
▼ 0
3.5
3
2.5
2
1.5
1
0.5
0
-0.5
-1
0
1
2
3
4
5
Time=100 min Surface: Phase indicator, phase 2
▲ 0.92
0.9
0.8
0.7
0.6
0.5
0.4
0.3
0.2
0.1
0
▼ 0
Time=130 min Surface: Phase indicator, phase 2
▲ 0.28
0.25
0.2
0.15
0.1
0.05
0
▼ 0

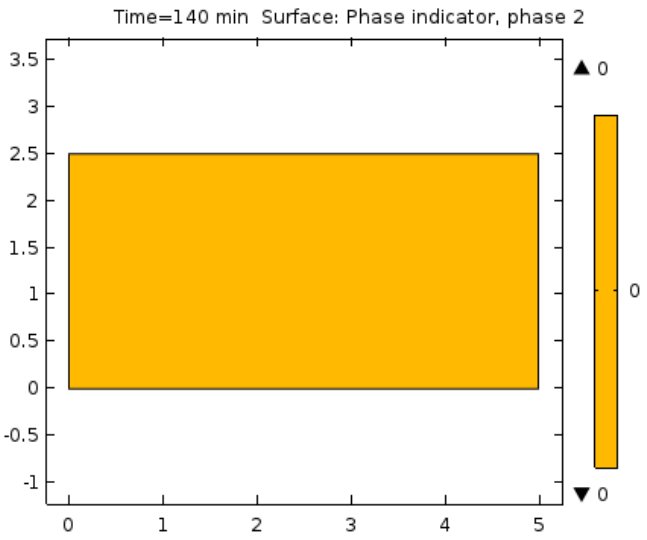

Figure 6.26: Water phase indicator variation on soils sample during time

6.2 COMSOL simulation: Pressure field

Focusing at the pore size, a mechanical model is presented to simulate the variation of pressure exerted by a volume of water under freezing condition. The simulation is done considering the ice as a solid with a certain thermal expansion coefficient. On the base of the temperature trend, already calculated by the energy conservation equation, the pressure due to the freezing is modeled.

The ice sample is considered as a solid elastic material, isotropic. The mechanical parameter of ice utilized are reported in the following pages. The geometry is the same already utilized for the temperature simulation: a sample of 2,5 cm height and 5 cm of diameter is considered. The results of this simulation will be compared with the experimental test results.

Mechanical model equations

The equilibrium equation for solid mechanics are given by Newton's second law.

$$\rho \frac{\partial^2 \mathbf{u}}{\partial t^2} = \nabla_X \sigma + \mathbf{f}_v \tag{6.13}$$

Where σ is the Cauchy stress tensor, f_v is a body force for unit deformed volume and ρ is the current mass density. The Comsol multiphysics utilized a material formulation writing the same equation of 6.13 in terms of the second Piola-Kirchoff stress tensor S:

$$\rho \frac{\partial^2 \mathbf{u}}{\partial t^2} = \nabla \cdot S + \mathbf{F}_v \tag{6.14}$$

Where F is the deformation gradient, and $\mathbf{F}_v$ is a body force which components are given with respect to the underformed volume.

Considering a Linear Elastic Material, Hooke's law relates the stress tensor to the elastic strain tensor:

$$\sigma = \sigma_{ex} + \mathbf{C} : \varepsilon_{el} \tag{6.15}$$

Where $\mathbf{C}$ is the elasticity tensor which depends on the Young Module and the Poisson's ratio, the ":" stands for the double-dot tensor product.

The term σ_{ex} is the contribute due to initial stress and viscoelastic stresses, if presents. The ε_{el} is the difference between the total strain ε and the inelastic strain ε_{inel}:

$$\varepsilon_{el} = \varepsilon - \varepsilon_{inel} = \varepsilon - \varepsilon_{th} \tag{6.16}$$

The inelastic strain ε_{inel} can be composed by several strain contributions as for instance: initial strain,thermal strain, plastic strain, viscoplastic strain.

In this case, only the thermal strain ε_{th} it is considered and it is obtained with the thermal expansion formula:

$$\varepsilon_{th} = \alpha(T - T_{ref}) \tag{6.17}$$

The thermal expansion is inserted to add an internal thermal strain caused by changes in temperature. The thermal strain depends on the thermal expansion coefficient α, the temperature T, and the strain-free reference temperature T_{ref}.

The total strain ε is linked to the velocity vector $\mathbf{u}$ from the relation:

$$\varepsilon = \frac{1}{2}\left[(\nabla \mathbf{u})^T + \nabla \mathbf{u}\right] \tag{6.18}$$

Parameters and steps of simulation

1. Step 1: The sample is considered at initial condition, in equilibrium conditions. The boundary condition imposed are: fixed constraint in the inferior side of the rectangular and two roller in the right and left side. So the pressure due to the weight force of the sample is computed, this is the initial value for the simulation, see fig.6.27.

2. Step 2: On the base of the results of step 1, the constraint in the superior part of the probe is imposed. The initial value of temperature is imposed, with the coupled temperature model.

3. Step 3 : The model solves firstly the temperature equations and then it calculate the pressure value on the base of the mechanical equations above reported.

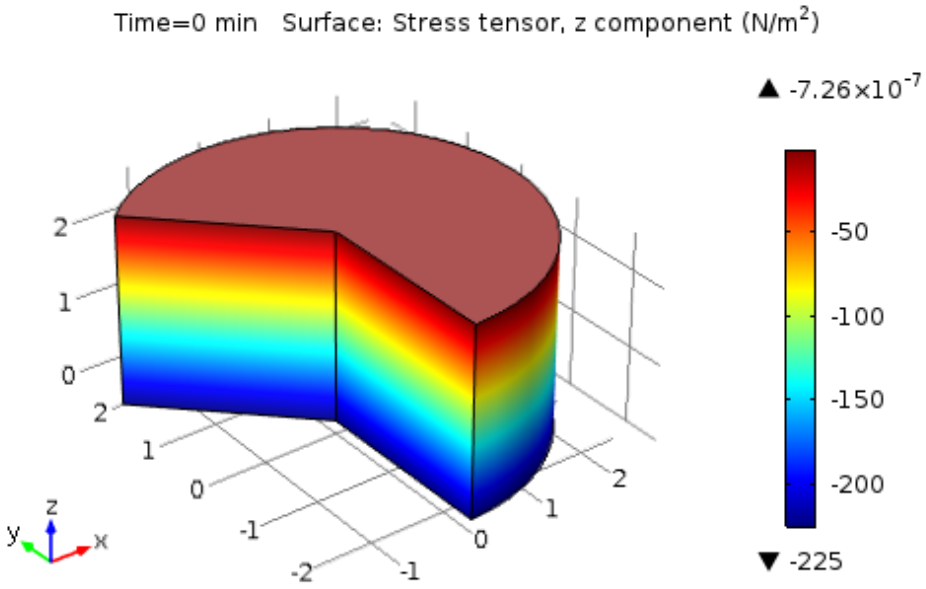

Figure 6.27: Initial value of stress tensor in the direction z at equilibrium conditions.

The parameter utilized for the simulation are summarize in the following table.

Symbols	Parameters	Value	Units
E	Young's modulus	9000	MPa
ν	Poisson's ratio	0.36	–
ρ^i	Ice density	916.8	$kg/(m^3)$
α	Coefficient of thermal expansion	$0.0872 \cdot 10^{-3}$	$1/K$
T_{ref}	Strain reference temperature	283.15	K

6.2.1 Boundary conditions

Running the simulation utilizing the same boundary condition utilized for the soils temperature simulation, some numerical problems emerges on the results. This was due to the fact that the temperature gradient was too high for the pressure computation. So, has been imposed as boundary condition a temperature function which varies from 5C to -10 C, see fig.6.28.

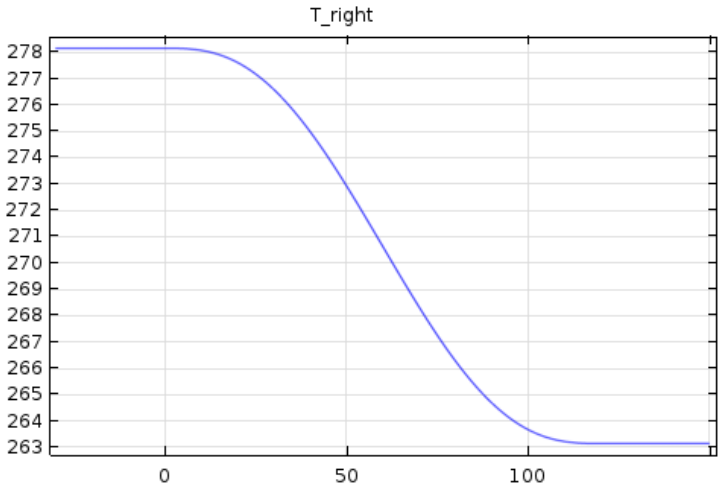

Figure 6.28: Temperature boundary condition at the superior side of the sample.

6.2.2 Results

Since the model considers the sample as a volume of only ice subjected to thermal deformation, it was necessary to insert the gradually formation of ice. To take into consideration that the volume is not totally made of ice from the first instant of the simulation, the coefficient of thermal expansion has been multiply to the ice phase parameter. In this way, the pressure is equal to zero when the temperature is higher than freezing temperature and then it grows gradually following the gradual creation of ice mass. This can be obtained thanks to the coupled thermo-mechanical multhiphsycs of COMSOL. The mechanical model is linked to the temperature model not only with the temperature variation but also with the variation of ice content.

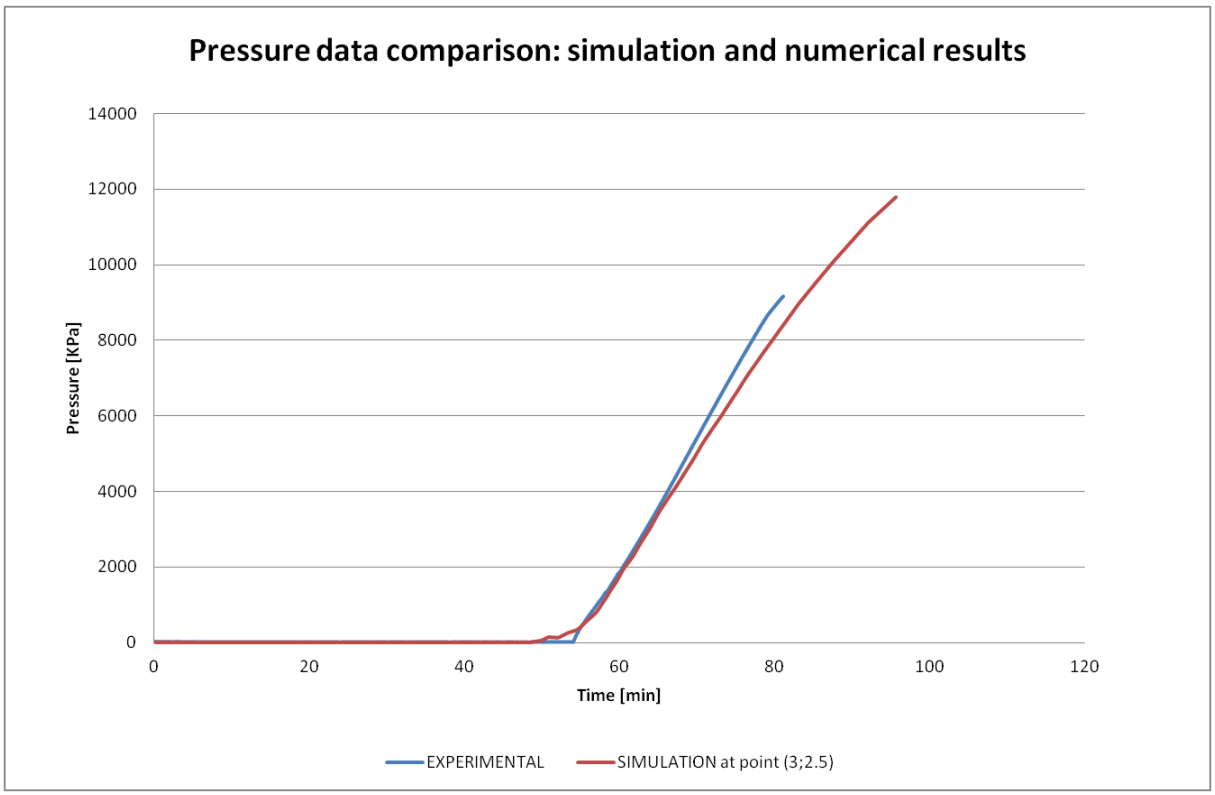

Figure 6.29: Comparison between pressure value from the thermo-mechanical simulation and experimental results.

The pressure trend has been calculated in a point on the superior side of the domain

to do a correlation between the simulated and experimental results. In the following graph (fig.6.29) it can be seen the pressure values obtained by the COMSOL simulation (in red). Comparing with the experimental results: it can be seen that the slope of the two curves are similar. As to be remarked that has been utilized a boundary condition which considers a very slow freezing process. This is made to reduce the numerical problems of COMSOL simulation, which surely find problem on the coupling modeling considering very high temperature gradient. This problem can be solved utilizing more advanced computational instrument, mesh more fitted but so also very higher computational time.

Since, the model utilized is a coupled thermo-mechanical model, the pressure values are measured at each step in the base of the temperature values. In fig.6.30 it is presented the temperature trend resulted by the coupled thermal-mechanical simulation.

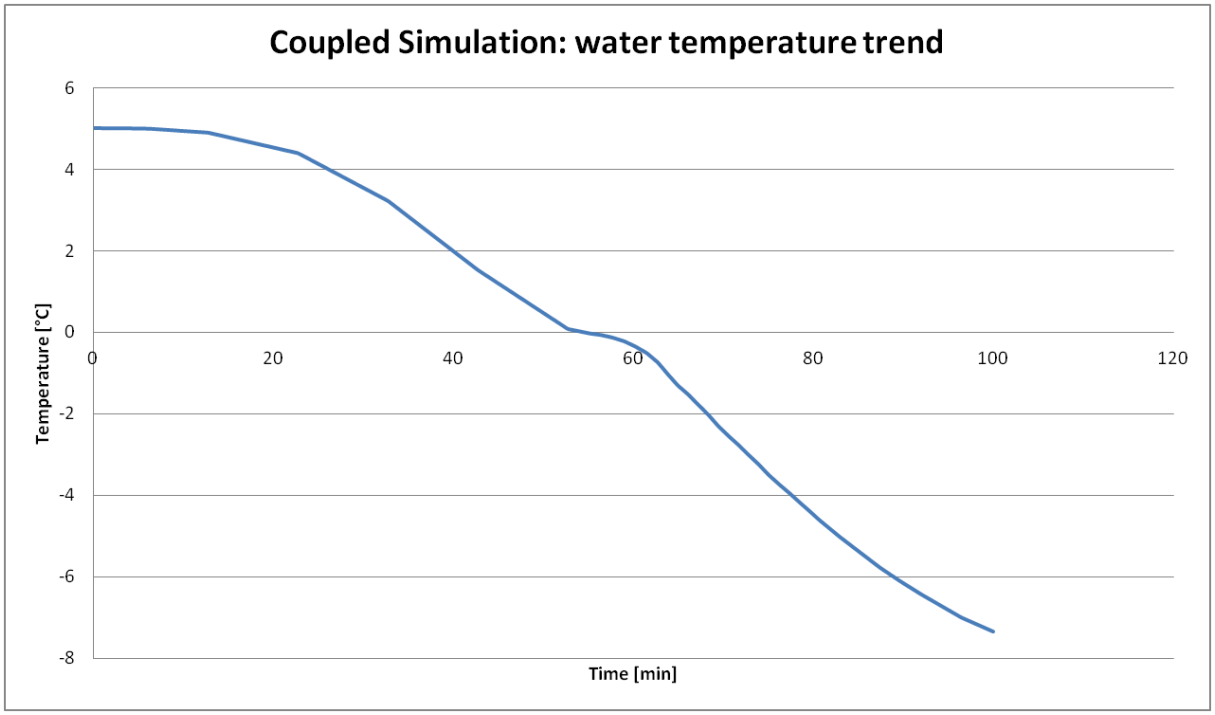

Figure 6.30: Temperature value obtained by the thermo-mechanical simulation at pore-size.

These temperature values correspond to the pressure trend already presented.

6.3 Proof of concept: Soil pressure evaluation

The final aim of the pressure analysis and simulation is to find a correlation between the pressure value simulated at pore-scale dimension with the pressure registered experimentally on the soils. If this correlation is founded, this mechanical model can be used to solve the mechanical part related to the system of equations presented in Chapter 3; and so it will be a way of obtain the value of the pressure exerted on the solid skeleton (p_s) taking into account of the real ice pressure under freezing conditions.

As a preliminary step on the research of the correlation, it has been compared the water pressure simulated with the soil pressure registered experimentally at the end of the freezing process.

The temperature at the end of freezing process, can be obtained zooming the previous graph.

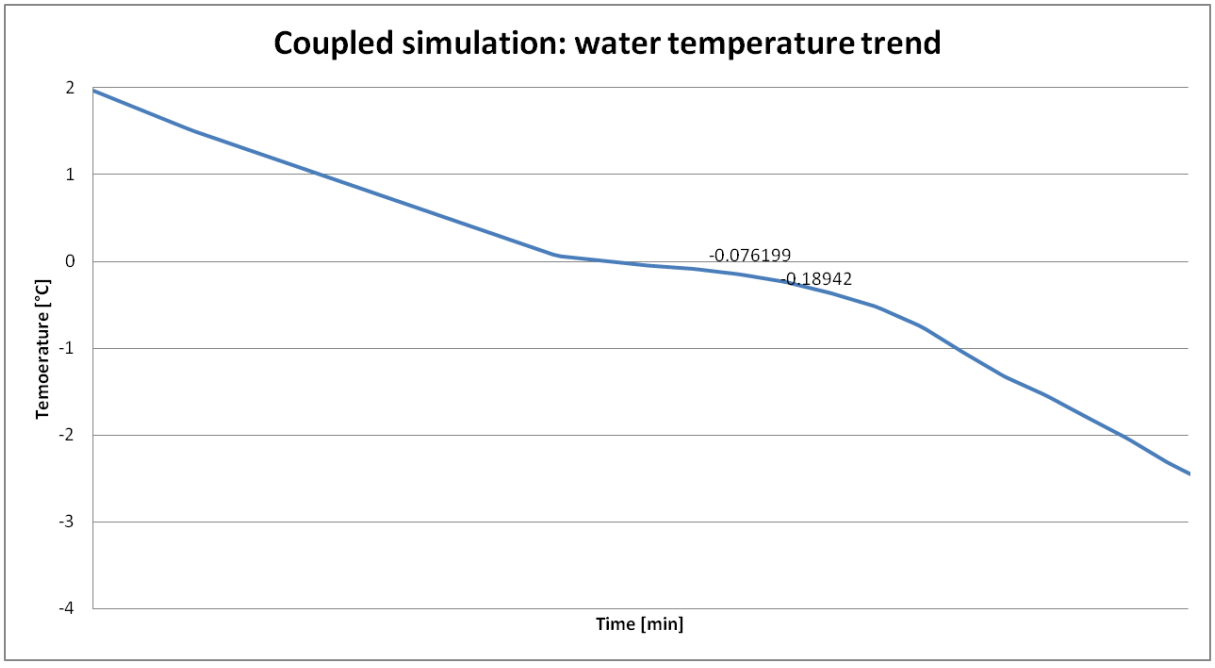

Figure 6.31: Zoom of the temperature obtained by the thermo-mechanical simulation at pore-size.

As it can be seen from fig.6.31, it is difficult to understand at which temperature the

freezing process ends, because the plateau is not well defined. Since the values are taken into a point very nearer to the superior side of the sample, the freezing process takes place in very small time. So it will be taken a series of point, from -0.076 to -0.01894, and the correspondent value of force.

In the figure 6.32, there are presented some temperature and corresponding force values taken at some points at the ending of freezing process of the simulation results.

Pore size simulation: Ice pressure			
Time	T	P	F
[min]	[°C]	[kPa]	[N]
56.40	-0.076	128.37	251.93
56.60	-0.085	142.12	278.91
56.80	-0.095	161.52	316.98
57.00	-0.105	181.43	356.06
57.2	-0.11555	201.85	396.13
57.4	-0.12563	222.78	437.21
57.6	-0.13572	244.21	479.26
57.8	-0.14771	260.89	512.00
58	-0.16162	273.16	536.08
58.2	-0.17552	286.34	561.94
58.4	-0.18942	300.41	589.55

Figure 6.32: Temperature and corresponding value of force at the end of freezing process resulting from the thermo-mechanical simulation.

The value of soil force is evaluated multiplying the value of water force for the porosity ($\varepsilon = 0.46$). In this way, it is obtained the force exerted by a volume of water equal to the total volume of water presented in the soils pore. This values of force is compared with the soil pressure registered in Test 4, Test 5 and Test 7 at the end of freezing (that correspond to the maximum value of force registered).

As can be seen from the results in the table in fig.6.33, a correlation can be found. The soil force obtained multiplying the simulated pore-size force (of only water) for the porosity is similar to the experimental soil force values.

This study it is only at the first stage. It has to be remarked that the coupled simulation

Soil pressure SIMULATION	
F	P
[N]	[kPa
115.89	59.05
128.30	65.38
145.81	74.30
163.79	83.46
182.22	92.85
201.11	102.48
220.46	112.34
235.52	120.01
246.60	125.65
258.49	131.72
271.20	138.19

Soil pressure EXPERIMENTAL		
F	P	
[N]	[kPa	
129.21	65.84	*TEST 4*
147.79	75.31	*TEST 5*
255.98	130.43	*TEST 7*

Figure 6.33: Comparison of soil force obtained experimentally and force evaluated by the simulation.

is done utilizing as a boundary condition a very slow freezing function, to reproduce the experimental pressure at the best. Moreover, from the temperature trend taken very near to the superior side of the sample is difficult to see at which temperature the freezing process ended. So, the correlation can be done considering a series of temperature and respective force values.

Besides all these approximations, it can be seen that the value of soil force simulated with this correlation are of the same order of magnitude of the ones registered experimentally.

Chapter 7

Conclusions

With COMSOL simulation a model with a coupled system of energy and mechanical equations is presented. Comparing the simulation results to the experimental results, it can be seen that:

- Applying the model at the pore-size dimension, it is able to reproduce the water pressure exerted during the freezing process, using specific boundary conditions.
- Solving the energy equations considering soils sample, the model it is able to well reproduce the temperature trend. The comparison has been done looking at the temperature trend in a point of the domain.
- On the bases of the model results, a first stage of evaluating the soil force has been done. The soil force has been evaluated multiplying the water force exerted at the end of freezing for the porosity. Comparing the soil pressure evaluated in this way and the experimental soil force it can be seen that the values are of the same order of magnitude.

Looking at the system proposed in the chapter 3, the energy equation has been solved for soils and the comparison with the experimental results shows that the change of phase

modeled is well representative of the real physical process. Moreover, it is proposed a way to evaluate the pressure exerted on the soil skeleton considering the ice pressure exerted during the freezing process, utilizing a coupled thermo-mechanical model. This is presented as a proof of concept because the correlation utilized is very simplified and there is the necessity to further studies to have a certain level of precision. However, the comparison of the soil pressure simulated in this way and the experimental soil pressure under-light that this can be a possibly way of proceeding. Indeed, the value of force obtained are of the same order of magnitude and can be quietly good compared with the experimental ones.

Analyzing the experimental set-up and results, the results shows a congruence with the theory. The laboratory test results, both for water and soils, shows an increase of pressure exerted in correspondence of the start of freezing process. The temperature data registered follow the trend expected: there is a decreasing part of the curve and the temperature stays constant for all the freezing process. From the test results with soils sample, it can be seen that the temperature of freezing is below the zero, as expected by the theory explained by the Clapeyron equation. It can be concluded that the set-up and laboratory equipment designed is able to measure and register the various aspects of the physics of the problem.

The results of pressure measurement with water showed a peak of 20000N (corresponding to a pressure of 10151.91 kPa). This is a optimal result from two points of view. On one hand, from this results it can be say that the confining structure it is able to support high values of pressure. On the other hand, it under-light the greatness of strength that a water sample of 5 cm of diameter and 2,5 cm of height can reaches.

Looking at the soils sample test the force measured reaches a maximum value of 255N (corresponding to a pressure of 130.43 kPa). The pressure measurement shows a decreasing part of the curve at the end of the freezing process. This can be explained as a problem linked to the set-up of the test and is a issue which have to be analyzed in further studies.

Moreover, the thermal effects of the confining structure are visible in the results. The disturb of the deformation of confining structure can be reduced inserting before the test, only the confining structure in the fridge. As showed by the results, following this procedure the pressure exerted by the thermal effects of steel structure are reduced.

Looking at the future applications of the entire project, the laboratory experiment set-up can be adopted to do a huge range of studies such as considering different type of soils in different conditions. For future applications, the drawback linked to the thermal effect of the confining structure can be totally overcome with a different way of freezing the sample. For instance, modifying the structure of sample cell such that the temperature gradient is imposed only at the sample and not at the entire confining structure and load sensor.

The experimental set-up can be easily modified to permits the realization of different type of test,for instance,it can be add a liquid water reserve to take into account also the cryostatic effects.

The numerical modeling it is at a first stage for soils, but can be implemented to solve also the hydrological part of the phenomena. The energy equations gives as an output the temperature and change of mass parameter for each time. These two unknowns of the general system can be inserted into the mass conservation equation and Clapeyron equation. Moreover, further researches on the proposed mechanical model can lead to a way of evaluation of the pressure exerted on the solid skeleton. In this way, also the unknown p_s of the system can be calculated.

The study in every aspects (mathematical, experimental and numerical) has a huge potentiality to reach a better understand of freezing soils phenomena and it set the basis for an exhaustive and complete model which can represents a possible way of resolution of this complex problem.

Appendix A

Clapeyron equation

Clapeyron equation is a relevant relation whit a verified importance on the study of water freezing in soils. As can be seen by the literature overview,it is widely utilized in different forms and under different assumption.

Referring to freezing soils it is necessary to make it in light the real applications of every different forms.

First of all, the meaning of the equation is to represent the decreasing of water freezing point under the normal freezing point (0°C), because it is influenced by a pressure change.

If we consider a general pressure increment dP applied equally to both phase ice and water, and so $\Delta P_i = \Delta P_w$, we can write:

$$\frac{dT}{dP} = \frac{(V_w - V_i)T_0}{L_f} \tag{A.1}$$

V_w = specific volume of water m^3kg^{-1}

V_i = specific volume of ice m^3kg^{-1}

L_f= heat of fusion of ice Jkg^{-1}

T= temperature K

and dT is the change of freezing point, T_0 is the normal freezing point (0°C) when the

pressure is atmospheric.

The increasing of pressure is so considered as a total pressure applied to both water and ice in the same way. Although this is normally assumed, it is not the condition which happens in the case of water freezing in soil.

Considering now a different change of pressure for ice and water, ΔP_i is not equal to ΔP_w. For instance, examining the case when pressure on the water is lowered and pressure of ice remains at a constant value we can apply:

$$\frac{P_w}{dT} = \frac{L_f}{TV_w} \tag{A.2}$$

This equation cannot be applied if the ice has a pressure higher than atmospheric (for example,due to the weight of overlaying material).

In the case of freezing soils,the variation of water pressure and ice pressure are different and ice pressure is higher of atmospheric pressure. In this situation the previous equation can not be used but must be used a combination of the two equations:

$$T - T_0 = \frac{(P_w V_w - P_i V_i)T}{L_f} \tag{A.3}$$

In this equation compare the difference $P_i - P_w$ which have a relevant role on the pressure behavior in freezing soils [12].

The eq. A.3 can be obtained also following another approach. In the book "Hilgardia" ([21], pag.118, eq.201) they demonstrate this formulation:

$$v_2\frac{dP_w}{dT} - v_1\frac{dP_i}{dT} + \frac{dp}{dT}(v_2 - v_1) = \frac{L_f}{T} \tag{A.4}$$

P_w = pressure of water

P_i = pressure of ice

v_2 = specific volume of water

v_1 = specific volume of ice

p = pressure of gas L_f= heat of fusion of ice

T= temperature

Neglecting the gas pressure we obtain:

$$\frac{(v_2 dP_w - v_1 dP_i)}{dT} = \frac{L_f}{T} \tag{A.5}$$

Reorganizing:

$$\frac{T(v_2 dP_w - v_1 dP_i)}{L_f} = dT \tag{A.6}$$

we obtain the same formula written in eq.A.3.

and considering that the specific volume can be written as: $1/\rho$, we obtain:

$$\frac{1}{\rho^w}\frac{dP_w}{dT} - \frac{1}{\rho^i}\frac{dP_i}{dT} = \frac{L_f}{T} \tag{A.7}$$

$$\frac{1}{\rho^w}dP_w - \frac{1}{\rho^i}dP_i = L_f\frac{dT}{T} \tag{A.8}$$

Integrating T from T_0 to $T_{f/m}$ we obtain:

$$\frac{P_w}{\rho^w L_f} - \frac{P_i}{\rho^i L_f} = ln(\frac{T_{f/m}}{T_0}) \tag{A.9}$$

Finally:

$$T_{f/m} = T_{ref} exp[\frac{1}{\rho^w L_f}(P^w - \frac{\rho^w}{\rho^i} P^i)] \tag{A.10}$$

Appendix B

Mass Conservation equation

$$\frac{\partial(\varepsilon s^{\alpha}\rho^{\alpha})}{\partial t} + \nabla \cdot (\varepsilon s^{\alpha}\rho^{\alpha}\mathbf{v}^{\alpha}) = e_{wi} \tag{B.1}$$

$$\frac{\partial[(1-\varepsilon)\rho^{s}]}{\partial t} + \nabla \cdot [(1-\varepsilon)\rho^{s}\mathbf{v}^{\mathbf{s}}] = 0 \tag{B.2}$$

We can writing the Darcy velocity considering a velocity for each phase relative to the solid velocity:

$$\mathbf{q}^{\alpha} = s^{\alpha}\varepsilon(\mathbf{v}^{\alpha} - \mathbf{v}^{s}) \tag{B.3}$$

At this point substituting this in eq. B.1 we can eliminate $\mathbf{v}^{\alpha}$ from the equation.

$$\frac{\partial(\varepsilon s^{\alpha}\rho^{\alpha})}{\partial t} + \nabla \cdot (\rho^{\alpha}\mathbf{q}^{\alpha}) + \nabla \cdot (\varepsilon s^{\alpha}\rho^{\alpha}\mathbf{v}^{s}) = e_{wi} \tag{B.4}$$

We can apply now the product rule to expand the first term, and we obtain:

$$\rho^{\alpha}s^{\alpha}\frac{D\varepsilon}{Dt} + \varepsilon\rho^{\alpha}\frac{Ds^{\alpha}}{Dt} + \varepsilon s^{\alpha}\frac{D\rho^{\alpha}}{Dt} + \nabla \cdot (\rho^{\alpha}\mathbf{q}^{\alpha}) + \varepsilon s^{\alpha}\rho^{\alpha}\nabla \cdot \mathbf{v}^{s} = e_{wi} \tag{B.5}$$

In single-phase subsurface flow studies the solid velocity can be considered only implicitly. So, putting in evidence $\mathbf{v}^s$ from eq.B.2:

$$\nabla \cdot \mathbf{v^s} = -\frac{1}{(1-\varepsilon)\rho^s}\frac{D[(1-\varepsilon)\rho^s]}{Dt} \tag{B.6}$$

Substituting eq.B.6 into eq.B.5 we obtain:

$$\varepsilon\rho^\alpha\frac{Ds^\alpha}{Dt} + \rho^\alpha s^\alpha\frac{D\varepsilon}{Dt} + \varepsilon s^\alpha\frac{D\rho^\alpha}{Dt} + \nabla\cdot(\rho^\alpha\mathbf{q}^\alpha) - \frac{\varepsilon s^\alpha\rho^\alpha}{(1-\varepsilon)\rho^s}\frac{D[(1-\varepsilon)\rho^s]}{Dt} = e_{wi} \tag{B.7}$$

Considering now that the

$$\rho^\alpha s^\alpha\frac{D\varepsilon}{Dt} = -\rho^\alpha s^\alpha\frac{D(1-\varepsilon)}{Dt} = -\frac{\rho^\alpha s^\alpha}{\rho^s}[\rho^s\frac{D(1-\varepsilon)}{Dt}] \tag{B.8}$$

Expanding the last term with the product rule:

$$\rho^s\frac{D[(1-\varepsilon)]}{Dt} = \frac{D[(1-\varepsilon)\rho^s]}{Dt} - (1-\varepsilon)\frac{D(\rho^s)}{Dt} \tag{B.9}$$

Next combining eq.B.9 and eq.B.7 we obtain:

$$\begin{aligned}\varepsilon\rho^\alpha\frac{Ds^\alpha}{Dt} - \left[\frac{\rho^\alpha s^\alpha}{\rho^s} + \frac{\varepsilon s^\alpha\rho^\alpha}{(1-\varepsilon)\rho^s}\right]\frac{D[(1-\varepsilon)\rho^s]}{Dt} + \frac{\rho^\alpha s^\alpha(1-\varepsilon)}{\rho^s}\frac{D\rho^s}{Dt} \\ +\varepsilon s^\alpha\frac{D\rho^\alpha}{Dt} + \nabla\cdot(\rho^\alpha\mathbf{q}^\alpha) = e_{wi}\end{aligned} \tag{B.10}$$

Finally we obtain:

$$\begin{aligned}\varepsilon\rho^\alpha\frac{Ds^\alpha}{Dt} - \frac{\rho^\alpha s^\alpha}{(1-\varepsilon)\rho^s}\frac{D[(1-\varepsilon)\rho^s]}{Dt} + \frac{\rho^\alpha s^\alpha(1-\varepsilon)}{\rho^s}\frac{D\rho^s}{Dt} \\ +\varepsilon s^\alpha\frac{D\rho^\alpha}{Dt} + \nabla\cdot(\rho^\alpha\mathbf{q}^\alpha) = e_{wi}\end{aligned} \tag{B.11}$$

To obtain the compressibility terms we will convert the derivates of the variables into derivated of pressure. Considering that the effects of temperature, chemical composition and strength on density are negligible, the density is function only of pressure $\rho^\alpha = \rho^\alpha(p^\alpha)$.

Considering Matrix compressibility α^β

$$\alpha^\beta = \frac{1}{(1-\varepsilon)\rho^s}\frac{\partial[(1-\varepsilon)\rho^s]}{p^s} \tag{B.12}$$

$$\beta^s = \frac{1}{\rho^s}\frac{\partial \rho^s}{\partial p^s} \tag{B.13}$$

$$\beta^\alpha = \frac{1}{\rho^\alpha}\frac{\partial \rho^\alpha}{\partial p^\alpha} \tag{B.14}$$

Inserting the derivate respect to pressure we obtain the final general form:

$$\varepsilon\rho^\alpha\frac{\partial s^\alpha}{\partial t} + s^\alpha\rho^\alpha\{[\alpha^\beta + (1-\varepsilon)\beta^s]\frac{\partial p^s}{\partial t} + \varepsilon\beta^\alpha\frac{\partial p^\alpha}{\partial t}\} - \nabla\cdot(\rho^\alpha\mathbf{q}^\alpha) = e_{wi}. \tag{B.15}$$

$\alpha = w, i, a$

Considering the expression of Darcy velocity we obtain

$$\mathbf{q}^\alpha = \left[\frac{k^{s\alpha}}{\mu^\alpha}\cdot(\nabla p^\alpha - \rho^\alpha g)\right] \tag{B.16}$$

$$\varepsilon\rho^\alpha\frac{\partial s^\alpha}{\partial t} + s^\alpha\rho^\alpha\{[\alpha^\beta + (1-\varepsilon)\beta^s]\frac{\partial p^s}{\partial t} + \varepsilon\beta^\alpha\frac{\partial p^\alpha}{\partial t}\} - \nabla\cdot[\rho^\alpha\frac{k^{s\alpha}}{\mu^\alpha}\cdot(\nabla p^\alpha - \rho^\alpha g)] = e^\alpha_{\alpha s} + e^\alpha_{wn}. \tag{B.17}$$

$\alpha = w, i, a$

Appendix C

Energy Conservation equation

To quantify the energy content in V, we consider the internal energy U [18]. It is defined as

$$U = U_s + U_i + U_w \tag{C.1}$$

where U_s, U_i and U_w are the internal energies of solid, ice and liquid water.

Each of these internal energies can be written with respect to a reference temperature (T_{ref}, in K, see again [18]:

- $U_s = \rho^s c^s (1-\varepsilon)(T - T_{ref})$
- $U_i = \rho^i c^i \varepsilon s^i (T - T_{ref})$
- $U_w = \rho^w \varepsilon s^w \left[L_f + c_w (T - T_{ref})\right]$

where c_s, c_w and c_i are specific thermal capacities for minerals, liquid water and ice (in J/kg/K) and L_f is the latent heat of fusion (in J/kg). It follows that

$$U = C_{eff}\,(T - T_{ref}) + \rho^w L_f \varepsilon s^w \tag{C.2}$$

, with

$(C_p)_{eff} = \rho^s(1-\varepsilon)C_p^s + \rho^w \varepsilon s^w C_p^w + \rho^i \varepsilon s^i C_p^i$

is usually called total (or volumetric) thermal capacity of the soil volume [10, 18]. Henceforth, $T - T_{ref} = T^\star$.

The one-dimensional conservation equation for U reads:

$$\frac{\partial U}{\partial t} + \nabla \cdot (\mathbf{G} + \mathbf{J}) = 0 \tag{C.3}$$

The first term of eq.C.3 can be writted as:

$$\frac{\partial U}{\partial t} = C_{eff}\frac{\partial T}{\partial t} + \rho^w L_f \varepsilon \frac{\partial s^w}{\partial t} \tag{C.4}$$

The terms **G** and **J** indicates respectively the heat flux due to conduction and advection.

The conduction flux is modeled as:

$$\mathbf{G} = -\lambda_{eff}\nabla T \tag{C.5}$$

Where $\lambda_{eff} = \lambda^s + \lambda^w + \lambda^i$ is the thermal conductivity of the soil.

The convection flux is defined as:

$$\mathbf{J} = \rho^w c_p^w \mathbf{v}^w T^* + \rho^w L_f \mathbf{v}^w \tag{C.6}$$

Substituting into eq.C.3 we obtain:

$$(\rho C_p)_{eff}\frac{\partial T^*}{\partial t} + \rho^w L_f \varepsilon \frac{\partial s^w}{\partial t} + (\rho^w C_p^w v^w)\nabla T^* - \nabla \cdot (\lambda_{eff}\nabla T^*) = 0 \tag{C.7}$$

Where:

$(\rho C_p)_{eff} = \rho^s(1-\varepsilon)C_p^s + \rho^w \varepsilon s^w C_p^w + \rho^i \varepsilon s^i C_p^i$

$\lambda_{eff} = \lambda^s + \lambda^w + \lambda^i$

$T^* = T - T_{f/m}$

The second term of eq.C.10 indicates the rate at which soil water turns into ice. Since this term depends on temperature we can introduce an apparent heat capacity combining the first and second term as follow:

$$\begin{aligned}(\rho C_p)_{eff}\frac{\partial T^*}{\partial t} - \rho^i L_f \varepsilon \frac{\partial s^i}{\partial t} &= (\rho C_p)_{eff}\frac{\partial T^*}{\partial t} - \rho^i L_f \varepsilon \frac{\partial s^i}{\partial T}\frac{\partial T}{\partial t} \\ &= \left((\rho C_p)_{eff} - \rho^i L_f \varepsilon \frac{\partial s^i}{\partial T^*}\right)\frac{\partial T^*}{\partial t}\end{aligned} \tag{C.8}$$

Calling C_a apparent capacity, written as:

$$\begin{aligned}C_a &= (\rho C_p)_{eff} - \rho^i L_f \varepsilon \frac{\partial s^i}{\partial T^*} \\ &= \rho^s(1-\varepsilon)C_p^s + \rho^w \varepsilon s^w C_p^w + \rho^i \varepsilon s^i C_p^i - \rho^i L_f \varepsilon \frac{\partial s^i}{\partial T^*}\end{aligned} \tag{C.9}$$

We obtain the final equation:

$$(\rho C_a)\frac{\partial T^*}{\partial t} + (\rho^w C_p^w v^w)\nabla T^* - \nabla \cdot (\lambda_{eff}\nabla T^*) = 0 \tag{C.10}$$

Bibliography

[1] Dobinski, W. *Permafrost.* Earth-Sci. Rev. 108 (3âĂŞ4), 158âĂŞ169, (2011).

[2] T.E. Osterkamp, C.R. Burn *Permafrost.*

[3] Kurylyk, Barret L., Kerry TB MacQuarrie, and Jeffrey M. McKenzie. *Climate change impacts on groundwater and soil temperatures in cold and temperate regions: Implications, mathematical theory, and emerging simulation tools.* Earth-Science Reviews 138 (2014): 313-334.

[4] Louis L. Ray *Permafrost.* U.S. Department of the Interior / U.S. Geological Survey.

[5] Lorraine Manz *Frost heave* Geo News, 32 (2), pages 18âĂŞ24,July 2011.

[6] Andrew C. Fowler, William B. Krantz *A generalized secondary Frost Heave Model.*. SIAM Journal on Applied Mathematics, Vol. 54, No. 6.,pages 1650-1675,Dec 1994

[7] Kevin O'Neill, Robert D. Miller *Exploration of a Rigid Ice Model of Frost Heave.* Water Resources Research, VOL. 21, NO. 3, Pages 281-296, March 1985

[8] Alan W. Rempel *Frost Heave.* Journal of Glaciology, Vol. 56, No. 200, 2010.

[9] Daichao Sheng, Sven Knutsson *Frost Heave due to Ice Lens Formation in Freezing Soils 1. Theory and Verification.*. Hydrology Research, 1995.

[10] Klas Hansson,* Jirka SËĞ imuÂř nek, Masaru Mizoguchi *Water Flow and Heat Transport in Frozen Soil: Numerical Solution and FreezeâĂŞThaw Applications.* Vadose Zone Journal 3:693âĂŞ704, 2004.

[11] Andrew C. Fowler; William B. Krantz *A generalized secondary frost heave model.* SIAM Journal on Applied Mathematics, Vol. 54, No. 6. , pages 1650-1675, Dec. 1994

[12] Williams, P., Smith, M. *THERMODYNAMIC BEHAVIOUR OF FROZEN SOILS. In The Frozen Earth: Fundamentals of Geocryology* . Cambridge University Press ,pages 174-201, 1989

[13] Apostolos Kantzas,Jonathan Bryan,Saeed Taheri. *Fundamentals of Fluid Flow in Porous Media.* http://perminc.com/resources/fundamentals-of-fluid-flow-in-porous-media/chapter-2-the-porous-medium/compressibility-of-porous-rocks/

[14] Pinder, George F., and William G. Gray. *Essentials of multiphase flow in porous media.*. John Wiley and Sons, 2008.

[15] L.A. Richards *Capillary Conduction of Liquids through Porous Mediums.* Journal of Applied Physics, 1, 318-333,1931.

[16] Global climate change https://climate.nasa.gov/vital-signs/global-temperature/

[17] J. Bear. *Dynamics of fluids in porous media.* Dover Publications, 1972.

[18] M. Dall'Amico, S. Endrizzi, S. Gruber, and R. Rigon. *A robust and energy-conserving model of freezing variably-saturated soil. The Cryosphere*, 5(2):469–484, 2011. doi: 10.5194/tc-5-469-2011. URL `http://www.the-cryosphere.net/5/469/2011/`.

[19] Koniorczyk, Marcin, Dariusz Gawin, and Bernhard A. Schrefler *Modeling evolution of frost damage in fully saturated porous materials exposed to variable hygro-thermal conditions.* Computer Methods in Applied Mechanics and Engineering 297 (2015): 38-61.

[20] Lewis, R. W.; Schrefler, B.A. *The Finite Element Method in the Static and Dynamic Deformation and Consolidation of Porous Media*. 1987.

[21] California Agricultural Experiment Station. *Hilgardia*. 2011

[22] Y. Mualem. A new model for predicting the hydraulic conductivity of unsaturated porous media. *Water Resources Research*, 12, 1976.

[23] H. Saito, J. Šimůnek, and B. P. Mohanty. Numerical analysis of coupled water, vapor and heat transport in the vadose zone. *Vadose Zone Journal*, 5:784–800, 2006.

[24] C. Truesdell. The rational mechanics of materials. In *On the Foundations of Mechanics and Energetics*, pages 293–304. Gordon & Breach, 1965.

[25] L. Zhao, D. M. Gray, and D. H. Male. Numerical analysis of simultaneous heat and mass transfer during infiltration into frozen ground. *Journal of Hydrology*, 200:345 – 363, 1997.